THE UNIVERSITY OF QUEENSLAND

AUSTRALIA

Vegetation Effects on Soil Moisture and Groundwater Recharge in Subtropical Coastal Sand Dunes

Junliang Fan

BEng, MEng

A thesis submitted for the degree of Doctor of Philosophy at

The University of Queensland in 2014

School of Civil Engineering

Abstract

Vegetation can potentially have a strong influence on the water budget and hydrological processes in vegetated ecosystems due to canopy rainfall interception and the partitioning of rainfall into throughfall and stemflow, as well as root water uptake from the vadose zone or groundwater table. This study aims to explore the potential effects of vegetation on soil moisture dynamics and groundwater recharge in a subtropical coastal area of eastern Australia. This area is characterized by highly permeable sands, intense summer rainfall events and three typical vegetation covers (exotic pine plantation, native woodland and grassland).

First of all, the spatial variability of both throughfall and stemflow at the soil surface was investigated in a 12-year-old managed pine plantation over one year on Bribie Island using tipping-bucket rain gauges. Rainfall loss by canopy interception and subsequent evaporation from this pine plantation and a native banksia woodland were also quantified and compared using field measurements and two analytical models of rainfall interception. In addition, the potential hydrological impacts of changes in vegetation cover in this shallow sandy groundwater system (depth to water table < 2 m) was evaluated by estimating groundwater recharge and discharge by evapotranspiration (ET_g) under the three contrasting vegetation covers over a 2-year period using the water table fluctuation method and the White method, respectively.

To further monitor the actual water percolation processes in deep sand dune profiles (depth to water table > 10 m), spatial patterns and seasonal dynamics of root-zone soil moisture were quantified under three contrasting vegetation covers on North Stradbroke Island by combining two geophysical techniques: surface electric resistivity tomography (surface ERT) and spatial time domain reflectometry (spatial TDR). Based on the field investigations of rainfall and root distributions at the under-canopy and inter-canopy zones, spatial distributions of vadose zone soil moisture and deep drainage in this subtropical coastal forest overlying deep sand dunes were finally simulated using HYDRUS models.

On the Bribie Island sites, the highest throughfall was found on the east side of the tree trunks (~85% of gross rainfall) and the lowest in the midway between tree rows (~68% of gross rainfall) in the pine plantation. These spatial patterns persist for around 84% of recorded rainfall events. This is explained by canopy interception of the inclined rainfall resulting from the prevailing easterly wind direction throughout the experiment. Annual

rainfall interception loss in the banksia woodland was lower (~16% of gross rainfall) than that in the pine plantation (~23% of gross rainfall) due to the lower canopy storage capacity and higher aerodynamic resistance of the banksia woodland. The RGAM and WiMo models predicted the interception losses from these forest stands reasonably well. The average annual gross recharge was largest at the sparse grassland site, followed by the exotic pine plantation and then native banksia woodland. Lower recharge values at forested sites are most likely resulted from higher rainfall interception losses and shallower water table depths. The pine plantation extracted more groundwater through ET_g than the banksia woodland, whereas sparse grassland was found not consuming groundwater.

In the open pine forest on North Stradbroke Island, the joint use of surface ERT and spatial TDR methods allowed spatially monitoring of root-zone moisture dynamics of the forest soils and the detection of typical features of rainfall interception, root water uptake and preferential infiltration of stemflow. Both surface ERT measurements and HYDRUS modelling identified higher soil moisture and deep drainage at the inter-canopy area relative to those under the canopy due to lower rainfall interception loss and higher root water uptake. The HYDRUS modelling experiments indicated deep drainage was underestimated by 130 mm to 162 mm (9.7%–12.0% drop compared to baseline scenario) as a consequence of uniform representation of spatial root systems in one- or two-dimensional HYDRUS models.

The results of this study confirmed the vegetation in these coastal systems has a significant impact on the spatial distribution of rainfall at the soil surface and root water uptake, changing water infiltration and evapotranspiration patterns. Recharge in these shallow sandy aquifers is governed by seasonal rainfall but restricted in the wet season by wet antecedent soil moisture when the water table is approaching the soil surface, i.e., potential recharge is rejected. Groundwater use by vegetation is largely driven by potential ET but also limited by the depth to water table. The establishment of commercial pine plantations in these areas of native vegetation may reduce deep drainage and ultimately groundwater recharge, especially during extensive dry seasons, due to higher interception losses and groundwater uptake. In recharge modelling, our HYDRUS simulations show that translating the hydrological effect of the two-dimensional tree structure (rainfall redistribution and heterogeneous roots) to a one-dimensional lumped vertical conceptualization needs to be undertaken with caution.

Declaration by author

This thesis is composed of my original work, and contains no material previously published or written by another person except where due reference has been made in the text. I have clearly stated the contribution by others to jointly-authored works that I have included in my thesis.

I have clearly stated the contribution of others to my thesis as a whole, including statistical assistance, survey design, data analysis, significant technical procedures, professional editorial advice, and any other original research work used or reported in my thesis. The content of my thesis is the result of work I have carried out since the commencement of my research higher degree candidature and does not include a substantial part of work that has been submitted to qualify for the award of any other degree or diploma in any university or other tertiary institution. I have clearly stated which parts of my thesis, if any, have been submitted to qualify for another award.

I acknowledge that an electronic copy of my thesis must be lodged with the University Library and, subject to the General Award Rules of The University of Queensland, immediately made available for research and study in accordance with the *Copyright Act 1968*.

I acknowledge that copyright of all material contained in my thesis resides with the copyright holder(s) of that material. Where appropriate I have obtained copyright permission from the copyright holder to reproduce material in this thesis.

Publications during candidature

Peer-reviewed papers

1. **Fan, J.**, Oestergaard, K. T., Guyot, A., Jensen, D. G., & Lockington, D. A. (2014). Spatial variability of throughfall and stemflow in an exotic pine plantation of subtropical coastal Australia. *Hydrological Processes* (in press). DOI: 10.1002/hyp.10193.

2. **Fan, J.**, Oestergaard, K. T., Guyot, A., & Lockington, D. A. (2014). Measuring and modelling rainfall interception losses by a native banksia woodland and an exotic pine plantation in subtropical coastal Australia. *Journal of Hydrology* 515, 156-165.

3. **Fan, J.**, Oestergaard, K. T., Guyot, A., & Lockington, D. A. (2014). Estimating groundwater recharge and evapotranspiration from water table fluctuations under three vegetation covers in a coastal sandy aquifer of subtropical Australia. *Journal of Hydrology* 519, 1120-1129.

4. **Fan, J.**, Scheuermann, A., Baumgartl, T., & Lockington, D. A. (2014). Quantifying spatiotemporal dynamics of root-zone soil moisture in a mixed forest on subtropical coastal sand dunes using surface ERT combined with spatial TDR. *Journal of Hydrology* (under review).

5. **Fan, J.**, Baumgartl, T., Scheuermann, A., & Lockington, D. A. (2014). Modelling effects of rainfall redistribution and root water uptake on spatiotemporal soil moisture dynamics and deep drainage in a subtropical coastal sand dune forest. *Vadose Zone Journal* (under review).

6. Guyot, A., Ostergaard, K. T., Lenkopane, M., **Fan, J.**, & Lockington, D. A. (2013). Using electrical resistivity tomography to differentiate sapwood from heartwood: application to conifers. *Tree physiology* 33, 187-194.

Conference papers

Scheuermann, A., Gonzales, C., **Fan, J.**, Braga, B., Baumgartl T., Lockington, D., Schlaeger, S., Becker, R., Wagner N., & Hübner C. (2014). Spatial Time Domain

Reflectometry (spatial TDR) in geo-environmental engineering. The 9th IEEE Sensors Applications Symposium (SAS), Queenstown, New Zealand.

Publications included in this thesis

This thesis contains two jointly-authored accepted papers, two jointly-authored submitted papers and one jointly-authored paper to be submitted for publication. These papers are incorporated as chapters of this thesis (Chapters 2–6). I was responsible for the majority of the work in these papers, including developing ideas, designing experiments, collecting and analysing data as well as drafting the papers. Contributions by co-authors are indicated below the citations.

1. **Fan, J.**, Oestergaard, K. T., Guyot, A., Jensen, D. G., & Lockington, D. A. (2014). Spatial variability of throughfall and stemflow in an exotic pine plantation of subtropical coastal Australia. *Hydrological Processes* (in press). DOI: 10.1002/hyp.10193. Incorporated as Chapter 2.

Oestergaard, K. T. (5%) and Guyot, A. (5%) critically commented and revised the paper. Jensen, D. G. (5%) conducted the experiments on small-scale spatial variability of gross rainfall. Prof. Lockington, D. A. (10%) contributed to the conception and design of the project.

2. **Fan, J.**, Oestergaard, K. T., Guyot, A., & Lockington, D. A. (2014). Measuring and modeling rainfall interception losses by a native banksia woodland and an exotic pine plantation in subtropical coastal Australia. *Journal of Hydrology* 515, 156-165. Incorporated as Chapter 3.

Oestergaard, K. T. (5%) and Guyot, A. (5%) critically commented and revised the paper. Prof. Lockington, D. A. (10%) contributed to the conception and design of the project.

3. **Fan, J.**, Oestergaard, K. T., Guyot, A., & Lockington, D. A. (2014). Estimating groundwater recharge and evapotranspiration from water table fluctuations under three vegetation covers in a coastal sandy aquifer of subtropical Australia. *Journal of Hydrology* 519, 1120-1129. Incorporated as Chapter 4.

Oestergaard, K. T. (5%) and Guyot, A. (5%) critically commented and revised the paper. Prof. Lockington, D. A. (10%) contributed to the conception and design of the project.

4. **Fan, J.**, Scheuermann, A., Baumgartl, T., & Lockington, D. A. (2014). Quantifying spatiotemporal dynamics of root-zone soil moisture in a mixed forest on subtropical coastal sand dunes using surface ERT combined with spatial TDR. *Journal of Hydrology* (under review). Incorporated as Chapter 5.

Scheuermann, A. (5%) and Baumgartl, T. (5%) critically commented and revised the paper. Prof. Lockington, D. A. (10%) contributed to the conception and design of the project.

5. **Fan, J.**, Baumgartl, T., Scheuermann, A., & Lockington, D. A. (2014). Modelling effects of rainfall redistribution and root water uptake on spatiotemporal soil moisture dynamics and deep drainage in a subtropical coastal sand dune forest. *Vadose Zone Journal* (under review). Incorporated as Chapter 6.

Baumgartl, T. (5%) and Scheuermann, A. (5%) critically commented and revised the paper. Prof. Lockington, D. A. (10%) contributed to the conception and design of the model.

Contributions by others to the thesis

No contributions by others.

Statement of parts of the thesis submitted to qualify for the award of another degree

None.

Acknowledgements

I would first like to express my sincere appreciation and gratitude toward my supervisors, Prof. David Lockington, Dr Alexander Scheuermann and Dr Thomas Baumgartl. Without their constructive advice, guidance and encouragement throughout my doctoral research, I would not have completed my Ph.D. study. I am particularly grateful that they gave me the freedom to pursue my own research interests while gently steering me towards the right direction. Thanks are also given to the other two members of my thesis committee, Professor Ling Li and Professor William Clarke, for their contributions during my study.

I would next like to thank Dr. Kasper Oestergaard and Dr. Adrien Guyot for their intellectual assistance during field studies and making useful comments on the manuscripts. I am also grateful to Jeremy Canard for driving me around, testing and setting up the instrumentation during the countless field trips to Bribie Island and North Stradbroke Island. The assistance and support of the technicians from School of Civil Engineering Laboratories, especially Troy Brooks, is gratefully acknowledged. Special thanks are due to HQPlantation Pty Ltd and Seqwater for providing trees and access to the study sites. I also extend my sincere thanks to all the friends and nice people that I have met during my stay in Australia.

I would finally like to thank my family for their steady encouragement and support. I sincerely thank my wife, Nan Qi, for always making me happy even during the most stressful times and being there all the time with patience and understanding throughout my Ph.D. process. Finally, I acknowledge the following agencies for supplying financial support to my Ph.D. studies: the University of Queensland (UQ), the National Centre for Groundwater Research and Training (NCGRT) and the China Scholarship Council (CSC).

Keywords

rainfall interception loss, throughfall, stemflow, root water uptake, pine plantation, banksia woodland, water table fluctuation method, geophysical method, HYDRUS model

Australian and New Zealand Standard Research Classifications (ANZSRC)

ANZSRC code: 090509, Water Resources Engineering, 100%

Fields of Research (FoR) Classification

FoR code: 0905, Civil Engineering, 100%

Table of Contents

List of Figures

List of Tables

List of Abbreviations and Symbols

Abbreviations

AHD	Australian Height Datum
BD	Bulk density
BW	Banksia woodland
CV	Coefficient of variation
DBH	Diameter at breast height
E_a	Actual evaporation
E_i	Interception loss
E_p	Potential evaporation
EMI	Electromagnetic induction
ERT	Electrical resistivity tomography
ET	Evapotranspiration
ET_g	Groundwater evapotranspiration
GPR	Ground penetrating radar
LAI	Leaf area index
LCLU	Land cover/land use
mbls	m below land surface
ME	Mean error
MRC	Master recession curve
PET	Potential evapotranspiration
P_g	Gross rainfall
P_n	Net rainfall
PP	Pine plantation
RGAM	Revised Gash's analytical model
RH	Relative humidity

RMSE	Root mean square error
SD	Standard deviation
SEQ	Southeast Queensland
S_f	Stemflow
SVR	Volume per mm of rain
TDR	Time domain reflectometry
T_f	Throughfall
Tp	Potential transpiration
TSV	Total stemflow volumes
USDA	United States Department of Agriculture
WB	Water balance
WD	Wind direction
WiMo	Wind controlled canopy interception capacity model
WTF	Water table fluctuation
1D	One-dimensional
2D	Two-dimensional
3D	Three-dimensional

Symbols

A	Area
c	Canopy cover
c_p	Specific heat of the air
d	Index of agreement
D	Median raindrop diameter
G	Soil heat flux
i	Rainfall intensity
K_s	Saturated hydraulic conductivity

n	Number
p	Canopy gap fraction
R	Recharge
r_a	Aerodynamic resistance
R_n	Net radiation
S	Canopy storage capacity
S_e	Effective saturation
$S(h)$	Sink term
T	Temperature
u	Wind velocity
u_r	Terminal fall velocity of raindrops
α	Rainfall inclination angle
$\gamma(h)$	Water stress response function
θ	Soil moisture content
θ_r	Residual soil moisture content
θ_s	Saturated moisture content
λ	Latent heat of vaporization of water
ρ	Soil resistivity
ρ_a	Air density

Chapter 1. Introduction

1.1 Background

Changes in the groundwater balance are determined by rates of recharge and discharge as well as the hydraulic characteristics of the aquifer. The rate at which groundwater is replenished is important in determining the sustainable rate at which groundwater can be extracted. Therefore, quantification of groundwater recharge rates and patterns (timing and location) is essential for sustainable groundwater management. This fundamentally requires us to be able to quantify and model recharge processes including the impact of alternative management scenarios, e.g., changes in land cover/land use (LCLU) and climate variability (Scanlon et al., 2002).

In southeast Queensland (SEQ), Australia, valuable resources of generally high quality groundwater are located in onshore sand mass systems and on nearby sand islands (e.g., Bribie Island and North Stradbroke Island). These areas are typically characterized by aquifers with highly permeable sands and a climate characterized by intense summer rainfall. The groundwater is mainly exploited for water supply to coastal communities. It is also required to maintain the health of associated coastal and estuarine wetland vegetation. This coastal area has experienced rapid growth and changes in LCLU over the past several decades. Exotic pine plantations have been developed largely in the natural distribution areas of native vegetation (e.g. banksia woodland and grassland) for timber production. SEQ has the second largest plantation area in Australia with 9.6% of the national total plantation area (FPQ, 2010). Transforming vegetation cover from native ecosystems to exotic species plantations can potentially affect soil moisture dynamics and subsequently groundwater recharge.

Groundwater recharge in forested areas is largely determined by the interplay of climate, vegetation and soils, of which vegetation acts as the primary link between the atmosphere and subsurface water. Vegetation affects the groundwater yields indirectly by rainfall interception losses and extraction of infiltrating rainwater before it reaches the water table, or directly through groundwater uptake, where it draws on water from the water table or capillary fringe (Le Maitre et al., 1999). With pine plantation and native ecosystems being the dominant covers in recharge areas of these sand mass systems, it is essential to understand and quantify their effects on recharge in these areas.

1.2 Problem statement

The assessment and management of groundwater resources, estimates of spatially and temporally varied groundwater recharge are usually required either as inputs to groundwater models, or as calibration targets. Traditionally, most regional-scale groundwater models often simplify (or even neglect) vadose zone flow processes (Harbaughet al., 2000), generally assuming recharge is a simple percentage of rainfall. This approach does not consider the effects of local vegetation cover and water table depth on recharge. For example, MODFLOW, the most commonly used groundwater flow model, was originally designed with independent recharge and ET packages. These packages specify recharge as a source term for the groundwater and simulate discharge of water through transpiration with a maximum ET rate and a user-defined ET extinction depth. This simplified representation of vadose zone flow appears to be arbitrary and subject to very large uncertainty because groundwater and surface water are in continuous dynamic interaction. It is likely that the uncertainty will be more pronounced for systems where vegetation introduces significant non-uniformity in flow patterns or where the transport through the vadose zone introduces significant lag between rainfall and recharge.

To reduce the uncertainty associated with vadose zone processes in groundwater modelling, some one-dimensional packages have been recently developed and incorporated into MODFLOW, e.g., the Unsaturated Zone Flow (UZF1) package (Niswonger et al., 2006) and the HYDRUS package (Seo et al., 2007). These packages are intended to reasonably characterise the vadose zone processes in groundwater models. Nevertheless, this large-scale lumped modelling inevitably induces a loss of detail in the representation of the fundamental recharge processes. Therefore, the uncertainties of modelling recharge with lumped one-dimensional (1D) vadose models compared to two- or three-dimensional (2D/3D) models need to be determined to confidently model recharge.

Achieving a better understanding of the mechanisms that control groundwater recharge beneath forests is a crucial step towards improving groundwater management. Water flow in the vadose zone especially affects the transfer rates between the land surface and the groundwater table. Vadose zone soil moisture and groundwater recharge in vegetated ecosystems can be influenced by canopy architecture and root systems (e.g., Vrugt et al., 2001; Sansoulet et al., 2008). For instance, water fluxes in the subsurface can vary between the under-canopy and inter-canopy zones. These spatial patterns have important hydro-ecological consequences because they significantly affect the magnitude and

distribution of groundwater recharge and solute transport (Tanaka et al., 1996; Nikodem et al., 2013). Understanding the spatial variability caused by vegetation under forests is also useful for designing both recharge monitoring and modelling strategies at larger scale. However, little attention has been paid to quantifying the fundamental water percolation processes and correlating them with recharge in forest systems, especially in subtropical coastal environments. For these systems, the proposed research questions are as follows.

(1) How does local vegetation affect the net rainfall input and spatial rainfall distribution at the soil surface?

(2) Is the vegetation type important for groundwater recharge in shallow groundwater systems?

(2) How does the rainwater infiltration and percolation differ at the under-canopy or inter-canopy areas?

(3) How should we represent the vegetation (2D/3D information) in 1D lumped modelling such that it captures the main features of recharge processes?

1.3 Aims and objectives

We aim to improve our fundamental understanding of, and quantify and model, the vegetation-related mechanisms and processes affecting groundwater recharge in the subtropical coastal environments (e.g., rainfall interception loss and its partitioning into throughfall stemflow, root water uptake). The specific objectives are as follows:

(1) to determine how the canopy of exotic pine trees redistributes rainfall under the canopy and at the intercanopy area through partitioning of rainfall into throughfall and stemflow, and how the redistributed rainfall affects the local soil water infiltration patterns;

(2) to quantify and model how much rainfall reaches the soil surface after canopy interception as net rainfall input for potential recharge under different vegetation covers (pine plantation and banksia woodland);

(3) to estimate the actual gross recharge and groundwater losses by evapotranspiration through root water uptake using the water table fluctuation methods in order to explore the effect of vegetation on recharge in shallow water table environment;

(4) to test the applicability of two geophysical techniques in these environments for monitoring actual 2D soil water transport processes at the under-canopy and inter-canopy areas as well as the interactions between vegetation and soil moisture;.

(5) to model physics of the mechanisms and processes associated with vegetation using a variably saturated water flow model (HYDRUS 2D/3D), investigate the effects of vegetation on soil moisture and deep drainage through scenario analysis and identify the uncertainties for representing the detailed field information with 2D/3D and 1D models.

1.4 Overview of study sites

We performed comparative experiments on stand-scale plots to investigate the rainfall interception and groundwater recharge under three different vegetation covers: pine plantation, banksia woodland and sparse grassland. Three study sites were established in a shallow sandy aquifer area (depth to water table < 2 m) on Bribie Island with similar topography and soils (Figure 1.1). A fourth site was established in a mixed forest overlying a deeper aquifer (depth to water table > 10 m) on North Stradbroke Island (Figure 1.1) to monitor detailed soil moisture dynamics and recharge processes.

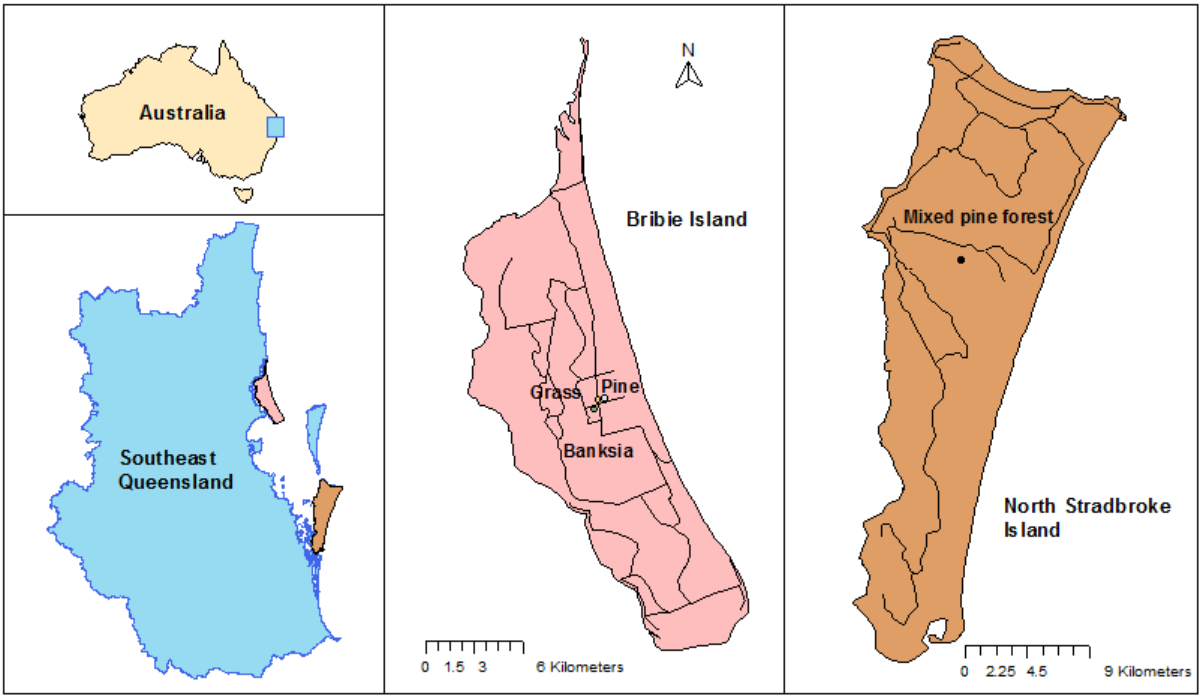

Figure 1.1 Location map of study sites on Bribie Island and on North Stradbroke Island, southeast Queensland, Australia

1.4.1 Bribie Island

The first three study sites were located in the commercial State Forest on Bribie Island (26°59´04´´S, 153°08´18´´E, ~9 m a.m.s.l.), approximately 65 km north of Brisbane. The island stretches approximately 30 km from north to south and has an average width of 5 km with a total area of 144 km^2 (Isaacs and Walker, 1983). Bribie Island has an average elevation of ~5 m Australian Height Datum (AHD) with the maximum value of 13 m AHD. The topography consists largely of the elevated areas which correspond to two parallel sand dune ridges and a separating swale. However, the island is generally considered to be one of low relief. The extensive unconfined upper aquifer consists of fine to medium sands lying over cemented low permeability layers, with an average water table depth of ~1.3 m below land surface. This area experiences a humid subtropical climate (Köppen climate classification *Cfa*) characterized by hot humid summers (December–February) and mild dry winters (June–August). According to the rainfall data from Australian Bureau of Meteorology (Figure 1.2), the mean annual rainfall (± SD) over the last 30 years is 1405 (± 338) mm, with 1082 mm (77.0% of annual rainfall) occurring during the wet season (November–April). Average monthly temperature is 21.4 ℃, varying from 16.2 ℃ in July to 26.6 ℃ in January. The average annual pan evaporation is ~1700 mm (Jackson, 2007). Prevailing winds blow from east to west, particularly during rainfall events. The exotic pine trees have replaced large areas of native vegetation in the two major beach ridge systems on the island.

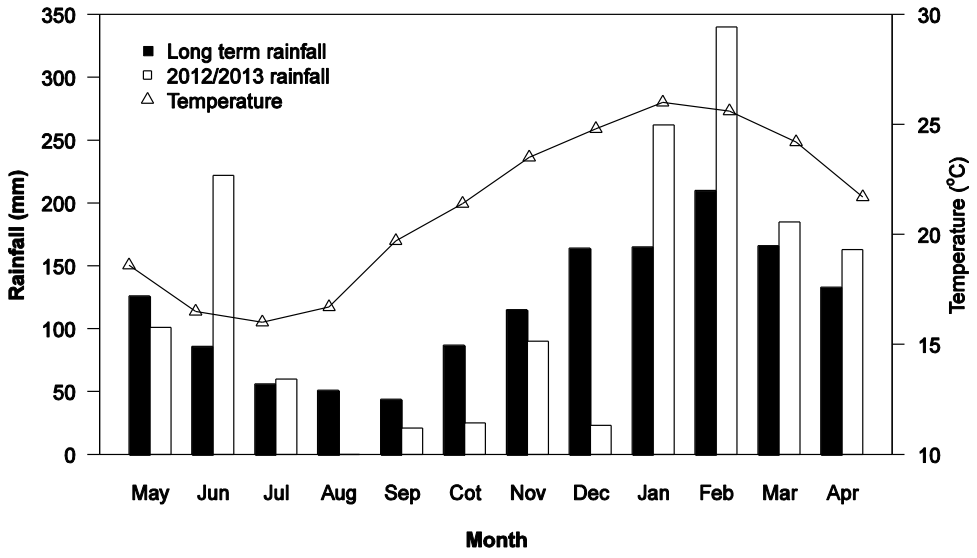

Figure 1.2 Seasonal trend in rainfall for 30-year average and the 2012/2013 season, and mean monthly temperature on Bribie Island.

Two representative study sites were established in adjacent pine plantation (PP) and banksia woodland (BW), approximately 400 m from each other. The PP site had an area of

0.25 ha (50 m × 50 m, ~8.4 m AHD) and was surrounded by similar stands. The 12-year-old pine hybrid of *Pinus elliottii* Engelm. × *Pinus caribaea* Morelet var. *hondurensis* (second rotation) was planted in rows (roughly 5.0 m between tree rows and 2.5 m between the trees in a row). The pine trees reached an average height of 13.3 m and the tree crowns were slightly overlapping above the rows (5%–10%), leaving a gap area of ~1.5 m width between rows. The stem density was 840 trees ha^{-1} and stand basal area was 23.6 m^2 ha^{-1}. The native banksia woodland site had an area of 0.06 ha (25 m × 25 m, ~7.8 m AHD) and was largely dominated by wallum banksia (banksia *aemula* R.Br.) with a sparse understory of grass species. The woodland had with an average tree height of 6.8 m, a stem density of 371 tree ha^{-1} and a basal area of 21.3 m^2 ha^{-1}. The sparse grassland was located on a 30 m wide track (~9.3 m asl) that boards the pine stands. A third grassland site (*Leptocarpus tenax* R.Br.) between the other two sites (but closest to the pine plantation at around 50 m distance) was covered with sparse grasses (Leptocarpus tenax R.Br.) and with an area of 30 m × 30 m and a higher surface elevation of ~9.3 m AHD.

1.4.2 North Stradbroke Island

The fourth study site was located in a sand dune area covered by open forests mainly consisting of exotic slash pine (*Pinus elliottii* Engelm), native wallum banksia (banksia *aemula* R.Br.) and understory grass (*Lomandra elongata* Ewart) on North Stradbroke Island (27°30´40´´S, 153°26´44´´E, 115 m above sea level) of southeast Australia (Figure 1.1). North Stradbroke Island is the world's second largest sand island, with a cover area of ~280 km^2 and dune elevations of mainly between 100 m and 150 m Australia Height Datum (Moss et al., 2013). This area also had a subtropical climate with a hot humid summer (December–February) and a mild dry winter (June–August). The mean annual rainfall, based on 1983–2013 data from Australian Bureau of Meteorology, is 1605 mm and 68.3% of the annual rainfall occurs during the wet season (November–April). The coldest and warmest months are July and January, with average monthly temperatures of 14.2 ℃ and 29.3 ℃, respectively. This study site was a former pine plantation and abandoned approximately in 2000. The pine trees had an average height of 10.5 m, with a stem diameter at breast height of 0.23 m. The banksia trees had a tree height of 5.3 m and a stem diameter of 0.20 m. The extensive unconfined aquifer consists of fine-grained sands based on particle size distribution.

1.5 Thesis structure

The structure of the thesis is as follows.

Chapter 1 provides the background and a general review of the vegetation effects on vadose zone water processes. It also states the current problems and objectives of the thesis, introduces the study sites and thesis structure.

Chapter 2 consists of a detailed study on spatial variability of throughfall and stemflow in the exotic pine plantation on Bribie Island to investigate the spatial distribution of net rainfall reaching the forest floor. This chapter identifies the patterns and magnitudes of variability in gross rainfall, throughfall and stemflow, explores the main driving factors for spatial variability of throughfall and stemflow, and determines the proportions of throughfall, stemflow and interception loss in this plantation. Results from this chapter can be used for numerical models in Chapter 6.

Chapter 3 consists of a comparison of rainfall interception losses by the exotic pine plantation and native banksia woodland on Bribie Island based on field observations and two analytical rainfall interception models. This chapter explores the underlying causes of differences in rainfall interception between the native and exotic forests, calibrates and validates the RGAM and WiMo models for both forest stands, and assesses the canopy and climatic parameters required to apply the models. Results from this chapter will be used in Chapter 4.

Chapter 4 estimates groundwater recharge and discharge by evapotranspiration from water table fluctuations under the three vegetation covers (pine plantation, native banksia woodland and sparse grassland) on Bribie Island. This chapter examines how water table depth varies daily and seasonally under a pine plantation, a banksia woodland and a sparse grassland; determines depth-dependent specific yields under both rising and falling conditions; estimates daily and seasonal groundwater recharge and ET_g under different vegetation covers; and explores the controlling factors on groundwater yields in shallow sandy aquifer systems.

Chapter 5 quantifies spatiotemporal dynamics of root-zone soil moisture in the mixed forest on North Stradbroke Island using surface ERT combined with spatial TDR. This chapter evaluates and validates the capability of spatial TDR and surface ERT to monitor 1D/2D moisture distribution in sandy forest soils; explores and compares seasonal

dynamics of subsurface soil moisture under various vegetation types at the plant scale; investigates how rainfall redistribution by canopy and root water uptake affect the spatial distribution of root-zone moisture content and subsequent deep drainage.

Chapter 6 studies spatial rainfall distributions at the under-canopy and inter-canopy areas caused by pine canopy interception and the heterogeneous root distribution on North Stradbroke Island. HYDRUS models are then used to investigate the spatial characteristics of soil moisture and deep drainage along the canopy-intercanopy transect to provide insight into the percolation processes in the deep vadose zone. Finally, a discussion of translating the effects on recharge of two-dimensional tree structure (rainfall redistribution and heterogeneous roots) to a one-dimensional unsaturated flow model was provided.

Chapter 7 summarizes the major results from Chapters 2 through 6, and brings the studies together. The implications of these findings in terms of field monitoring and modelling groundwater hydrology in subtropical coastal environments are discussed. It also includes recommendations for future research.

Chapter 2. Spatial Variability of Throughfall and Stemflow in an Exotic Pine Plantation of Subtropical Coastal Australia

2.1 Introduction

Partitioning of gross rainfall (P_g) into throughfall (T_f), stemflow (S_f) and interception loss (E_i) by forest canopies exerts a significant role in the water budget of forest ecosystems (Llorens and Domingo, 2007). The presence of trees affects the volume and also the spatial distribution of net rainfall reaching the forest floor via throughfall and stemflow. The variable throughfall and stemflow fluxes and related solute inputs are of great importance, because they can produce "hot spots" and "hot moments" of hydrological and biogeochemical processes within soils (McClain *et al.*, 2003), e.g. water availability for plants (Ford and Deans, 1978; Bouillet *et al.*, 2002; O'Grady *et al.*, 2005), nutrient concentration and cycling (Whelan *et al.*, 1998; Laclau *et al.*, 2003; Zimmermann *et al.*, 2007) and localized groundwater recharge (Taniguchi *et al.*, 1996; Liang *et al.*, 2009; Guswa and Spence, 2012). Additionally, the spatial patterns of throughfall and stemflow will determine the accuracy of estimates on stand-scale interception losses (Loustau *et al.*, 1992; Shinohara *et al*., 2010). Consequently, the spatial variability of throughfall and stemflow is potentially a significant control on forest hydrology and biogeochemistry (Hopp and McDonnell, 2011; Levia *et al.*, 2011; Coenders-Gerrits *et al.*, 2013).

Field investigations have exhibited considerable variability in throughfall over diverse forest types globally (e.g. Llorens and Domingo, 2007; Wullaert *et al.*, 2009; Krämer and Hölscher, 2009; Mululo Sato *et al*., 2011). Stemflow has demonstrated even higher variability than throughfall (e.g. Lloyd and Marques, 1988; Loustau *et al.*, 1992; Levia *et al.*, 2010). Variability of throughfall and stemflow is influenced by a number of factors, including canopy structure and architecture (e.g. Crockford and Richardson, 2000, Loescher *et al.*, 2002; Deguchi *et al.*, 2006; Ziegler *et al.*, 2009), rainfall intensity and duration (e.g. Huber and Iroumé, 2001; Carlyle-Moses *et al.*, 2004; Zhan *et al.*, 2007), wind direction and speed (e.g. Herwitz and Slye, 1995; Šraj *et al*., 2008; Van Stan *et al*., 2011).

Apart from throughfall and stemflow, open-field gross rainfall is also characterized by high spatial variability from sub-kilometer scale to large catchment scale (Syed *et al.*, 2003; Ciach and Krajewski, 2006; Villarini *et al.*, 2008; Fiener and Auerswald, 2009). For example, Krajewski *et al.* (2003) analyzed the small-scale (<5 km^2) gross rainfall variability

in different climatic regimes and identified large variability at the small distances. McConkey et al. (1990) studied the spatial variability of gross rainfall using 10 tipping-bucket rain gauges spaced between 800 to 4,000 m apart and suggested that gross rainfall must be observed within a few hundred meters of the study site to obtain reliable gross rainfall. However, the spatial patterns of gross rainfall at finer scales (sub-hundred-meter scale) at which most throughfall experiments were performed, have seldom been examined.

In subtropical Australia, as in many other regions and countries, exotic pine plantations have been largely developed for timber production in recent decades (Kanowski *et al*., 2005). To optimize the management of these plantations in terms of soil water and nutrition availability, a better understanding of the spatial distribution of rainfall within forests and its controls is required. Although researchers have investigated the throughfall and stemflow in areas of pines (e.g. Valente *et al*., 1997; Shachnovich *et al*., 2008; Molina and Del Campo, 2012), few studies have focused on the spatial variability in both throughfall and stemflow, as well as their drivers in managed pine plantations. Particularly, the spatial variability of throughfall and stemflow in pine forests planted under subtropical coastal conditions characterized by hot humid summers with frequent intense thunderstorms and mild dry winters, have hitherto not been reported.

Here, we examine the heterogeneity of gross rainfall, throughfall and stemflow, as well as the resulting interception loss in a typical pine plantation of subtropical Australia. Specific objectives of this study are to: (1) identify the patterns and magnitudes of variability in gross rainfall, throughfall and stemflow; (2) explore the main driving factors for spatial variability of throughfall and stemflow; (3) determine the proportions of throughfall, stemflow and interception loss in this plantation.

2.2 Materials and methods

2.2.1 Site description

The present study was conducted on Bribie Island (Figure 1.1). A detailed site description is presented in the overview of study sites in Chapter 1. The representative study plot (50 m × 50 m) was established in a pine stand surrounded by similar stands, extending 0.8 km, 1.2 km, 2.1 km and 4.3 km to the west, east, north and south, respectively (Figure 2.1a).

The plot was established at least 15 m (15–20 m) away from the tracks to the south and the west to minimize the edge effect.

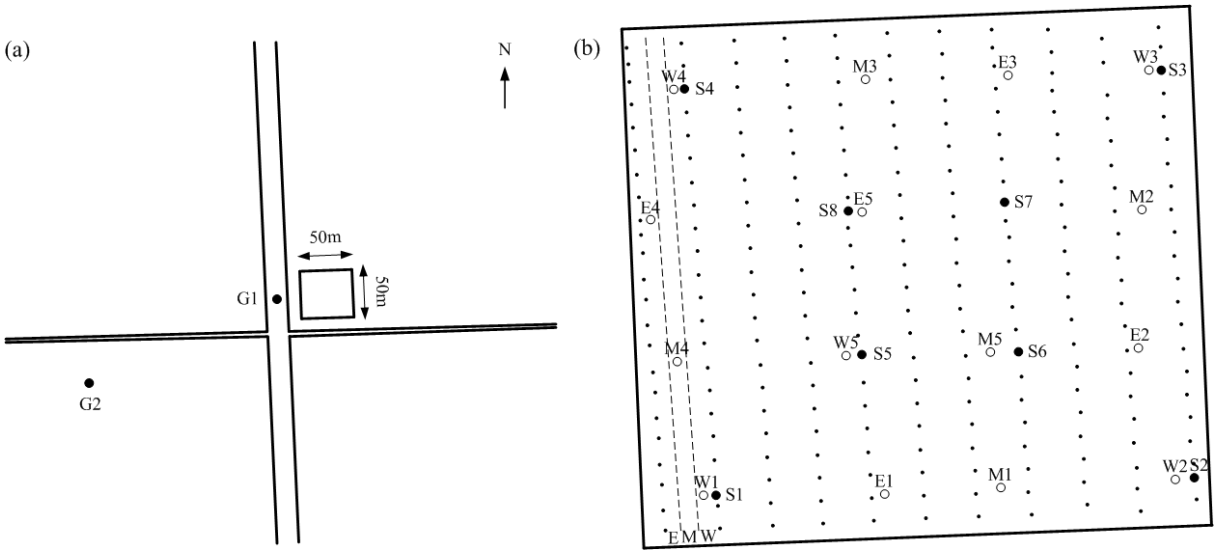

Figure 2.1 (a) Locations of two gross rainfall gauges (G1, G2) on the track and in the nearby clearing. The 50 m × 50 m study plot used for throughfall measurements was represented by the square; (b) Locations of the 15 throughfall gauges deployed at three tree zones (E, W and M): tree trunk to east edge of projected crown area (E1−E5), tree trunk to west edge of projected crown area (W1−W5) and pathway in between edges of projected crown area (M1−M5), and 8 stemflow gauges (S1−S8).The dots represent locations of pine trees.

2.2.2 Measurement of stand characteristics

The forest canopy height was measured from the ground to the top of the tree canopy using a clinometer and a tape measure. The crown radius was determined as the horizontal distance from the tree trunk to the projected edge of the crown along four main compass directions (N, S, W, E). The stem diameter at breast height (*DBH*, 1.3 m above ground surface) was obtained using a diameter caliper. The number of trees and stem diameter were surveyed within the experimental plot to obtain stem density and stand basal area. The canopy gap fraction (*p*) and leaf area index (LAI) were seasonally measured 1.0 m above each rain gauge in the late evening using a LAI-2000 plant canopy analyzer (LI-COR, Lincoln, USA). The *p* and LAI above each throughfall gauge was determined for the circle with a radius of ~1.3 m at the canopy height, equivalent to a zenith angle of 7°. The *p* was calculated as the ratio of below- and above-canopy readings and the canopy cover (*c*) was then determined as 1-*p*. The LAI-2000 plant canopy analyzer tends to underestimate LAI for conifers due to the clumping effects (Gower and

Norman, 1991). The estimated LAI values were thus corrected by a factor of 1.11, based on the measurements in a pine stand of same species in southeast Queensland by Baynes and Dunn (1997). The canopy storage capacity (*S*) above each throughfall gauge was estimated by the method of Leyton *et al.* (1967), as the negative intercept of linear regression between gross rainfall and throughfall for rainfall events that were sufficient to saturate the canopy.

2.2.3 Meteorological variables

An automatic weather station was set up in the center of the study plot to measure temperature and relative humidity (HMP155 sensor, Vaisala, Finland), wind speed and direction (Model 03002 wind sentry set, RM Young, USA), net radiation (CNR4 net radiometer, Kipp & Zonen, The Netherlands) and soil heat flux (HFP01 soil heat flux plates, Hukseflux, The Netherlands). The weather station was mounted on a 15-meter-high mast, which was ~1.5 m above the tree canopy. These meteorological variables were continuously measured at 5-min intervals and automatically recorded to a datalogger (CR3000, Campbell Scientific, USA) at 15-min intervals. Gross rainfall was measured using two HOBO tipping-bucket rain gauges with a 177 cm^2 orifice (RG3-M, Onset Computer Corp., USA), one in the middle of a ~30 m wide track next to the study plot and the other in the center of a nearby clearing at a distance of ~400 m (Figure 2.1a). The bucket tipping time (0.5 s resolution) and numbers were automatically recorded by a self-constructed datalogger.

2.2.4 Experimental design

To investigate the spatial variability of gross rainfall and quantify potential instrumental errors in rain gauge records, 16 tipping-bucket rain gauges were deployed within a 50 m × 50 m plot in the nearby clearing from 5 December 2011 to 14 March 2012 before the throughfall and stemflow measurements. These rain gauges were set up in a lattice-like arrangement at 16 m × 16 m spacing. All the tipping-bucket rain gauges used in this study were placed 50 cm above the ground to avoid droplet splash effects and the screen covers on rain gauges were cleaned and maintained every one or two months to prevent from clogging by leaves and other debris. These rain gauges were calibrated to 0.2 mm per tip in the lab, and dynamically recalibrated in the field seasonally to ensure the accuracy of the rain gauges (Calder and Kidd, 1978).

Throughfall and stemflow were simultaneously measured from 20 March 2012 to 23 March 2013. Throughfall was sampled using 15 rain gauges identical to those used for gross rainfall measurements. To quantify the impact of tree rows on the spatial variability of throughfall, rain gauges were distributed over three tree zones (Figure 2.1b). Within each zone, five rain gauges were placed at a fixed position throughout the experiment period to evaluate the effects of rainfall characteristics on spatial variability of throughfall. Ten rain gauges were positioned ~0.75 m from the tree trunk on east and west sides of the trunks and the other five rain gauges were located in the midway between tree rows.

Stemflow was collected on eight trees using spiral-type stemflow collectors made of wired rubber hose with 2.5 cm in diameter (Toba and Ohta, 2005). Each collector channel was wrapped at least one and a half loops around the tree stem and the collected stemflow was diverted to a HOBO tipping-bucket rain gauge. The upscaled equivalent stand-scale stemflow depth was obtained following Hanchi and Rapp (1997):

$$S_f = \sum_{i=1}^{n} \frac{S_i \cdot m_i}{A \cdot 10^4} \tag{2.1}$$

where S_f is the stand-scale stemflow depth (mm) for the study area of A (m^2); n is the number of *DBH* classes; S_i and m_i are the average stemflow volume (ml) and the number of trees in the DBH class, respectively.

2.2.5 Determination of rainfall inclination angle

The rainfall inclination angle (α, in degree from the vertical) was computed following a series of empirical equations (Herwitz and Slye, 1995):

$$D = 2.23\left(0.03937i\right)^{0.102} \tag{2.2}$$

$$u_r = 3.378 \ln D + 4.213 \tag{2.3}$$

$$\tan\alpha = u/u_r \tag{2.4}$$

where D is the median raindrop diameter (mm); i is the rainfall intensity (mm h^{-1}); u_r is the terminal fall velocity of raindrops (m s^{-1}) and u is the wind velocity (m s^{-1}). The rainfall inclination angle was calculated at 15-min intervals and the average inclination angle for each rainfall event was computed as the mean of all 15-min values.

2.2.6 Time stability of spatial variability of throughfall

To evaluate the time stability of throughfall patterns, throughfall collected by each throughfall gauge during all rainfall events was normalized using Equation (5) (Keim *et al.*, 2005):

$$\tilde{T} = \frac{T_i - \bar{T}}{SD} \quad (2.5)$$

where $\tilde{T}$ is the normalized throughfall; T_i is the throughfall at a sampling point; $\bar{T}$ is the mean throughfall for all sampling points and *SD* is standard deviation of throughfall for all sampling points.

2.2.7 Data analysis

Data analyses were carried out using statistical software SPSS (version 16.0, SPSS Inc., USA). The Kolmogorov-Smirnov statistic was used to test the normality of mean throughfall distribution (Molina and Del Campo, 2012). Differences in total throughfall among three tree zones were tested by nonparametric tests (Kruskal-Wallis test) because the (transformed) throughfall data were deviated significantly ($p<0.05$) from normal distribution. The spatial variability of gross rainfall, throughfall and stemflow were indicated by the coefficient of variation (*CV*). The relationships between throughfall, stemflow, canopy structure and climate variables were studied by correlation analysis.

2.3 Results

2.3.1 Rainfall characteristics

A rainfall event was defined as a rainfall period from preceding and succeeding rainfall being separated by at least 6 h to entirely dry the wet canopy (Murakami, 2006). A total of 107 rainfall events were thus identified and analyzed. The annual gross rainfall amounted to 1579 mm, which was higher than the long-term mean annual rainfall of 1405 mm. Specifically, the observed wet-season rainfall of 1250 mm was 171 mm greater than usual whereas the dry-season rainfall of 321 mm remained similar to the usual mean of 326 mm. Based on the rainfall amounts, the gross rainfall was divided into five classes: <5 mm, 5-10 mm, 10-20 mm, 20-50 mm and >50 mm (Table 2.1). Most rainfall events were less than 20 mm (80.6% of total events). Small rainfall events (<5 mm) occurred frequently (46.9%

of total events), but their contribution to the annual rainfall was less than 8.0%. Although only 7 heavy storms (>50 mm) were recorded, they accounted for 41.4% of the annual rainfall. The average rainfall intensity during each rainfall event varied from 1.6 to 11.4 mm h^{-1}, with the maximum intensity of 58 mm h^{-1}. Eighty-six percent of rainfall events were accompanied by easterly winds (38% NE and 48% SE) and the rest by NW and SW winds (Figure 2.2). The average wind speed observed during rainfall mainly ranged from 1.5 to 4.0 m s^{-1}, with minimum and maximum wind speeds reaching 0.5 and 11.8 m s^{-1}, respectively. The rainfall inclination angle varied from 5° to 47°, but was dominantly between 10° and 30°, accounting for 78.6% of all sampled events (Figure 2.2).

Table 2.1 Throughfall measured at three tree zones for different rainfall classes (mean ± standard error). Within each rainfall class, values followed by the same letter are not significantly different ($p < 0.05$).

Rainfall classes (mm)	Frequency (%)	Gross rainfall (mm)	Throughfall (mm)		
			West side of trunk	East side of trunk	Midway between tree rows
<5	46.9	118.0	67.6 ± 1.6 a	75.6 ± 1.8 b	50.2 ± 2.2 c
5-10	20.4	165.8	117.6 ± 1.2 a	129.2 ± 4.5 b	94.8 ± 2.8 c
10-20	13.3	202.2	158.1 ± 5.7 a	168.0 ± 1.8 b	130.2 ± 6.5 c
20-50	13.3	440.6	363.5 ± 2.6 a	397.4 ± 5.7 b	314.1 ± 9.4 c
>50	6.2	652.8	560.7 ± 9.5 a	576.2 ± 16.2 a	483.9 ± 18.4 b
All	100.0	1579.4	1267.5 ± 14.9 a	1346.4 ± 24.3 b	1073.3 ± 37.6 c

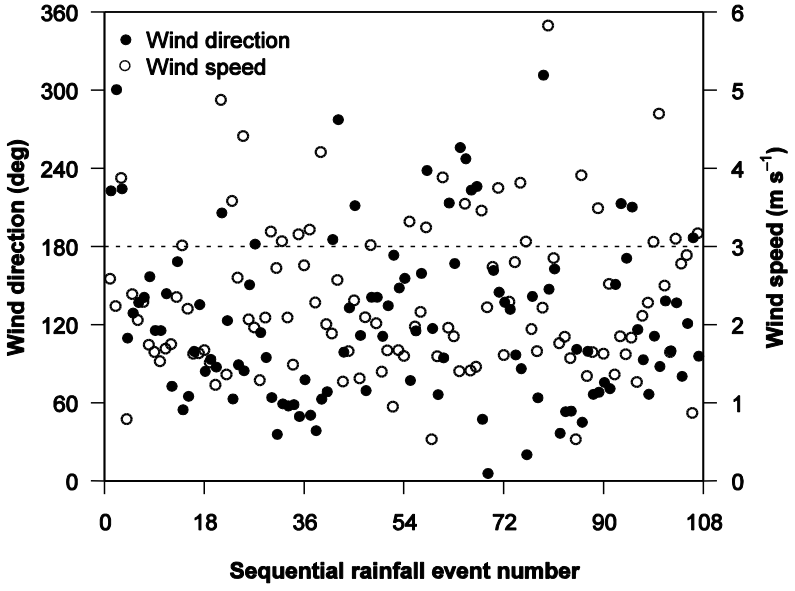

Figure 2.2 Mean wind direction and speed during individual rainfall event.

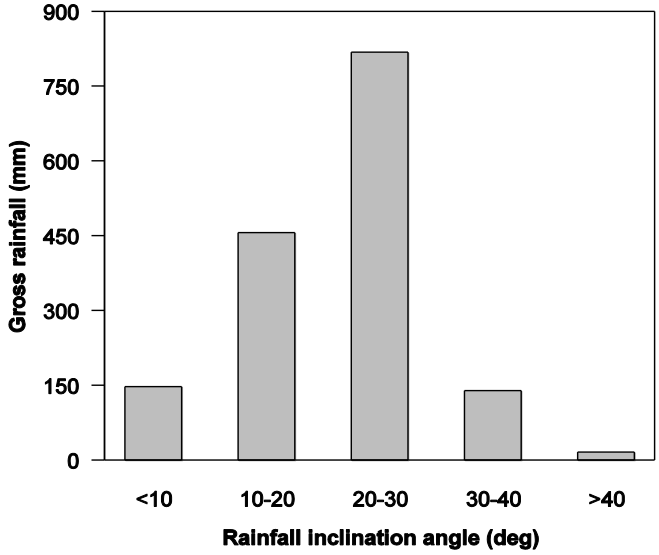

Figure 2.3 Total gross rainfall for different classes of rainfall inclination angle over the study period.

2.3.2 Small-scale variability of gross rainfall

The collected gross rainfall by 16 rain gauges showed a small variability from each other especially for rainfall events >5 mm and the CV_g remained almost constant at 3.5% for these rainfall events (Figure 2.4). The average standard error of mean gross rainfall was estimated at 2.1%, ranging from 3.7% to 1.2% in case of 1 mm and 170 mm rainfall events, respectively. It was thus assumed that gross rainfall was uniformly distributed over the small-scale plot (50 m × 50 m), but the resulting CV_g was incorporated into the analysis of spatial variability of throughfall afterwards.

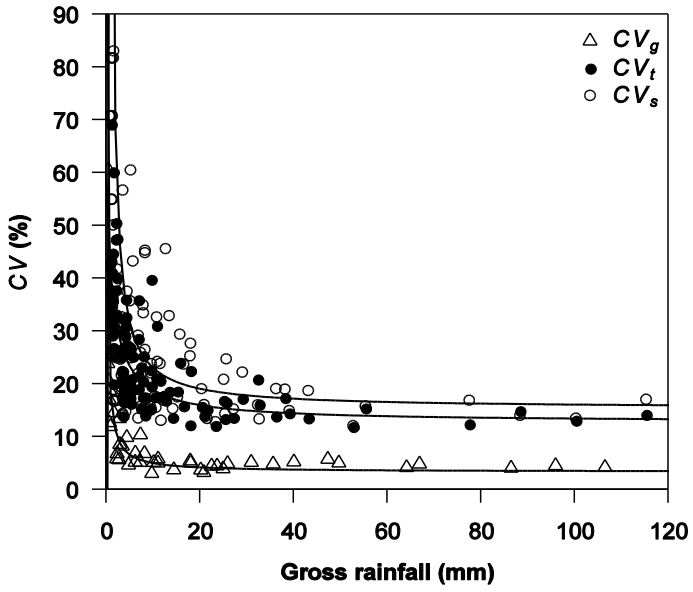

Figure 2.4 Coefficient of variation of gross rainfall (CV_g), throughfall (CV_t) and stemflow (CV_s) against gross rainfall.

2.3.3 Variability of throughfall

A strong and positive linear correlation was revealed between throughfall and gross rainfall (T_f=0.802P_g-1.023, R^2=0.996, n=107, Figure 2.5a). Annual throughfall was 1231 mm, representing 77.9% of the annual gross rainfall of 1579 mm. The relative throughfall (TF_r, expressed as percentage of gross rainfall) ranged from 21% to 85%, averaged 64%, and tended to quasi-constant 81% as gross rainfall increased (Figure 2.5b). The coefficient of variation of throughfall (CV_t) coupled with CV_g was greatly affected by the rainfall amount when gross rainfall was below 10 mm and it was larger among these small rainfall events (mean=40%, range=13%–66%). However, the CV_t decreased down to 20% for gross rainfall of 20 mm, and remained at ~16.5% for greater rainfall events.

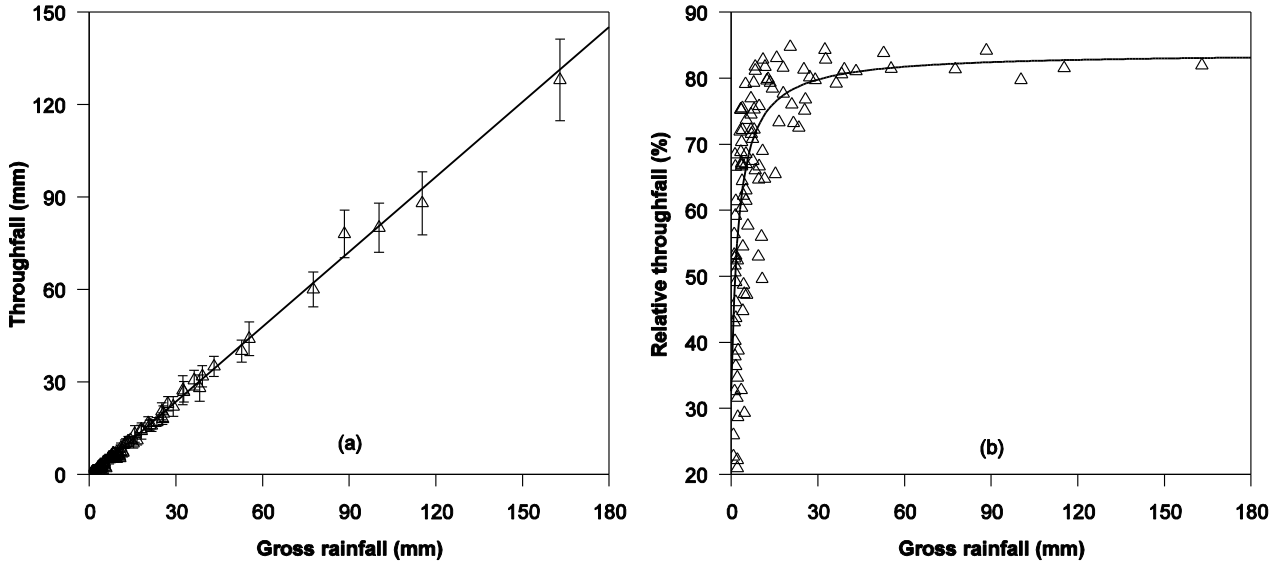

Figure 2.5 (a) Spatially averaged throughfall (mean ± standard deviation) and (b) relative throughfall (expressed as percentage of gross rainfall) as a function of gross rainfall.

Based on the nonparametric tests, significant differences in throughfall among different tree zones were revealed for 93 of 107 rainfall events (p<0.05). The throughfall in the midway between tree rows was the lowest and throughfall on east side of tree trunks was the highest, but this difference was not statistically significant for heavy rainfall events (> 50 mm), especially for throughfall gauges close to tree trunks (Table 2.1). The confidence intervals of estimated throughfall varied from ±6% to ±17% of the mean throughfall, with 89 out of 107 being less than 10% of the estimates, and the confidence interval of the estimated annual throughfall was ±7% of mean annual throughfall.

Throughfall patterns indicated that the distribution of throughfall was heterogeneous but the spatial patterns appeared to be stable among rainfall events (Table 2.1), which was further confirmed by the time stability of spatial variability of throughfall (Figure 2.6). Persistence of higher and lower throughfall was detected close to tree trunks and in the midway between tree rows, respectively. More rainfall was collected on east side of tree trunks than on west side. However, rain gauges in the midway showed slightly lower variability of normalized throughfall than gauges close to tree trunks, indicated by error bars.

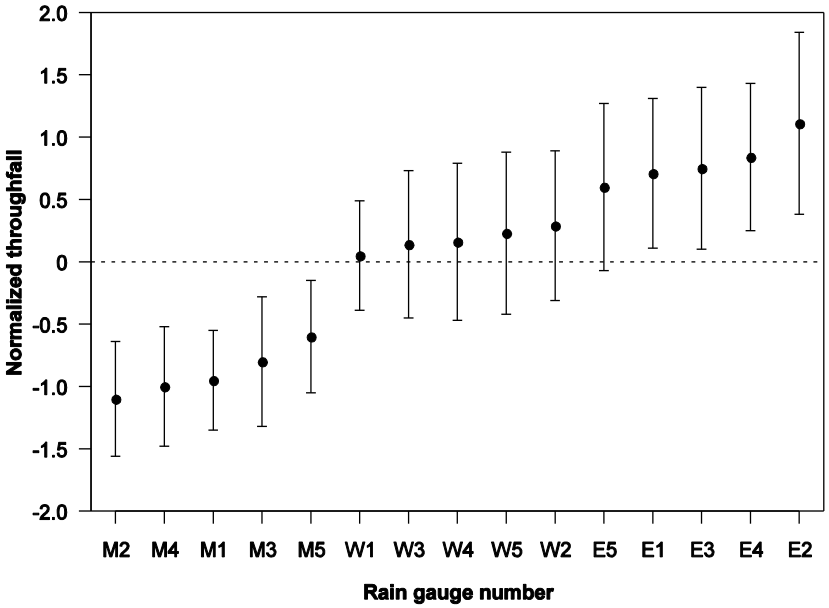

Figure 2.6 Time stability plot of normalized throughfall. The gauges were plotted along the horizontal axis and ranked by mean normalized throughfall and error bars are plus and minus one standard deviation.

The estimated canopy storage capacity above the 15 throughfall gauges based on relationship between throughfall and gross rainfall, ranged between 0.61 mm and 1.67 mm during the study period, with a mean of 1.12 mm. The measured canopy cover within a zenith angle of 7° above the 15 throughfall gauges was on average 57%, ranging from 23% to 91%. The corresponding LAI ranged from 1.22 $m^2 m^{-2}$ to 2.56 $m^2 m^{-2}$, with a plot-average of 1.97 $m^2 m^{-2}$. A negative exponential correlation was revealed between relative throughfall and canopy storage capacity ($TF_r = 115.313e^{-0.283S}$, $R^2 = 0.761$, $n = 15$, Figure 2.7a). However, positive power correlations were found between relative throughfall and LAI ($TF_r = 68.596LAI^{0.332}$, $R^2 = 0.679$, $n = 15$, Figure 2.7b) and canopy cover ($TF_r = 94.234c^{0.178}$, $R^2 = 0.801$, $n = 107$, Figure 2.7c).

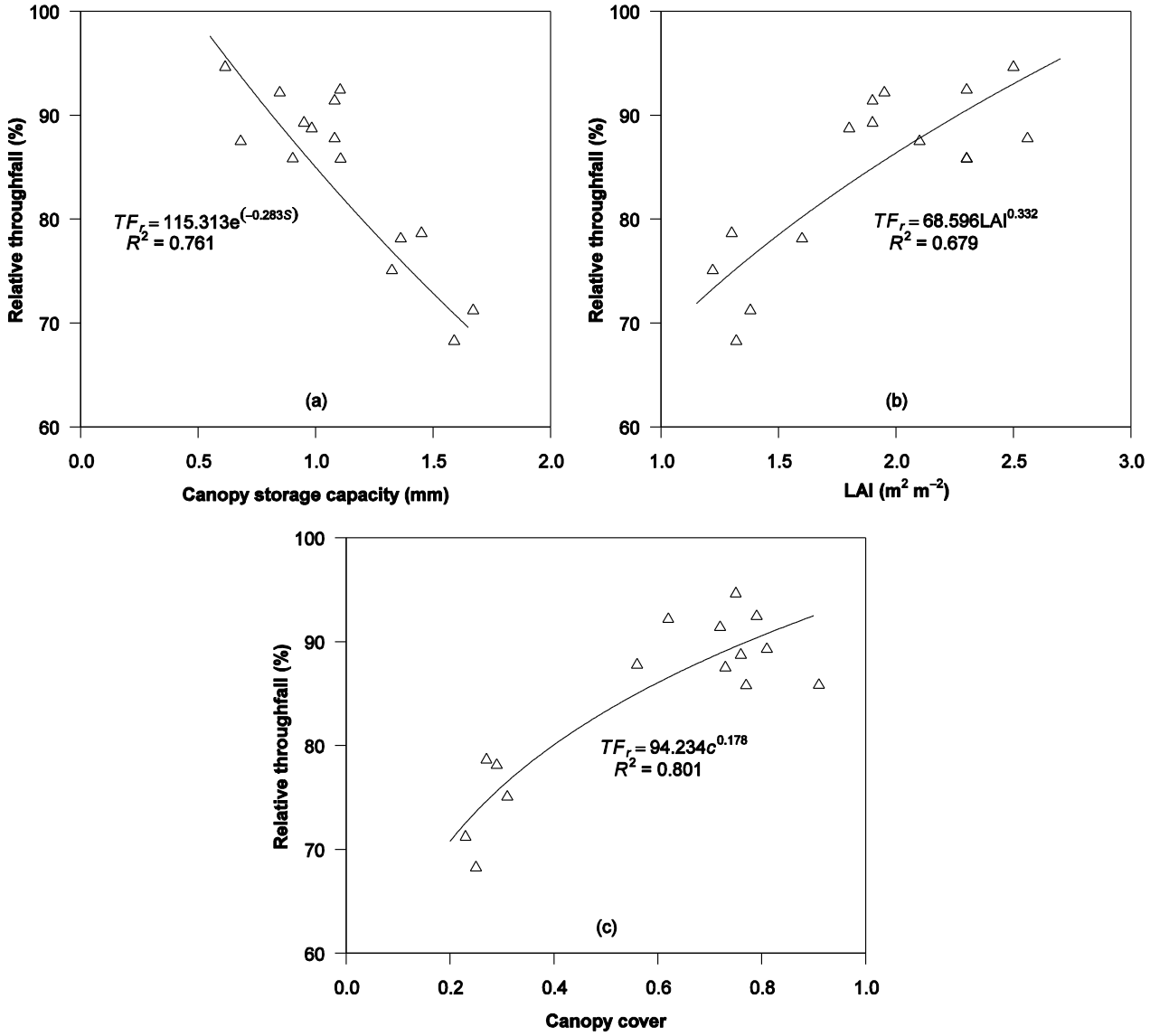

Figure 2.7 Relationships between relative throughfall (TF_r, as percentage of gross rainfall) and (a) canopy storage capacity (S), (b) Leaf area index (LAI), and (c) canopy cover (c).

The wind direction was found to significantly influence the distribution of throughfall within different tree zones (Figure 2.8). The highest throughfall occurred on the windward side of tree trunks. However, throughfall gauges in between tree rows received lowest throughfall under both easterly and westerly wind conditions. No correlation was found for maximum rainfall intensity but a negative relationship was revealed between variability of throughfall and the average rainfall intensity (Figure 2.9). Generally, the coefficient of variation of throughfall tended to decline with increase in rainfall intensity.

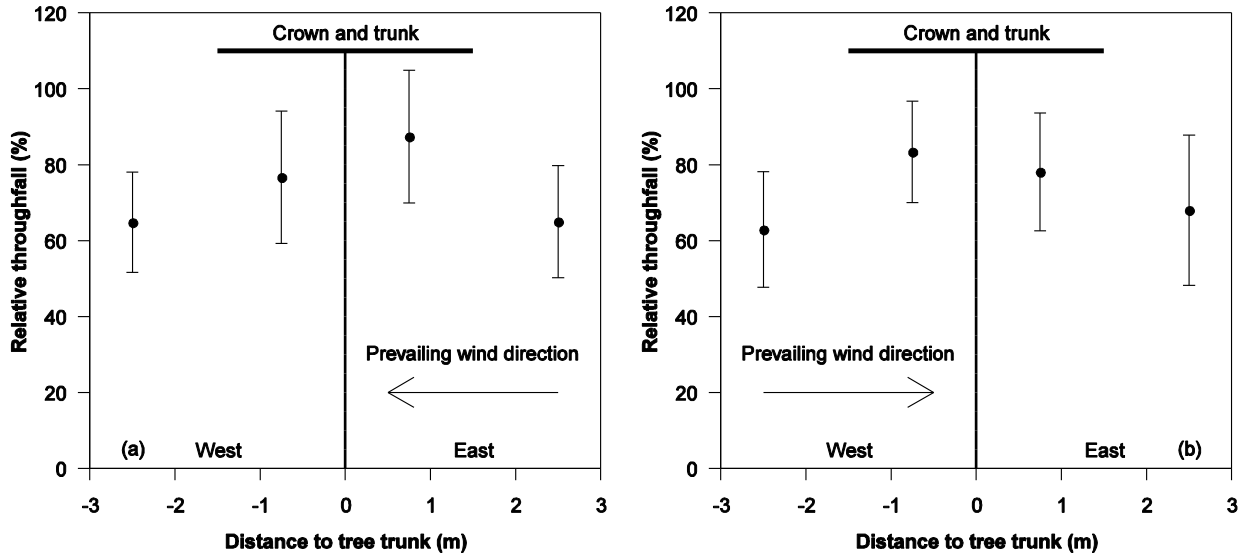

Figure 2.8 Distribution of mean relative throughfall (± standard deviation) within three tree zones: (a) during easterly wind-driven rainfall events (*n*=89); (b) during westerly rainfall events (*n*=18).

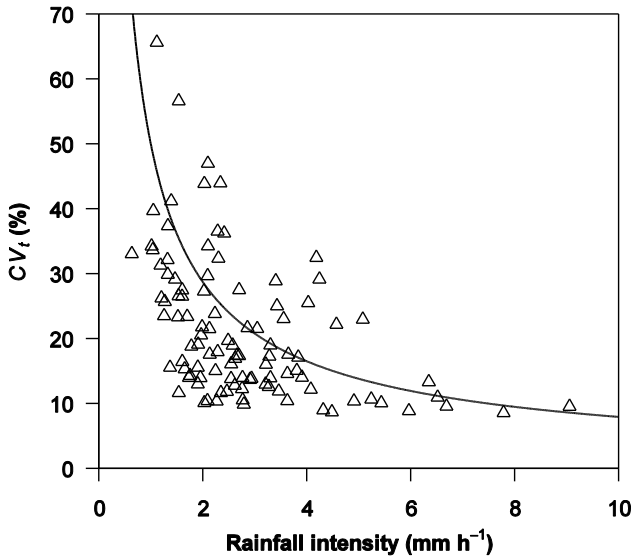

Figure 2.9 Coefficient of variation of throughfall (CV_t) against mean rainfall intensity.

2.3.4 Variability of stemflow

Average annual stand-scale stemflow was 15 mm, accounting for only 1.0% of the annual gross rainfall. Stemflow was well correlated to gross rainfall and increased with increasing gross rainfall (Figure 2.10a). The stemflow was small for rainfall less than 30 mm. For rainfall larger than 50 mm, the stemflow varied from 1.0% to 1.3% of gross rainfall (Figure 2.10b). The coefficient of variation of stemflow (CV_s) among trees greatly depended upon the gross rainfall (Figure 2.4). The average CV_s was 0.46 for rainfall below 5 mm. As

observed for throughfall, the CV_s tended to decline asymptotically to 18% as gross rainfall increased, but the CV_s was higher than CV_t. The higher variability of stemflow caused much larger confidence intervals of estimated stemflow than throughfall (12%–49% of mean stemflow).

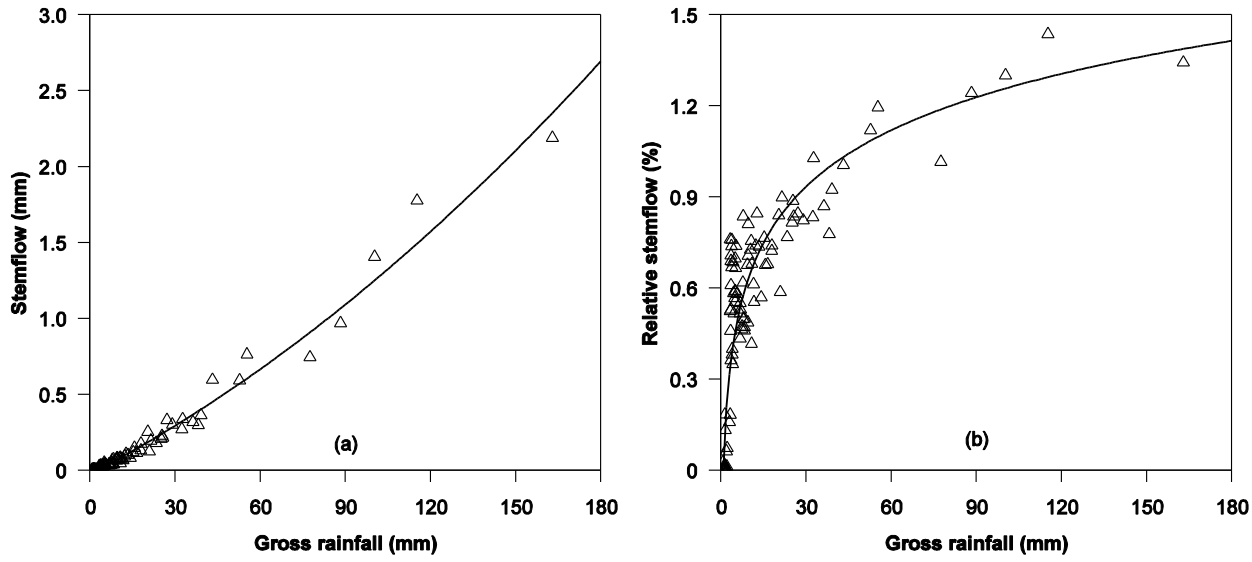

Figure 2.10 (a) Stand-scale stemflow and (b) relative stemflow (expressed as percentage of gross rainfall) as a function of gross rainfall.

The total stemflow volumes (TSV) differed among individual sample trees (Table 2.2). The TSV received by the largest sample tree (tree 6) was 2.5 times larger than that sampled by the smallest sample tree (tree 1). Generally, positive relationships were obtained between volume per mm of rain (SVR) and PCA (SVR = 0.0202 PCA-0.0003, R^2 = 0.77, n=8) and DBH (SVR = 0.0194 DBH-0.2137, R^2 = 0.67, n=8).

Table 2.2 Tree size characteristics, total stemflow volume (TSF) and stemflow volume per mm of rain (SVR). PCA and DBH represent projected crown area and diameter at breast height, respectively.

Tree number	Canopy height (m)	PCA (m^2)	DBH (cm)	TSV (L)	SVR (L mm^{-1})
1	11.5	5.7	15.3	173	0.11
2	12.1	4.5	17.4	186	0.12
3	12.7	9.6	21.4	234	0.15
4	13.5	8.6	21.2	276	0.17
5	12.4	5.7	16.5	135	0.09
6	14.1	11.3	22.3	431	0.27
7	13.4	10.8	20.3	334	0.21
8	13.8	7.1	19.6	258	0.16

2.3.5 Derived rainfall interception loss

Interception loss was estimated by the difference between the measured gross rainfall and net rainfall (throughfall plus stand-scale stemflow). The derived annual interception loss was 333 mm, representing 21.1% of gross rainfall. The interception loss increased as gross rainfall increased, but relative interception loss declined with increasing gross rainfall. Relative interception loss was large (average=64%, range=23%–81%) for rainfall below 5 mm, around 30% for rainfall of 10 mm and was nearly stable (~20%) for heavier rain events (> 30 mm). The total interception loss for rainfall below 5 mm only occupied 13% of the annual interception loss, while that for rainfall > 30 mm accounted for 34% of the annual interception. The confidence intervals of interception loss were averaged at ±31% of the mean interception loss.

2.4 Discussion

2.4.1 Spatial variability of gross rainfall

The assumption of uniform distribution of gross rainfall within the experimental plot is usually applied when investigating the spatial variability of throughfall. The low coefficient of variation (3.5%) and average standard error (2.1%) of gross rainfall in the present study indicated that this assumption could be valid over a small study plot (50 m × 50 m) in subtropical coastal areas. Particularly, the variability of gross rainfall measured at this small scale can be most likely subject to the stochastic errors from tipping-bucket rain gauges (Krajewski et al., 2003). Therefore, the variability of variation resulted from these instrumental errors needs to be considered when analyzing the spatial variability of throughfall.

2.4.2 Spatial variability of throughfall

The minimum number of throughfall gauges (N_{min}) required to estimate throughfall within a preset percentage of mean (E) at 95% confidence interval can be estimated from CV_t following Kimmins (1973):

$$N_{\min} = \frac{z_c^{\,2} \times CV_t^{\,2}}{E^2} \tag{2.6}$$

where z_c is the critical value of the 95% confidence level (approximately 2.0).

To estimate the throughfall within 10% of mean at the 95% confidence interval based on CV_t, the required number of throughfall gauges would be on average 17 (range=4−66) for gross rainfall events > 3 mm. For gross rainfall events < 3 mm, much more throughfall gauges would be required (average=67, range=15−173). The 15 throughfall gauges used in the present study were sufficient to estimate the mean throughfall within the acceptable error limit of 10% for gross rainfall events > 3 mm (mean=±9%) and for the total throughfall over the study period (±7%).

Stationary collectors were found to typically produce higher CV_t than roving collectors (Holwerda et al., 2006; Levia and Frost, 2006). More collectors are thus required to obtain reliable estimates on plot-average throughfall. To minimize the number of gauges for throughfall estimates with high confidence level and low error, periodically relocating the collectors have been adopted (Ritter and Regaldo, 2012). In difficult-to-access areas, collecting troughs with larger sampling area are recommended (Ziegler et al., 2009; Mair and Fares, 2010). However, fixed gauges have to be used, as we did in this study, when focusing on the spatial distribution of throughfall and determining their drivers. Although the layout of throughfall gauges appeared to produce acceptable throughfall estimate in our study, the uncertainty in estimation of stand-scale throughfall resulted from the specific placement of gauges has to be acknowledged. The throughfall gauges were fixed in the center of each tree zone throughout the experiments, which could leave the other locations poorly sampled and thus cause sampling errors on stand-scale throughfall estimation.

The quasi-constant CV_t of ~16.5% appeared lower than generally reported values in non-subtropical pine forests. Gash and Stewart (1977) reported that the variability of throughfall in a Scots pine plantation was around 22% based on 24 roving gauges. Using 40 rain gauges, Zhan et al. (2007) found CV_t remained at 18% in a Chinese pine plantation. Similarly, Loustau et al. (1992) found the CV_t to be around 19% in a maritime pine stand using 52 fixed gauges. However, the present result was higher than the findings by Llorens et al. (1997) in a Mediterranean mountainous *Pinus sylvestris* forest, where a lower steady CV_t of 6% was revealed. In the above studies, number and type of rain gauges, forest and rainfall characteristics were different from this study. The lower canopy cover and higher canopy openness in this studied young pine plantation may reduce potential drip points and hence produced less spatial variability in throughfall (Carlyle-Moses et al., 2004). Besides, the lower variability of throughfall may be ascribed to relative high rainfall intensity from summer storms in the humid subtropical areas where the canopy was

saturated in a short time (Zhan et al., 2007). Finally, the lower variability of throughfall could be caused by the limited sampling points of throughfall, as discussed above.

Time stability analyses confirmed the persistence of higher relative throughfall close to the pine trees and lower relative throughfall in the midway between tree rows among rainfall events. In contrast, Whelan et al. (1998) found less throughfall close to the spruce trunks, while Loustau et al. (1992) found the throughfall in between pine trees was the highest for light rainfall but the lowest for heavy rainfall events. Keim et al. (2005) reported higher throughfall close to tree trunks in young coniferous forests, but lower throughfall occurred close to trunks in old stands of conifers, which was attributed to the difference in tree structure.

The average *S* of 1.12 mm determined with the regression method compared favorably with observed values in coniferous forests, ranging from 0.3 mm to 3.0 mm (Llorens and Gallart, 2000). However, the negative relationship between *S* and LAI indicates that estimated *S* values for the canopy above the individual throughfall collectors were modified by the winds. In general, relative throughfall decreases with increase in LAI and canopy cover (Molina and Del Campo, 2012). However, our results revealed the opposite tendency, which indicates that the meteorological variables had a greater effect on the spatial viability of throughfall than did the canopy structure.

Intense and wind-driven rainfall events occur frequently in subtropical coastal areas. As reported by earlier studies, the variability of throughfall decreases with increasing rainfall intensity. As we found in this study, the windward canopy intercepted more rainfall than the leeward canopy and throughfall in between trees was the lowest at all times (Figure 2-8), which can be largely explained by the rain shadow effects. This further supports our conclusion that spatial distribution of throughfall is mainly controlled by meteorological conditions. Wind-driven rainfall is always inclined from a vertical pathway (Ford and Deans, 1978; Herwitz and Slye, 1995). The tree crowns probably create lateral rain shadowing effects on the leeward side and midway areas between tree rows. Only part of the inclined rainfall passes directly through small gaps in the canopy and falls in the shadowed midway areas as free throughfall, but the intercepted rainfall will drip down under canopy as released throughfall or evaporate to the atmosphere as interception loss. The dominant wind during the study period blew from east to west (86%), which caused slightly higher throughfall on the east side of tree canopy.

2.4.3 Spatial variability of stemflow

Stand-scale stemflow accounted for only a small percentage (1.0%) of gross rainfall, which was similar to the quantified values by other authors, e.g. 1.3% by Llorens et al. (1997), 1.4% by Shachnovich et al. (2008) and 0.88% by Shi et al. (2010). The low stemflow fraction was expected because of the low stem density and rough bark in our pine forests. Compared to throughfall, the stand-scale stemflow was considerably small, which would underestimate the actual stemflow input per unit area because stemflow only concentrates within a small area around tree trunks instead of the stand area (Levia and Frost, 2003). The concentrated stemflow are important inputs of water and nutrients to the soils. Liang et al. (2007, 2009), for example, has presented a coupled mechanism termed “double-funneling”, which led to a stemflow-induced preferential infiltration process along root pathways. Silva and Rodriquez (2001) have reported stemflow concentrations were enriched with leaching nutrients of C_u, F_e, M_n, and Z_n compared with gross rainfall concentrations in a pine forest (*Pinus pseudostrobus Lindl.*). Apparently, the effects of stemflow serving as highly localized inputs of rainfall on the spatial distributions of soil water and solutes in forested ecosystems cannot be ignored.

Total stemflow volumes among individual trees were different from each other. Variability of stemflow within the same tree species is commonly resulted from the differences in canopy size and tree architecture (Levia and Frost, 2003). The positive relationship between SVR and PCA and DBH showed that stemflow generation generally increased with increase in crown and stem sizes, which indicates the variability of stemflow among trees was mainly attributed to differences in tree size. However, the small sample size (eight trees) and relatively low coefficient of determination suggests that this conclusion has to be treated with a degree of caution. That’s because the difference in stemflow yields can be also due to architectural variables not measured in our study, e.g. branch angles and flow path obstructions (Ford and Deans, 1978). However, this study supported the findings by Llorens et al. (1997) that indicates tree size does affect stemflow yields. More trees should be studied in the future to confirm the conclusion and investigate the effect of tree architecture on stemflow production.

2.4.4 Interception loss estimation

Interception loss by the pine plantation as measured in the present study (21.1% of gross rainfall) was in the low range of observed values in other coniferous forests, mainly

ranging from 20%–40% (Carlyle-Moses, 2004; Komatsu et al., 2010), which was possibly due to the low canopy coverage and leaf area index in the young pine plantation. The relative error for the interception loss estimate was high due to the sampling errors on throughfall and stemflow. Since stemflow was relatively small, the major errors were considered from the throughfall measurements (Llorens et al., 1997). To reduce the confidence interval on the interception estimate to below 10%, it would require an increase in sample size of between three- to four-fold of throughfall rain gauges, especially for small rainfall events. Instead of employing a large number of rain gauges to integrate the variability of throughfall and minimize the sample errors, rovers or troughs are two feasible options to apply as suggested before. Compared to broadleaf forests, conifers generally produce higher rainfall interception losses mainly due to their higher canopy storage capacity (Carlyle-Moses, 2004), which indicate the conversions from native forests to commercial pine plantations may result in a reduction in the soil water availability of these forested ecosystems.

2.5 Conclusions

As presented in this work, annual gross rainfall in the subtropical pine plantation was partitioned as follows: 77.9% throughfall, 1.0% stemflow, and 21.1% interception loss. The spatial variability of gross rainfall over a small plot (50 m × 50 m) in subtropical coastal areas was found minimal. Throughfall proved to be spatially heterogeneous but the spatial patterns persisted among most individual rainfall events. Interception of inclined rainfall by tree crowns appeared to be the main driver of the spatial patterns of throughfall and nearly single prevailing wind direction caused stability of these patterns. The total stemflow volumes per tree were variable. The variability of stemflow was more related to the tree size (canopy area and stem diameter) than meteorological variables. This research suggests that the spatial variability of throughfall and stemflow in the subtropical pine plantation is sensitive to meteorological variables and canopy structure, respectively.

Chapter 3. Measuring and Modelling Rainfall Interception Losses by a Native Banksia Woodland and an Exotic Pine Plantation in Subtropical Coastal Australia

3.1 Introduction

Quantifying the amount of rainfall interception loss by tree canopies can be of considerable importance for the hydrological budgets of forested catchments (Whelan and Anderson, 1996). Previous investigations have demonstrated that the canopy interception loss generally represents 9%–36% of gross rainfall (Hörmann et al., 1996; Roth et al., 2007; Levia et al., 2011), while it has been estimated at up to 48% of gross rainfall for some coniferous forests (Rutter et al., 1975). Rainfall interception loss is largely dependent on the forest structure, rainfall characteristics and climatic variables governing the evaporation rates during and after rainfall events (Muzylo et al., 2009).

Interception loss (E_i) is usually quantified by the difference between measured gross rainfall (P_g) and net rainfall (P_n), defined as throughfall (T_f) plus stemflow (S_f). To predict interception losses using readily available meteorological variables, researchers have developed more than 15 physically-based rainfall interception models. Muzylo et al. (2009) compared these models and found the original and revised Gash's analytical models to be the most commonly employed. The revised Gash's analytical model (RGAM) was reformulated from the original model to predict E_i for sparse forests (Gash, 1979; Gash et al., 1995; Valente et al., 1997). Hörmann et al. (1996) developed a dynamic model of wind controlled canopy interception capacity (WiMo) in a coastal area of Germany which takes into account the effect of wind on canopy storage capacity, a factor that can be of importance in areas dominated by wind-driven rainfall.

The RGAM model has been extensively applied over various climate types around the world, *e.g.*, Mediterranean climate (Valente et al., 1997; Aboal et al., 1999; Šraj et al., 2008), continental climate (Carlyle-Moses and Price, 1999; Price and Carlyle-Moses, 2003), tropical monsoon and montane climates (Asdak et al., 1998; Van Dijk and Bruijnzeel, 2001; Cuartas et al., 2007; Wallace and McJannet, 2008). Compared to the RGAM model, few studies have evaluated the WiMo model for interception predictions in windy areas (Hörmann et al., 1996; Klingaman et al., 2007). Ghimire et al. (2012) applied the RGAM model to two forests under the subtropical monsoonal montane conditions of Central Nepal and demonstrated the modeled results corresponded well with actual values when the optimized wet-canopy evaporation rate was used. Klingaman et al. (2007)

compared three interception models for a leafless deciduous forest in the eastern United States and found the WiMo model performed better than the RGAM model. The RGAM and WiMo models, however, have not yet been applied under subtropical coastal forests and have seldom been compared against each other.

In subtropical Australia, as in many other regions and countries, exotic pine species have been largely planted for timber production (Kanowski et al., 2005), particularly in the natural distribution areas of native tree species like banksia. The changes in vegetation in these areas can potentially affect the local hydrological processes. For example, Swank and Douglass (1974) reported annual streamflow was greatly reduced (20%) by converting a mature deciduous hardwood to white pine. Bosch and Hewlett (1982) reviewed 94 catchment experiments and found pine forests caused higher change in water yield (40 mm) than deciduous hardwood (25 mm) per 10% change in vegetation cover. Ford et al. (2011) revealed annual evapotranspiration (interception plus transpiration) by planted pine stands doubled the value of hardwood stands.

The objectives of this research are to: (1) measure and compare E_i in a banksia woodland and a pine plantation located in subtropical coastal Australia, (2) explore the underlying causes of differences in E_i between the native and exotic forests, (3) calibrate and validate the RGAM and WiMo models for both forest stands, compare the predicted and measured E_i, and (4) assess the canopy and climatic parameters required to apply the models.

3.2 Materials and methods

3.2.1 Study area

The study plots are located in the commercial State Forest on Bribie Island (Figure 1.1). A detailed site description is presented in the overview of study sites in Chapter 1. The leaf area index (LAI) measured using a LAI-2000 plant canopy analyzer (LI-COR, Lincoln, USA) was on average 2.33 m^2 m^{-2} for BW and 2.05 m^2 m^{-2} for PP. The LAI changed seasonally from 2.13 m^2 m^{-2} in winter to 2.48 m^2 m^{-2} in summer for BW and from 1.87 m^2 m^{-2} to 2.16 m^2 m^{-2} for PP, indicating small seasonal variations. The other forest structural features are illustrated in Table 3.1.

Table 3.1 Forest structural characteristics of banksia woodland (BW) and pine plantation (PP).

Forest type	Stem density (tree ha^{-1})	DBH [a] (m)	Basal area (m^2 ha^{-1})	LAI [a] (m^2 m^{-2})	Canopy height [a] (m)	Crown diameter [a] (m)
BW	371	0.30±0.05	21.32	2.33±0.14	6.82±0.28	7.44±0.54
PP	840	0.21±0.02	23.65	2.05±0.08	13.34±0.41	3.56±0.36

[a] Data are given as mean ± standard deviation (n=25). LAI denotes leaf area index and DBH diameter at breast height.

3.2.2 Collection of gross rainfall, throughfall and stemflow

From 1 May 2012 to 30 April 2013, the measurements of P_g, T_f and S_f were conducted simultaneously for both forest stands. The P_g was measured using two HOBO RG3 tipping-bucket rain gauges (177 cm^2 orifice, Onset Computer Corp., Bourne, USA) and positioned at 0.5 m above the ground to avoid rain splash and prevent damage by animals. One rain gauge was situated in the middle of a 30 m wide track that borders the pine stands. The horizontal angle between the rain gauge and the top of the nearest trees was smaller than 45°, so little disturbance on gross rainfall measurement was caused by its surrounding environment (Asdak et al., 1998). The other rain gauge was located in a nearby well-exposed clearing next to the banksia woodland. All the tipping-bucket rain gauges used in this study were calibrated to 0.2 mm per tip in the lab and recalibrated after deployments in the field every three months to ensure the accuracy of the rain gauges (Llorens et al., 1997). The bucket tipping time and numbers were automatically recorded by a self-constructed datalogger. The raw tip-time data were further converted into 15-min rain rates to coincide with the weather station data.

The T_f was sampled under and between trees in the pine plantation using 15 rain gauges identical to those used for gross rainfall measurements. In the banksia woodland, the T_f was collected using 16 U-shaped troughs connecting to 8 Hobo tipping-bucket rain gauges. The troughs were made of split UPVC pipes, 1.0 m long by 0.1 m wide and randomly located within the plot. The collection troughs with larger collecting areas were used to integrate the spatial variability of T_f and reduce the sampling error (Limousin et al., 2008), since the BW plot was more heterogeneous than the PP plot. The S_f was measured on eight representative pine trees (0.15 m < DBH < 0.30 m) and on six banksia trees (0.20 m < DBH < 0.40 m). The S_f was collected using spiral-type stemflow collars constructed from wired rubber. Each stemflow collar was fixed around the tree trunk and sealed with silicon sealant. The collected stemflow was diverted to a HOBO tipping-bucket rain gauge using a

rubber hose with 2.5 cm in diameter. Following Hanchi and Rapp (1997), the tree-level S_f was upscaled to the stand-level S_f for both forest stands using Equation (3.1):

$$S_f = \sum_{i=1}^{n} \frac{S_n \cdot m}{A \cdot 10^4} \quad (3.1)$$

where S_f is the upscaled stemflow depth (mm) for a specified stand area of A (m^2), n the number of DBH classes, and S_n the average stemflow volume (ml) collected from m trees in the DBH class.

3.2.3 Meteorological instruments

Meteorological variables were observed from an automatic weather station mounted on a 15-meter-high mast (~1.5 m above the pine canopy) in the center of the PP plot. Air temperature (T, ℃) and relative humidity (RH, %) were measured with an HMP155 sensor (Vaisala, Vantaa, Finland). Wind speed (WS, m s^{-1}) and direction (WD, deg) were measured by a wind sentry set (model 03002, RM Young, Michigan, USA). A CNR4 net radiometer was deployed to measure net radiation (R_n, W m^{-2}) (Kipp & Zonen, Delft, The Netherlands). Two HFP01 soil heat flux plates (Hukseflux, Delft, The Netherlands) were buried at 5 cm depth to measure soil heat flux (G, W m^{-2}). Meteorological data were automatically sampled at 5-min intervals and recorded at 15-min intervals by a CR3000 datalogger (Campbell Scientific, Logan, USA).

3.2.4 Model descriptions

3.2.4.1 The RGAM Model

The RGAM model was used to model interception losses based on a series of individual rainfall events, with enough time to completely dry the tree canopy between two successive events (Gash, 1979). The model requires canopy and climatic parameters for interception calculations, which include the canopy storage capacity (S), canopy cover (c, assumed to be one minus free throughfall coefficient p), rainfall fraction converted to stemflow (p_t), trunk storage capacity (S_t), mean rainfall intensity ($\overline{R}$) and mean evaporation rate ($\overline{E}$) during rainfall. The amounts of rainwater needed to entirely saturate the canopy (P_g') and the trunk (P_t') were calculated using Equations (3.2) and (3.3), respectively:

$$P_g' = -\overline{R}/\overline{E}_c \, S_c \ln(1-\overline{E}_c/\overline{R}) \quad (3.2)$$

$$P_t' = S_t / p_t \tag{3.3}$$

where S_c is the canopy storage capacity per unit area of canopy cover, calculated as $S_c = S/c$, and $\overline{E}_C$ is the mean evaporation rate during rainfall upscaled to canopy cover, defined as $\overline{E}_C = \overline{E}$ /c.

The RGAM model distinguishes three sequential phases, i.e., a wetting-up phase, a saturating phase during rainfall, and a drying-out phase after rainfall. Evaporative losses from the canopy take place during each phase and the total interception for a given event is obtained as the sum of different components listed in Table 3.2 (Gash et al., 1995).

Table 3.2 Components of interception in the revised Gash's analytical model.

Components of interception	Equation
1. For *m* rainfall events $P_g<P_g'$	
(1) Evaporation from unsaturated canopy	$c\sum_{j=1}^{m} P_{g,j}$
2. For *n* rainfall events $P_g>P_g'$	
(2) Wetting up the canopy	$nc\left(P_g' - S_c\right)$
(3) Wet canopy evaporation during rainfall	$c\overline{E_c}/\overline{R}\sum_{j=1}^{n}\left(P_{g,j} - P_g'\right)$
(4) Evaporation after rainfall ceases	ncS_c
(5) Evaporation from trunks for *q* events, which saturate the trunks ($P_g>P_t'$)	$qS_t + P_t\sum_{j=1}^{n-q} P_{g,j}$

3.2.4.2 The WiMo model

The WiMo model incorporates a dynamic *S* based on the maximum wind speed (u_{max}) during each rainfall event. The E_i is calculated using a bucket model at hourly time steps as shown in Table 3.3 (Hörmann et al., 1996). The rainfall (P_g^i) falling on leaves is added to the canopy storage content of last hour (C_{i-1}) and actual evaporation (E_a^i) is subtracted from the canopy until *S* is empty. The throughfall (T_f^i) is calculated as the difference of hourly water balance (WB_i) and canopy storage content (C_i) when WB_i exceeds C_i.

Table 3.3 Algorithm used in the WiMo model to calculate throughfall for time step *i*.

Parameter	Equation
Maximum wind speed (u_{max})	Input
Rainfall (P_g)	Input
Actual evaporation (E_a)	Input
Canopy storage capacity (S)	S=f(u_{max})
Water balance (WB)	Max(P_g^i +C_{i-1}- E_a^i , 0)
Throughfall (T_f)	If WB_i>C_i then WB_i-C_i, else 0
Canopy storage content (C)	If WB_i>C_i then C_i, else WB_i

3.2.5 Estimation of model parameters

3.2.5.1 Canopy parameters

Following Wallace and McJannet (2006), the S values for BW and PP were obtained as the negative intercept of linear regression between P_g and P_n,. The p values were derived as the slope of the linear regression of T_f against P_g for small rainfall events that were insufficient to exceed S (Jackson, 1975). The trunk parameters p_t and S_t were estimated by the method of Gash and Morton (1978), as the slope and negative intercept of the linear regression of S_f and P_g, respectively.

3.2.5.2 Mean rainfall intensity

The individual rainfall events in this study were separated by at least 6 h without rainfall to allow the tree canopy to be completely dried before the next rainfall (Murakami, 2006). The mean rainfall intensity ($\overline{R}$) during rainfall was calculated as the arithmetic mean of the individual event rainfall intensities or as the median value when rainfall intensity was not normally distributed. Small rainfall events less than 2 mm were, however, removed from the analysis of mean rainfall intensity because it was difficult to accurately determine their durations (Wallace and McJannet, 2006).

3.2.5.3 Mean wet-canopy evaporation rate

The mean evaporation rate ($\overline{E}$) from the wet canopy during rainfall was derived using three approaches. First, the evaporation rate ($\overline{E}_{PM}$) was estimated using Penman-Monteith (PM) equation (Monteith, 1965), assuming canopy resistance r_c =0:

$$\overline{E}_{MP} = \frac{\Delta R_n - G + \rho_a c_p D / r_a}{\lambda\Delta + \gamma} \quad (3.4)$$

where Δ is the slope of the saturation vapor pressure against temperature curve (kPa K^{-1}), R_n the net radiation at the canopy surface (W m^{-2}), ρ_a the air density (kg m^{-3}), G the soil heat flux (W m^{-2}), c_p the specific heat of the air (J kg^{-1} K^{-1}), D the vapor pressure deficit (kPa), λ the latent heat of vaporization of water (kPa K^{-1}), γ the psychometric constant (J kg^{-1}), and r_a the aerodynamic resistance (s m^{-1}), which is calculated by the logarithmic boundary layer equation for neutral stability conditions (Allen et al., 1998):

$$r_a = \frac{\ln\left[(z_u - d)/z_{om}\right]\ln\left[(z_e - d)/z_{ov}\right]}{k^2 u} \tag{3.5}$$

where u is the wind speed (m s^{-1}), z_u the height at which the wind speed was measured (m), z_e the height of the relative humidity instrument (m), d the zero plane displacement height (m), z_{om} the roughness height controlling momentum (m), z_{ov} the roughness height controlling transfer of vapor and heat (m), and k von Karman's constant (0.41).

Usually, d and z_{om} are estimated from the average canopy height h_c . For forest stands in this study, it is assumed that $d=0.7h_c$, $z_{om}=0.1h_c$ and $z_{ov}=0.5z_{om}$ (Brutsaert, 1979; Verseghy et al., 1993). The $\overline{E}_{PM}$ was then determined as the arithmetic mean of evaporation rates calculated for individual rainfall events using PM equation. The mean wet-canopy evaporation rate ($\overline{E}_{TF}$) was also determined from the value of $\overline{E}/\overline{R}$ as obtained from the linear regression of P_g against observed E_i. The mean evaporation rate ($\overline{E}_O$) was finally optimized by minimizing the root mean square error (RMSE) between paired simulated and observed E_i for all rainfall events.

3.2.5.4 Relationship between canopy storage capacity and maximum wind speed

The S for each rainfall event as a function of u_{max} was derived by the regression of the optimum canopy storage capacity (S_o) and u_{max}. To obtain the S_o for each rainfall event, a bucket model that calculates T_f^i at each hourly time step was used:

$$T_f^i = \begin{cases} cP_g^i & if\ C_i \le S \\ cP_g^i + C_i - S & if\ C_i > S \end{cases} \tag{3.6}$$

where C_i is

$$C_i = C_{i-1} + P_g^i - E_a^i \tag{3.7}$$

The C_i was reset to S at the end of the time step when it exceeded S.

A MATLAB program was used to find S_o for each rainfall event by running the bucket model from 0 mm and 3.0 mm. The S was optimized to yield the minimum RMSE between the modeled and measured T_f^i . Paired S_o and u_{max} from 15-minute meteorological observations for each rainfall event were fitted to generate a regression equation.

3.3 Results

3.3.1 Rainfall characteristics

The average relative error between two gross rainfall measurements was only 2.6%, so it is assumed that the spatial variability of gross rainfall over the study area was negligible and the average value was used as gross rainfall. Over the study period, 102 discrete rainfall events produced 1492.1 mm of annual gross rainfall, with 71.3% and 28.7% of gross rainfall occurring during the wet season and dry season, respectively. However, the frequency distributions of rainfall amount and intensity were similar between the wet and dry seasons (Figure 3.1). Small rainfall events (<5 mm) occurred much more frequently than heavier rainfall, especially during the dry season (Figure 3.1a). Average event rainfall intensities varied from 0.4 to 10.8 mm h^{-1}, with the maximum 15-min intensity reaching 58 mm h^{-1}. Rainfall events with intensity lower than 2 mm h^{-1} accounted for 30% of total rainfall, while 50% of rainfall intensities lay between 2 and 4 mm h^{-1} (Figure 3.3b). Since the distribution of rainfall intensity data deviated from normal distribution, the median rainfall intensity was thus used to estimate E_i.

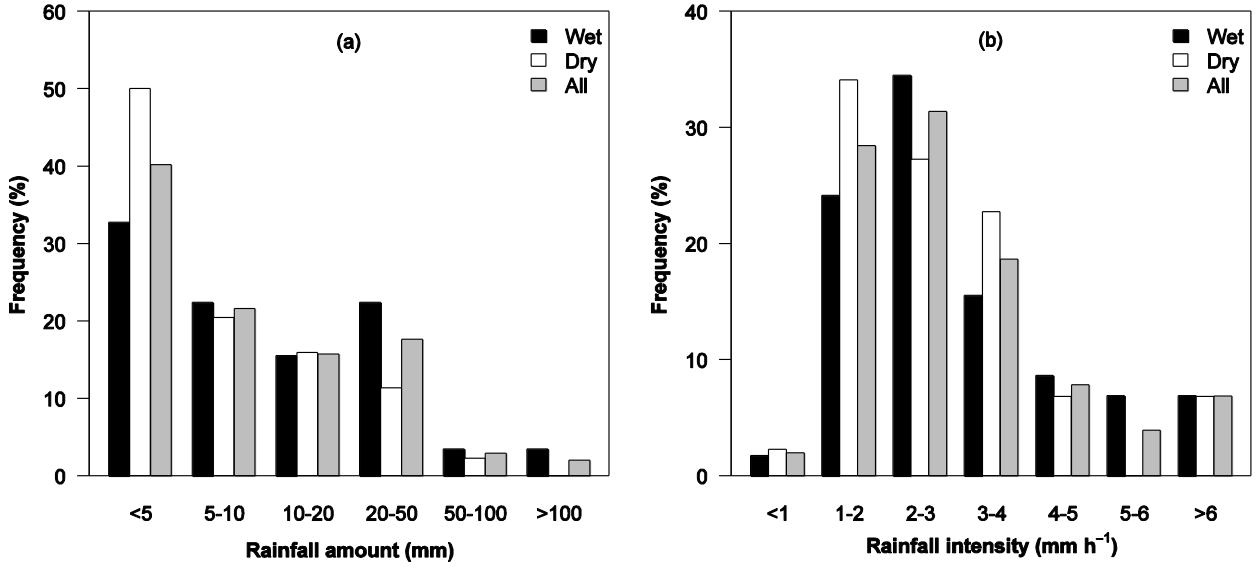

Figure 3.1 Frequency distributions of (a) rainfall amount and (b) rainfall intensity over the wet season (n=59), dry season (n=43) and entire year (n=102).

3.3.2 Throughfall, stemflow and interception loss

The measured annual T_f amounted to 1241.3 mm for BW and 1135.0 mm for PP, which accounted for 83.2% and 76.1% of P_g, respectively (Table 3.4). The average standard errors of mean T_f for individual events were 8.6% and 13.1% for BW and PP, respectively. The stand-level estimate of annual S_f for BW was only 0.4 % of P_g, while S_f for PP was slightly higher, estimated at 1.0% of P_g. The standard errors of the S_f estimates were much higher, 28.7% for BW and 20.4% for PP. By subtracting T_f and S_f from P_g, the annual E_i were estimated to be 245.0 mm for BW and 342.8 mm for PP, which accounted for 16.4% and 22.9% of P_g, respectively. The average standard errors of the E_i for individual events, which were calculated as the root sum of the variances of T_f and S_f, were 14.5% for BW and 17.8% for PP. The percentage of canopy interception was higher during the dry season than that during the wet season for both forest stands.

Table 3.4 Measured seasonal and annual gross rainfall, throughfall, stemflow, and interception losses for banksia woodland (BW) and pine plantation (PP).

Forest type	Season	Gross rainfall (mm)	Mean rainfall intensity (mm h^{-1})	Median rainfall intensity (mm h^{-1})	Throughfall (mm)	Stemflow (mm)	Interception (mm)
BW	Wet season	1063.4	3.25	2.76	898.2 (84.5%)	3.8 (0.4%)	161.4 (15.2%)
	Dry season	428.7	2.72	2.52	343.1 (80.0%)	2.0 (0.5%)	83.6 (19.5%)
	Annual	1492.1	3.02	2.62	1241.3 (83.2%)	5.8 (0.4%)	245.0 (16.4%)
PP	Wet season	1063.4	3.25	2.76	833.1 (78.3%)	10.6 (1.0%)	219.7 (20.7%)
	Dry season	428.7	2.72	2.52	301.9 (70.4%)	3.7 (0.9%)	123.1 (28.7%)
	Annual	1492.1	3.02	2.62	1134.9 (76.1%)	14.3 (1.0%)	342.8 (22.9%)

Values in parentheses are the percentage to corresponding gross rainfall.

3.3.3 Derived model parameters

3.3.3.1 Canopy parameters

The derivation of the average canopy parameters during wet season for both forest stands is presented in Figure 3.2. The following canopy parameters were determined for BW and PP, respectively: canopy storage capacity (S), 0.45 and 1.31 mm; free throughfall fraction

(*p*), 0.52 and 0.47, and thus canopy coverage (*c*), 0.48 and 0.53. The fraction of rainfall contributing to stemflow (p_t) and the trunk storage capacity (S_t) were obtained at 0.005 and 0.021 mm for BW, and at 0.014 and 0.066 mm for PP.

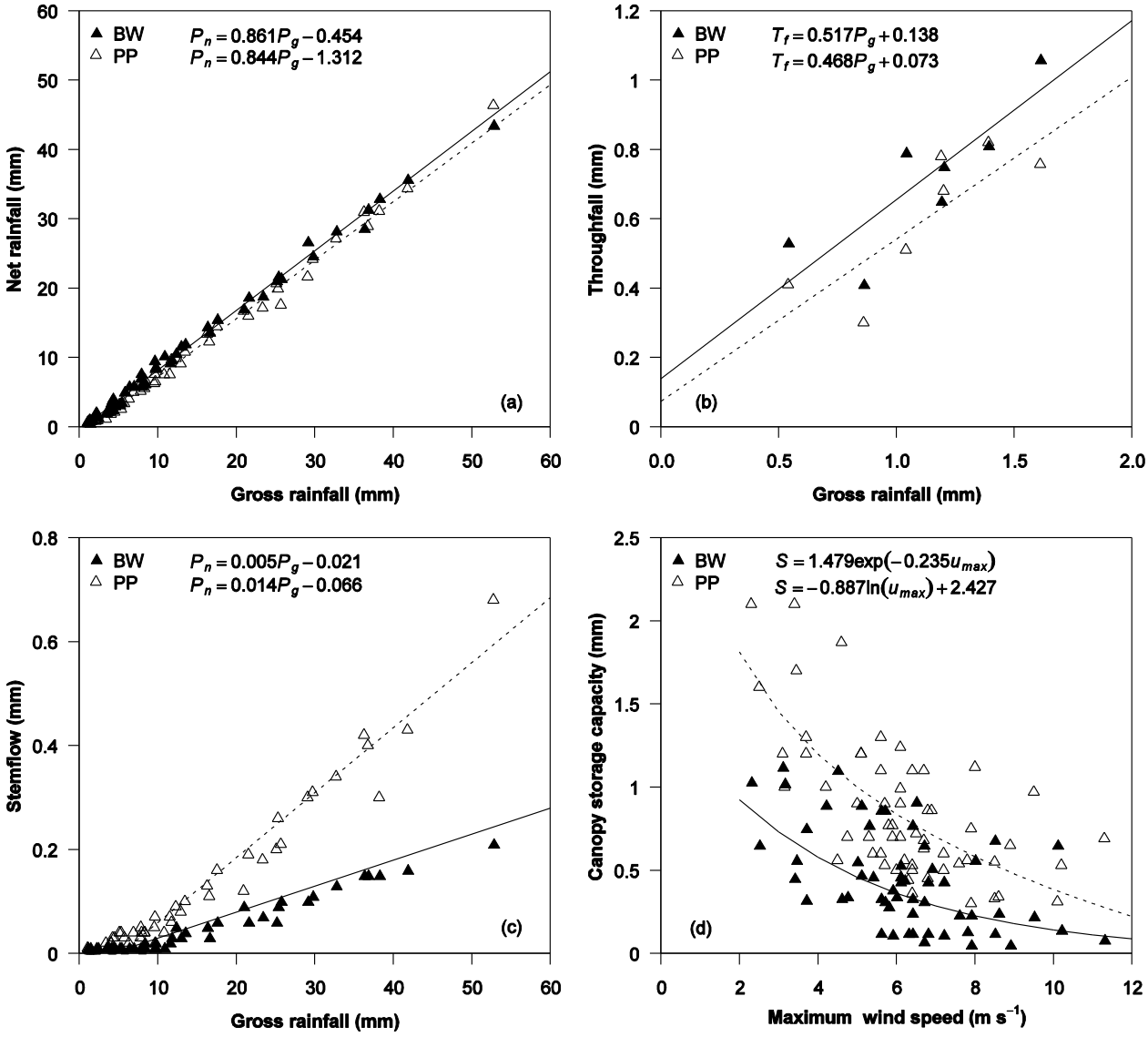

Figure 3.2 Estimation of (a) canopy storage capacity (*S*), (b) coefficient of free throughfall *p*, (c) the stemflow fraction (p_t) and trunk storage capacity (S_t), and (d) canopy storage capacity (*S*) as a function of maximum wind speed (u_{max}) for banksia woodland (BW) and pine plantation (PP).

3.3.3.2 Mean wet-canopy evaporation rate

The $\overline{E}_{PM}$ obtained using the PM equation were 0.19 mm h^{-1} for BW and 0.22 mm h^{-1} for PP. The estimated $\overline{E}/\overline{R}$ values from the regression method were 0.141 and 0.165 for BW and PP, respectively. Based on the median rainfall intensity of 2.76 mm h^{-1}, the resulted $\overline{E}_{TF}$ were 0.39 mm h^{-1} and 0.46 mm h^{-1} for BW and PP, respectively.

3.3.3.3 Relationship between canopy storage capacity and maximum wind speed

The effect of wind speed on the canopy storage capacity is shown in Figure 3.2d. The calculated S_o has a general tendency to decrease with increasing u_{max} despite scatter distribution. We derived a power regression equation (r^2=0.314, p<0.05) for BW and a logarithmic regression equation (r^2=0.488, p<0.05) for PP to calculate S in the WiMo model.

3.3.4 Model calibration and validation

The rainfall events observed during the wet season (n=59) were used to calibrate the RGAM and WiMo models, whereas the calibrated models were validated for the dry season (n=43). Canopy and climatic parameters used in the RGAM model for both forest stands are summarized in Table 3.5.

Table 3.5 Summary of canopy and climatic parameters used in the revised Gash's analytical model for banksia woodland (BW) and pine plantation (PP).

Forest type	Canopy parameters					Climatic parameters (mm h^{-1})			
	S (mm)	p	c	p_t	S_t (mm)	$\overline{R}$	$\overline{E}_{PM}$	$\overline{E}_{TF}$	$\overline{E}_O$
BW	0.45	0.52	0.48	0.005	0.021	2.76	0.19	0.39	0.34
PP	1.31	0.47	0.53	0.014	0.066	2.76	0.22	0.46	0.35

The observed and simulated total E_i during the wet season for three RGAM model runs and for the WiMo model are compared in Table 3-6. The predicted E_i by PM model was underestimated by 28.1% for BW and by 21.2% for PP. The predicted E_i using $\overline{E}_{TF}$ were closer to observed E_i with an overestimation of 11.6% for BW and 14.3% for PP. The optimized $\overline{E}_O$ for RGAM model using wet season rainfall data were 0.34 mm h^{-1} and 0.35 mm h^{-1} for BW and PP, respectively. Simulated E_i using $\overline{E}_O$ agreed well with observed values for both forest stands, underestimating by only 1.8% and 3.5%, respectively. The use of optimized wet-canopy evaporation rate improves RGAM interception predictions for both forests, where the error reduces from ~25% to ~2.5%, and the Nash-Sutcliffe efficiency (Nash and Sutcliffe, 1970) increases from ~0.70 to ~0.95. The simulated total E_i by WiMo model was underestimated by 7.7% for BW and by 4.3% for PP. Different components of the wet season E_i simulated by the optimized RGAM is presented in Table 3.6. The result suggested that 77.3% and 16.6% of E_i evaporated during and after rainfall

for BW, while the corresponding values for PP were 51.6% and 34.8%, respectively. Evaporation losses from other phases played a small role in total E_i for both forest stands.

Table 3.6 Comparison of observed total interception (I_o) and modeled total interception (I_m) by the RGAM model using different wet-canopy evaporation rates and by the WiMo model for the calibration and validation datasets from banksia woodland (BW) and pine plantation (PP).

Interception	Calibration (wet season)							
	Using E_{PM}		Using E_{TF}		Using E_O		WiMo	
	BW	PP	BW	PP	BW	PP	BW	PP
P_g (mm)	1063	1063	1063	1063	1063	1063	1063	1063
I_o (mm)	161	220	161	220	161	220	161	220
I_m (mm)	116	173	180	252	158	212	149	211
Modeled-observed (%)	-28.1	-21.2	11.6	14.3	-1.8	-3.5	-7.7	-4.3
Nash-Sutcliffe model efficiency	0.73	0.69	0.83	0.74	0.97	0.94	0.78	0.83

Interception	Validation (dry season)			
	Using E_O		WiMo	
	BW	PP	BW	PP
P_g (mm)	429	429	429	429
I_o (mm)	84	123	84	123
I_m (mm)	74	113	76	107
Modeled-observed (%)	-12.1	-8.5	-9.4	-12.7
Nash-Sutcliffe model efficiency	0.84	0.75	0.72	0.79

The optimized RGAM model and WiMo model were then used to estimate the dry season E_i from two forest stands (Table 3.6). As for the RGAM model, the predicted total dry season E_i was underestimated by 12.1% and 8.5% for BW and PP, respectively. The WiMo model also underestimated E_i during the dry season, with an agreement of 9.4% for BW and 12.7% for PP. Generally, the dry season E_i predicted by optimized RGAM model exhibits slightly lower error and higher Nash-Sutcliffe efficiency than those estimated by WiMo model. Totally, the cumulative simulated E_i by RGAM model using $\overline{E}_o$ over the entire year were 232 mm for BW and 325 mm for PP, with an underestimation of 5.3% and 5.2%, respectively (Figure 3.3). The corresponding values by WiMo model were 225 mm for BW and 318 mm for PP, with an underestimation of 8.2% and 7.3%, respectively. The

comparison between the observed and simulated E_i for individual rainfall events over the study period using the optimized RGAM and WiMo models is shown in Figure 3.4. The results indicated that the RGAM model generally underestimates E_i for small rainfall events but it overestimated E_i for some heavy events, which is not evident for the WiMo model.

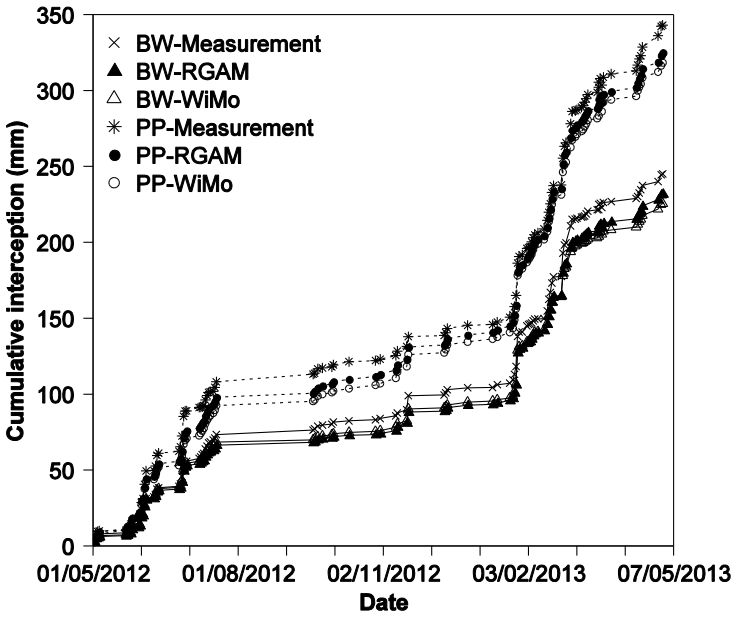

Figure 3.3 Cumulative measured and modeled interception over the one-year period using the RGAM and WiMo models for banksia woodland (BW) and pine plantation (PP).

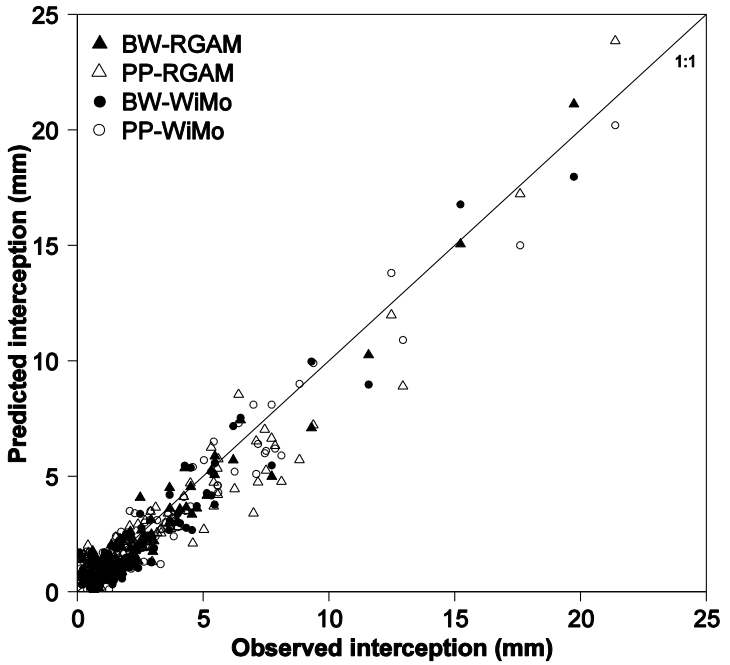

Figure 3.4 Measured and modeled interception for each rainfall event over the one-year period using the RGAM and WiMo models for banksia woodland (BW) and pine plantation (PP).

3.3.5 Parameter sensitivity

To identify the relative importance of the parameters in RGAM model, we conducted a sensitivity analysis with respect to canopy and climatic parameters (Figure 3.5), whereas no sensitivity analysis was performed for the parameter *S* in the WiMo model as it was calculated by the model itself. A decrease of 25% in *R* and *E* resulted in an increase 21% and a decrease of 16% in simulated E_i, but reducing *S* and *c* by 25% decreased E_i by only 6% and 3%. A change of 25% in p_t and S_t produced less than 0.5% changes in simulated E_i. The results showed that the RGAM model is highly sensitive to changes in climatic parameters *R* and *E*, less sensitive to canopy parameters *S* and *c*, but fairly insensitive to trunk parameters p_t and S_t.

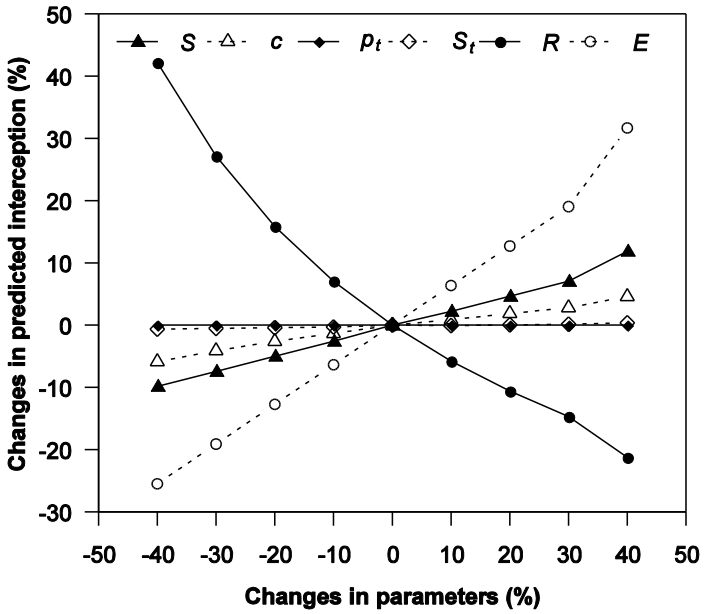

Figure 3.5 Sensitivity analyses of canopy parameters *S*, *c*, p_t and S_t, and climatic parameters *E* and *R* in the RGAM model on the predicted interception loss. Analyses were based on the average changes observed from two forest stands.

3.4 Discussion

3.4.1 Throughfall

The observed T_f for BW (83.2% of P_g) was comparable with the reported value in a Mediterranean banksia woodland of south Western Australia (Farrington and Bartle, 1991), ranging from 80% to 85% of P_g, but the T_f for PP (76.1% of P_g) was lower than those recorded in other pine forests of similar basal area, *e.g.*, 82%–87% by Farrington and

Bartle (1991) and 85% by Shi et al. (2010). Since the LAI was similar between two forests, the lower T_f fraction in the pine plantation relative to the banksia woodland was ascribed to its higher stem density. However, the lower T_f in our plantation relative to other studies was most likely resulted from the higher evaporation rates during rainfall events, which caused more intercepted rainfall water back to air and thus reduced throughfall through the canopy.

3.4.2 Stemflow

The stand-scale S_f accounted for a fairly low percentage of P_g, 0.4% and 1.0% of P_g for BW and PP, respectively. The steep branches of pine trees have a greater access of rainfall to the trunks than the low-angled branches of banksia trees and possibly caused higher stemflow for PP (Herwitz, 1987). The stemflow for PP was much lower than the other reported values, *e.g.*, 2.7% by Singh (1987), 4.9% by Meng et al. (2001) and 5.9% by Li et al. (2007) with stem density of 1,500–5,000 tree ha^{-1}, but it was closer to 0.88% by Shi et al. (2010) and 0.5% by Ghimire et al. (2012) found in pine forests with similar smaller stem density (600–800 tree ha^{-1}). This indicated that the lower stemflow fraction can be possibly explained by the low stem density in our plantation.

3.4.3 Interception loss

The E_i for BW (16.4% of P_g) was similar to the only reported value (average=15% of P_g) by Farrington and Bartle (1991). The observed E_i for PP (22.9% of P_g) was slightly higher than the earlier observations in pine forests with low stem density, *e.g.*, averaged 15% in a *Pinus pinaster* plantation by Farrington and Bartle (1991), 17.6% in a young pine *Pinus palustris* stand by Bryant et al. (2005), 14.2% in a natural *Pinus armandii* stand by Shi et al. (2010), and 19.4% in a planted pine forest reported by Ghimire et al. (2012). It is possible that the higher interception was due to the higher stand density in our study and higher evaporation rates during rainfall resulting from active advection of sensible heat at the coastal areas (Molen et al., 2006). The higher percentage of E_i for PP was expected, as E_i appears to be generally higher in coniferous forests than in broadleaf forests due to conifers' higher canopy storage capacity and the enhanced sensible heat transfer above the canopy caused by larger laminar boundary conductance from smaller leaves (Oke, 1992; Valente et al., 1997; Carlyle-Moses, 2004). Since the local climate and the canopy cover (*e.g.*, LAI) were similar in both forest stands, the higher E_i by the pine planation was

thus ascribed to its larger canopy storage capacity and smaller aerodynamic resistance at canopy surface as a result of its greater tree height (Valente et al., 1997).

3.4.4 Canopy parameters

The *S* estimate of 1.31 mm for PP compared favorably with observed values in coniferous forests, ranging from 0.3 mm to 3.0 mm (Llorens and Gallart, 2000). For broadleaf forests, the *S* values generally vary from 0.4 mm to 1.5 mm (Deguchi et al., 2006). The low *S* value (0.45 mm) for BW and estimated *S* value in the lower range for PP were consistent with the lower canopy coverage for both study plots. Similar to the finding by Hörmann et al. (1996), we found a decreasing trend in *S* with increasing wind speed, which is, however, contrary to the results of Klingaman et al. (2007). The decrease in *S* was because the captured rain droplets were shaken down from the canopy leaves by winds, which did not happen to the leafless stands of Klingaman et al. (2007).

The RGAM model was confirmed to be fairly insensitive to stemflow parameters S_t and P_t due to their small contributions to the total E_i, as shown in other studies (*e.g.*, Valente et al., 1997; Limousin et al., 2008; Shi et al., 2010; Ghimire et al., 2012). The *c* was not highly sensitive to the model compared with studies by Gash et al. (1995) and Limousin et al. (2008), but it was in agreement with the results of Dykes (1997) and Deguchi et al. (2006).

3.4.5 Mean rainfall intensity

The sensitivity analysis revealed that the RGAM model was mostly and highly sensitive to changes in climate parameters $\overline{R}$ and $\overline{E}$, which agrees well with the work by Loustau et al. (1992) and Limousin et al. (2008). The median rainfall intensity (2.76 mm h^{-1}) observed here was also comparable to what was reported in other tropical and subtropical regions, generally ranging from 2.5 to 5.0 mm h^{-1} (Van Dijk and Bruijnzeel, 2001; Limousin et al., 2008; Ghimire et al., 2012). Earlier investigations have shown that the separation time between two rainfall events did not significantly affect the resulted total E_i (Klaassen et al., 1998; Wallace and McJannet, 2006). Wallace and McJannet (2006) found that the uncertainty in rainfall intensity only brought less than 10% of the modeled E_i. The separation time in our study (at least 6 hours' dry period between successive rainfall events) was thus considered to be reasonable and would not sensibly affect the resulted E_i.

3.4.6 Mean wet-canopy evaporation rate

The calculated $\overline{E}_{PM}$ using PM equation were 0.19 mm h^{-1} and 0.22 mm h^{-1} for BW and PP, within the range of 0.07 mm h^{-1} to 0.70 mm h^{-1} found for most (sub)tropical forests (Carlyle-Moses 2007). The $\overline{E}_{PM}$ for BW and PP were approximately half of the corresponding $\overline{E}_{TF}$ obtained from regression method, while the $\overline{E}_{O}$ was closer to corresponding $\overline{E}_{TF}$. The optimized $\overline{E}_{O}$ in our study (0.34 mm h^{-1} for BW and 0.35 mm h^{-1} for PP) was slightly higher than the optimized values in subtropical montane forests (0.25–0.30 mm h^{-1}) by Ghimire et al. (2012), but much lower than those reported in the tropical coastal and montane rainforests (average=0.72 mm h^{-1}, range=0.44–1.20 mm h^{-1}) by Wallace and McJannet (2008).

Similar discrepancies between $\overline{E}_{PM}$ and $\overline{E}_{TF}$ have been reported in other rainfall interception studies (Wallace and McJannet, 2008; Holwerda et al., 2012) and the possible causes of this difference were discussed below. First, one-dimensional evaporation models like PM equation may be no longer valid for these sparse forests because the forest sparseness tends to enhance the turbulence and thus evaporation (Holwerda et al., 2012). Second, the assumed zero plane displacement height and roughness heights used to derive r_a in the PM equation can be questionable (Brutsaert, 1979; Verseghy et al., 1993). It is also possibly that PM equation fail in these coastal areas because of high advection of sensible heat from the nearby ocean during rainfall (Molen et al., 2006). Finally, the discrepancy between $\overline{E}_{PM}$ and $\overline{E}_{TF}$ can be caused by the difficulty in accurately measuring very high relative humidity during rainfall (Wallace and McJannet, 2008) and the evaporation of rain droplets splashed from tree canopy (Murakami, 2006).

3.4.7 Performance of the RGAM and WiMo models

In terms of the estimation error, the RGAM model generally performed better for BW than for PP. Although the model tended to underestimate E_i, it produced a reasonably good agreement between the predicted and observed total E_i using optimized wet-canopy evaporation rates, which confirmed the finding by Ghimire et al. (2012). The RGAM model was found typically underestimating the interception losses, *e.g.*, 2.9% by Valente et al. (1997), 4.3% by Llorens (1997) and 6.2% by Limousin et al. (2008). In our study, the model slightly overestimated the E_i for some heavy rainfall events, while E_i for smaller rainfall events tended to be underestimated, which is acceptable since interception losses are most often estimated over a season or a year instead of a single rainfall event. The errors resulting from underestimation of most small rainfall events were considered to be

the main factor that caused underestimations of the total E_i. The obtained Nash-Sutcliffe model efficiency (0.75–0.84) for RGAM model was comparable to the values for a hardwood forest (0.73–0.80) and pine forest (0.44–0.94) by Bryant et al. (2005). The WiMo model also tends to underestimate E_i, but it performed well with acceptable error (9.4%–12.7%) and relatively high Nash-Sutcliffe model efficiency (0.72–0.79). Klingaman et al. (2007) reported a similar Nash-Sutcliffe model efficiency (0.76) for the WiMo model but a lower value (0.50) for the RGAM model.

Compared to the wet season, the underestimation in dry season E_i by the RGAM model was much higher. The higher underestimates of E_i during the dry season is probably introduced by overestimation of rainfall intensity during the dry season, when small rainfall events occur more frequently and more actual evaporation is supposed to occur. However, closer errors were found between the dry season and wet season E_i simulated by the WiMo model, which is possibly because the empirically derived relationship between S and u_{max} can be applicable for both study periods. The relative high Nash-Sutcliffe model efficiency indicates the overall performance of the RGAM and WiMo models are satisfying.

Similar to Ghimire et al. (2012), fixed wet season parameters were used in the RGAM to predict seasonal and annual E_i in our study. Slight seasonal changes in canopy and climatic parameters can be expected due to changes in LAI and weather patterns, yet it is still possible to obtain satisfying estimates of seasonal and annual E_i using fixed parameters (Wallace and McJannet, 2008; Ghimire et al., 2012). Firstly, changes in seasonal LAI are small for both forests and the RGAM model is found to be less sensitive to canopy parameters in our study. Secondly, 71% of the annual rainfall in this area occurs during the wet season and the rainfall patterns are similar between wet and dry seasons. Finally, these model parameters may alter the seasonal proportion of interception, but changes in canopy and climatic parameters would compensate each other and the resulted errors in modeled interception using fixed parameters are considered to be minimal, as discussed by Wallace and McJannet (2008).

3.5 Conclusions

Rainfall interception losses were quantified and modeled for a native banksia woodland (BW) and an exotic pine plantation (PP) situated in subtropical coastal areas of Australia. Over the one-year period, measured throughfall, stemflow and interception loss were 83.2%, 0.4% and 16.4% of annual gross rainfall for BW, respectively. Corresponding

values for PP were 76.1%, 1.0% and 22.9%. A higher interception loss in the pine plantation can be explained by its higher canopy storage capacity and lower aerodynamic resistance. The simulated dry season and annual interception losses by the optimized RGAM and WiMo models were close to the observed values, with an underestimation of 5.2% to 12.7%. The RGAM is highly sensitive to climatic variables $\overline{R}$, $\overline{E}$, and less sensitive to canopy parameters *S*, *c*, but it was found to be fairly insensitive to the stem parameters S_t and p_t. The optimized RGAM model performed slightly better than the WiMo model, but both models appear to be robust and reliable to model seasonal or annual interception losses by banksia woodland and pine plantation under subtropical coastal conditions. The results indicate increase in interception losses by pine plantations would reduce the rainfall input on the forest floor, but further studies on changes in soil moisture dynamics and tree transpiration are needed to better understand the hydrological effects of exotic pine plantations in these subtropical coastal areas.

Chapter 4. Estimating Groundwater Recharge and Evapotranspiration from Water Table Fluctuations Under Three Vegetation Covers in a Coastal Sandy Aquifer of Subtropical Australia

4.1 Introduction

Vegetation plays a significant role in the groundwater hydrological cycle due to its impact on groundwater recharge and transpirative discharge; conversely, groundwater hydrology impacts sensitive vegetation in shallow water table environments (e.g., wetlands or riparian areas). Vegetation affects groundwater recharge, and thus sustainable yields, indirectly by rainfall interception losses as well as extraction of infiltrating rainwater before it reaches the water table (Le Maitre et al., 1999).

The impact of changes in vegetation cover on groundwater hydrology has been investigated for a range of environments, mostly in (semi)arid or temperate areas with deep aquifer systems (e.g. Scanlon et al., 2005; Mao and Cherkauer, 2009; Brauman et al., 2012; Nosetto et al., 2012). Deep-rooted woody vegetation was generally found to reduce streamflow and groundwater recharge (Matheussen et al., 2000; Crosbie et al., 2010), compared to shallower-rooted grasses and crops, and they tend to tap groundwater with deeper rooting systems (Benyon et al., 2006; Pinto et al., 2013). For example, Scanlon et al., (2005) found that the conversion of natural shrublands with agricultural ecosystems in southwest US altered the water flow from discharge through *ET* (i.e., no recharge) to recharge (9–640 mm yr^{-1}). Benyon et al. (2006) reported that plantations of *Pinus radiata* D.Don and *Eucalyptus globulus* Labill. used groundwater at an average rate of 435 mm yr^{-1} (40% of total water use) in the Green Triangle of southeast Australia. However, while coastal systems are under pressure from human development as well as potential stresses due to climate change, there are few studies quantifying the hydrological effects of vegetation cover changes in coastal areas characterized by shallow aquifer systems with highly permeable sediments.

Like other coastal and island sand mass aquifers around the world, significant resources of high quality groundwater are located on Bribie Island for water supply to coastal communities and local wetland vegetation. Over the past three decades, exotic pine tree plantations have been developed on the island largely for timber production, particularly in the natural distribution areas of native vegetation (e.g. banksia woodland and grassland).

The changes in vegetation cover can potentially affect the local hydrological processes, e.g., groundwater recharge and evapotranspiration (*ET*).

In shallow water table environments, groundwater recharge and groundwater use by vegetation via evapotranspiration (ET_g) can be estimated from analyses of water table fluctuations (*e.g.*, Scanlon et al 2005; Crosbie et al. 2005; Zhu et al., 2011; Yin et al., 2013; Fahle and Dietrich, 2014). For such analyses, quantification of the aquifer's specific yield (S_y) is considered the main source of uncertainty as its error is translated directly to final estimates (Scanlon et al., 2002; Loheide et al. 2005). Various methods (*e.g.*, laboratory experiment, field study and numerical modelling) are available for determining specific yield, but they usually produce inconsistent values (Neuman, 1987; Crosbie et al., 2005). Specific yield is often considered constant in hydrological studies. However, researchers have recognized that it is dependent on water table depth and drainage time (Duke, 1972; Nachabe, 2002; Shah and Ross, 2009), particularly in a shallow water table environment due to a the truncation of the equilibrium soil moisture profile (esp., capillary fringe) at the soil surface (Childs, 1960). Use of a constant specific yield can lead to the recharge and ET_g being significantly overestimated (Sophocleous, 1985; Loheide, 2005). Loheide et al. (2005) suggested the readily available specific yield can be used to obtain reasonable estimates of ET_g when the water table depths > 1 m, but the dependence of S_y on the water table depth needs to be considered for water table depths < 1 m. In spite of this, the depth-dependant specific yield has seldom been adopted for the estimation of recharge and ET_g in published studies (e.g., Crosbie et al., 2005; Carlson Mazur et al., 2013).

Here, we investigate shallow water table fluctuations in response to rainfall and ET_g under three vegetation covers to gain a better understanding of the hydraulic relationship between vegetation and groundwater in shallow sandy aquifers. Specific objectives of this study are to: (1) examine how water table depth varies daily and seasonally under a pine plantation, a banksia woodland and a sparse grassland; (2) determine depth-dependent specific yields under both rising and falling water table conditions and (3) estimate daily and seasonal groundwater recharge and ET_g under three contrasting vegetation covers.

4.2 Materials and methods

4.2.1 Site description

The study was undertaken on an unconfined surficial aquifer on Bribie Island (Figure 1.1). To minimize the effect of tides and groundwater pumping on water table fluctuations, three field sites with different vegetation cover were carefully selected in the interior of the island (Figure 1.1). These were along a belt transect which was normal to the coastline and crossing a relatively elevated section (dune). The transect is aligned with expected groundwater flow to adjacent wetlands. A detailed site description is presented in the overview of study sites in Chapter 1.

4.2.2 Field data acquisition

To characterize water table fluctuations for the vegetation covers, each field site was instrumented with a cluster of three monitoring wells (in triangle arrangement at 20–40 m spacing) equipped with pressure transducers (Level Troll 300, In-Situ Inc., USA). The average water levels obtained from three wells were used for estimates of recharge and ET_g at each site. Monitoring wells were installed to a depth of 2.0 m using a 51 mm diameter, 1.5 m long PVC screen and 1.5 m PVC riser. Augered sand was backfilled around the wells to a depth of 0.25 m below land surface and granular bentonite was then packed around land surface to avoid preferential flow. Apart from water pressure measurements, atmospheric pressure was monitored using a barometric datalogger (Baro Troll 100, In-Situ Inc., USA) to obtain water levels. The monitoring wells were vented to connect with the atmosphere and prevent air compression inside the PVC tubing. The water level data were measured from 1 November 2011 to 31 October 2013 and automatically recorded at 15-min intervals. Data were collected quarterly from the pressure transducers and the water table depth was manually measured by a dip meter during each field trip to check the logged water level values.

An automatic weather station was installed on a 15-meter-high mast located above the canopy and in the center of the pine plot to measure meteorological variables, including temperature and relative humidity, wind speed and direction, solar radiation and soil heat flux. Potential evapotranspiration (PET) was estimated using the Penman-Monteith equation (Monteith, 1965) with parameters obtained from the pine plantation (Fan et al., 2014). Gross rainfall was measured using a tipping-bucket rain gauges (RG3-M, Onset Computer Corp., USA) located in a nearby well-exposed clearing next to the banksia woodland. To obtain the net rainfall (throughfall plus stemflow) reaching the forest floor, throughfall was measured using 15 tipping-bucket rain gauges in the pine plantation and 8 troughs connected to 8 rain gauges in the banksia woodland. Stemflow was also collected

in the pine plantation and banksia woodland using 6 and 8 collars connected to rain gauges, respectively. A detailed description of rainfall and throughfall measurements was presented by Fan et al. (2014).

4.2.3 Groundwater recharge estimation using the water table fluctuation method

The water table fluctuation (WTF) method is widely used to estimate spatially-averaged gross recharge for unconfined shallow aquifers (Healy and Cook, 2002; Delin et al., 2007):

$$R = S_y(h)\frac{\Delta h}{\Delta t} \tag{4.1}$$

where R is the estimated gross recharge (m); $S_y(h)$ is the depth-dependent specific yield; Δh is peak rise in water level attributed to the recharge period (m); Δt is the time of the recharge period. The WTF method assumes rises of groundwater levels in unconfined aquifers are only due to recharge water arriving at the water table (Healy and Cook, 2002; Scanlon et al., 2002). The method is best applied in areas with shallow water tables that demonstrate sharp rises in water levels over short time periods, which is applicable in our coastal sandy environment.

The water level rise in Equation (4.1) during a recharge event was calculated as the difference between the peak of the water level rise and the low point of the extrapolated antecedent recession curve at the time of the peak, which is the trace that the well hydrograph would have followed in periods of no rainfall. Similar to Crosbie et al. (2005), the effects of evapotranspiration from the water table, lateral flow in and outwere coupled into the rate of water table decline. The master recession curve (MRC) approach was used to obtain the projected groundwater decline in each of the monitoring wells (Heppner and Nimmo, 2005; Crosbie et al., 2005; Heppner et al., 2007), rather than using more subjective graphical extrapolation methods. Generally, the MRC approach predicts higher water level declines at higher groundwater levels. During rain-free days, the decline rate was calculated as the decline in the groundwater level per day. To describe the relationship between rate of water table decline and depth to water table depth, regression functions are fitted to available data. The potential groundwater level that would have occurred under rain-free conditions can be calculated for a given groundwater level during rainfall events using these regression functions.

4.2.4 Groundwater evapotranspiration estimation using the White method

White (1932) developed an empirical method to quantify daily groundwater use by vegetation via evapotranspiration from the analysis of shallow water table fluctuations. The White method assumes: (1) diurnal water table fluctuations are caused by plant water use; (2) night-time water use from vegetation is negligible; and (3) a net inflow rate during night (midnight and 4 a.m.) is representative as a daily average rate. The daily groundwater evapotranspiration (ET_g) is obtained using the following equation:

$$ET_g = S_y(h)(24r \pm \Delta s) \tag{4.2}$$

where r is the net inflow rate between midnight and 4 a.m. (mm h^{-1}) and Δs is the net change of water table during a 24-h period (mm d^{-1}). A slight modification to the original White method suggested by Loheide et al. (2005) was applied in this study, where r was estimated as the average value of the net inflow rates calculated between midnight and 6 a.m. on the day of interest and the following day.

4.2.5 Determination of specific yield

The specific yield is defined as the volume loss or gain of water per unit area of aquifer associated with a corresponding unit drawdown or rise in water table (Freeze and Cherry, 1979):

$$S_y = \frac{V_w}{A\Delta z} \tag{4.3}$$

where V_w is the volume of water released or stored, A is the aquifer area and Δz is the change (decline or rise) in water table elevation. This definition is misleading as the specific yield can vary with depth to water table and with the time scale of observation (Duke, 1972; Said et al., 2005). The variation in specific yield beyond the daily time frame in this study was neglected due to the fast response of the water table in our sandy environment. To obtain reasonable estimates of recharge and ET_g, depth-dependent specific yields under falling and rising conditions were determined using laboratory-based drainage experiments on extracted cores (Cheng et al., 2013) and the ratio of water table rise to rainfall amount for different water table elevations using the field observations (Carlson Mazur et al., 2013), respectively.

Two undisturbed soil columns were excavated from the study sites using 80 cm high steel pipes with an inner diameter of 15 cm. In the laboratory, each column was slowly saturated from the bottom to minimize the trapped air and drained layer by layer using 8 taps identically spaced on the side of columns (3 replicates). Each drainage was stopped when a steady hydraulic state in the soils was reached (i.e., no further drainage out of column). Based on Equation (4.3), the specific yield was calculated for each layer using the weight of the drained water recorded by a balance (SP402 Scout-Pro, Ohaus, USA), cross-sectional area of the column (177 cm^2) and the drawdown in water table (10 cm). The calculated specific yield for each layer was considered as the value corresponding to the midpoint between two drainage levels.

Specific yield was also estimated from the response of the water table to each rainfall event as the ratio of water level rise to net rainfall depth at each site. Rainfall events were only included if the previous rainfall within one week had replenished the soil moisture over the entire unsaturated zone and thus caused water level rises. Large rainfall events when the water table was within 0.5 m of the surface with substantial runoff potential were not used for S_y estimation.

4.3 Results and discussion

4.3.1 Seasonal and diurnal water table fluctuations in response to rainfall and ET_g

Annual gross rainfall during the hydrological years 2012 and 2013 was 2093 mm and 1493 mm, respectively, which were higher than the long-term mean of 1405 mm. As we previously presented (Fan et al., 2014), the annual rainfall interception losses were estimated at 16.4% of gross rainfall for banksia woodland and 22.7% for pine plantation. Thus we take the resulting net rainfall under banksia woodland as 1737 mm in 2012 and 1239 mm in 2013, and the corresponding net rainfall under the pine plantation as 1633 mm and 1164 mm, respectively. The interception loss from sparse grassland was considered to be minimal since the grasses were small and sparsely distributed. Major rainfall that occurred during the wet season (November–April) accounted for ~76% of the annual rainfall (Figure 4.1). No rainfall occurred in both August 2012 and 2013, the driest months recorded since 1983.

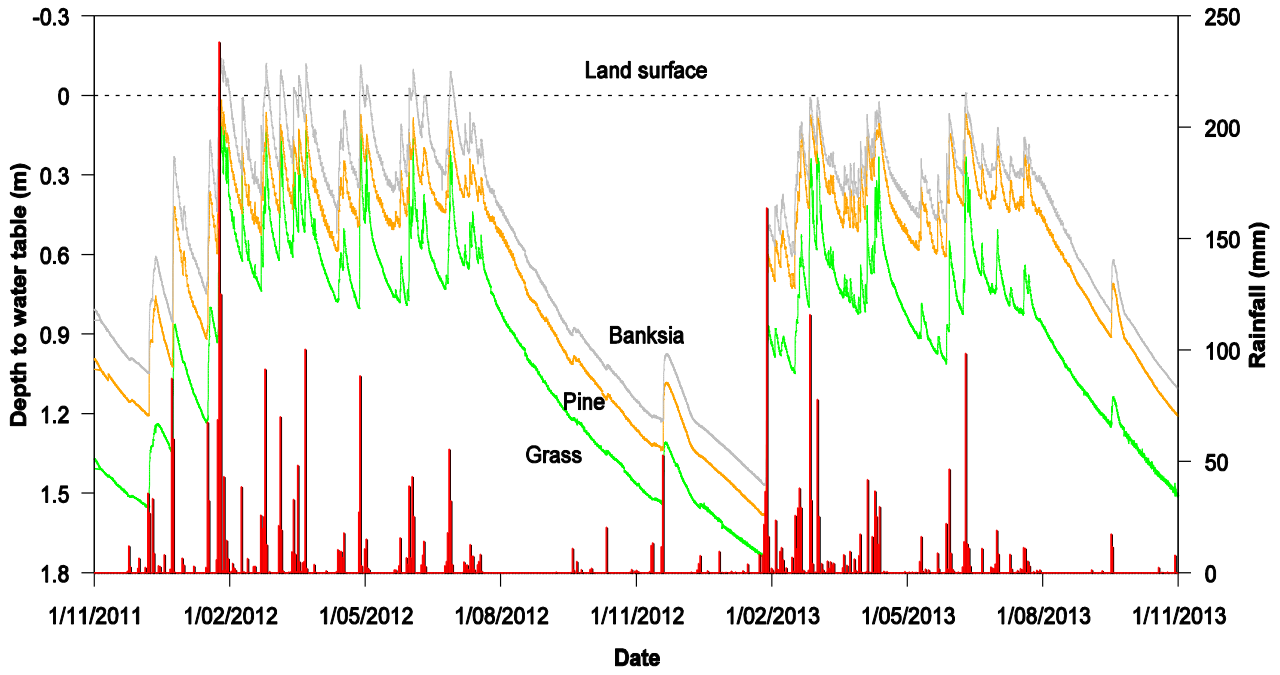

Figure 4.1 Seasonal rainfall distribution and average water table fluctuations observed from three monitoring wells at pine plantation, banksia woodland and sparse grassland, for the period from 1 November 2011 to 31 October 2013.

Seasonal fluctuations in water table depth were clear under the three vegetation covers and the fluctuation patterns were similar (Figure 4.1). Over the 2-year period, the depth to water table under the sparse grassland varied from 0.21 m to 1.77 m and averaged 1.02 m. The depth to water table averaged 0.55 m at the woodland wells and 0.68 m at plantation wells, ranging from ponded conditions to 1.47 m and from 0.02 m to 1.53 m, respectively. Water table fluctuations were not evaluated if the water table was above the land surface. Water table rises of between 0.02 m to 0.97 m were recorded in response to various rainfall events. Depending on the amount of rainfall and the initial depth to water table, the water table rise peaked from 0.5 to 73 hours of its initiation (Figure 4.2). This is an appropriate time frame (hours or a few days) for application of the water table fluctuation method (Healy and Cook 2002). However, these water table rises were not necessarily resulted from recharge. Infiltrating rainwater can trap air in the unsaturated zone and cause the Lisse effect (Heliotis and DeWitt, 1987). Trapped air potentially reduced the profile water storage capacity, with less water to raise the same water table relative to that without the entrapped air effects (Nachabe et al., 2004). The increase of air pressure in the unsaturated zone can partially cause the rises of water table. Although rapid water table rises were recorded by the pressure transducers (Figure 4.2), rises in water level comparable to expected values based on the depth of given rainfall and a gradual

dissipation of the water table rise indicated that the Lisse effect could be considered minimal in our coastal sandy environment (Healy and Cook, 2002; Crosbie et al., 2005).

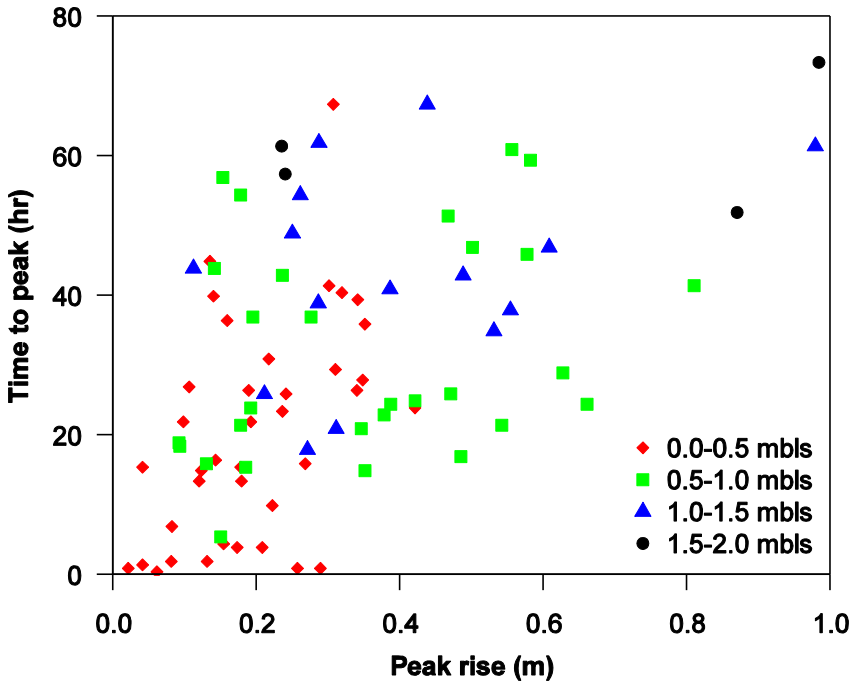

Figure 4.2 Relationship between time to peak and peak rise of water table for different groups of initial water table depths.

In the absence of rainfall events, diurnal fluctuations of groundwater levels were observed under the pine plantation and banksia woodland, whereas the sparse grassland hydrograph exhibited a continuous declining curve (Figure 4.3). Over the 2-year period, diurnal water table fluctuations were detected at a depth of up to ~1.0 m below land surface (mbls) in the pine plantation and ~0.8 mbls in the banksia woodland, but the fluctuation magnitude was significantly reduced beyond 0.8 mbls for pine plantation and 0.6 mbls for banksia woodland. The water table declined during the daytime because of tree water use and rebounded to a level slightly lower than the maximum level of the previous day during the night when transpiration significantly diminished or ceased. The daily highest water level occurred between 6 a.m. and 8 a.m. and the daily lowest water level occurred at 4 p.m.–6 p.m. Diurnal fluctuation of the water table suggests that both pine and banksia trees are accessing the groundwater.

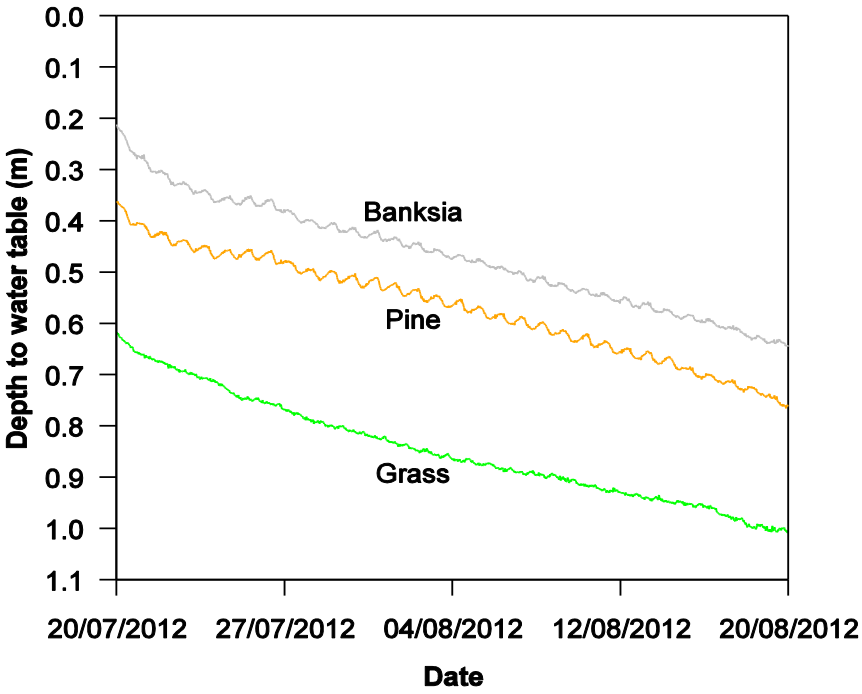

Figure 4.3 Example of average diurnal average water table fluctuations observed from three monitoring wells at pine plantation, banksia woodland and sparse grassland from 20 July to 20 August 2012.

The amplitudes of groundwater fluctuations at our tree sites suggest that the root zone there developed a maximum root depth of 1.0 m, with the majority of active roots in the upper 0.8 m for the pine plantation and 0.6 m for the banksia woodland. We observed the fine root (diameter < 2 mm) distributions of pine and banksia trees by excavation adjacent to trees and found a high root length density in the upper 0.5 m. In general, the rooting depths of woody vegetation have been found to be highly variable with a mean maximum depth of 7.0±1.2 m for trees and 5.1±0.8 m for shrubs (Canadell et al., 1996). The shallow and spreading rooting systems for trees at our sites were likely to be associated with their growth adapting to the shallow water table conditions. No diurnal water table fluctuation occurred at the grassland site because the grasses here had relatively shallow root depths (0.1 m) compared to trees, but the depth to water table at this site was often larger (> 0.3 m) than those at the forested sites due to its higher elevation. This undetectable fluctuation can also be ascribed to the low water requirements by the sparse grasses.

4.3.2 Variability of specific yield with depth in shallow water table environments.

In our laboratory experiments, the water drainage from each layer of the soil columns was fast due to the high conductivity of our well-sorted aeolian sands and normally ceased

within 24 hours of initiation. Considering the daily timeframe used in the White method, the time-dependency of specific yield at our sites is ignored. Similar to other studies (Schilling, 2007; Shah and Ross, 2009; Carlson Mazur et al., 2013), specific yields obtained from both laboratory and field methods were found to vary with water table depth, with low S_y values close to the soil surface (Figure 4.4). Specific yields then increase with increasing depth to water table as more groundwater is drained from the soil profile and finally approaches a quasi-constant of 0.25 when the water table is more than ~1.0 m from the surface. This is consistent with the finding by Loheide et al. (2005), who argued depth-dependency of specific yield has to be considered when water table depths < 1 m. We derived sigmoid functions (Venegas et al., 1998) to describe the dependence of specific yield on depth to water table (p<0.05).

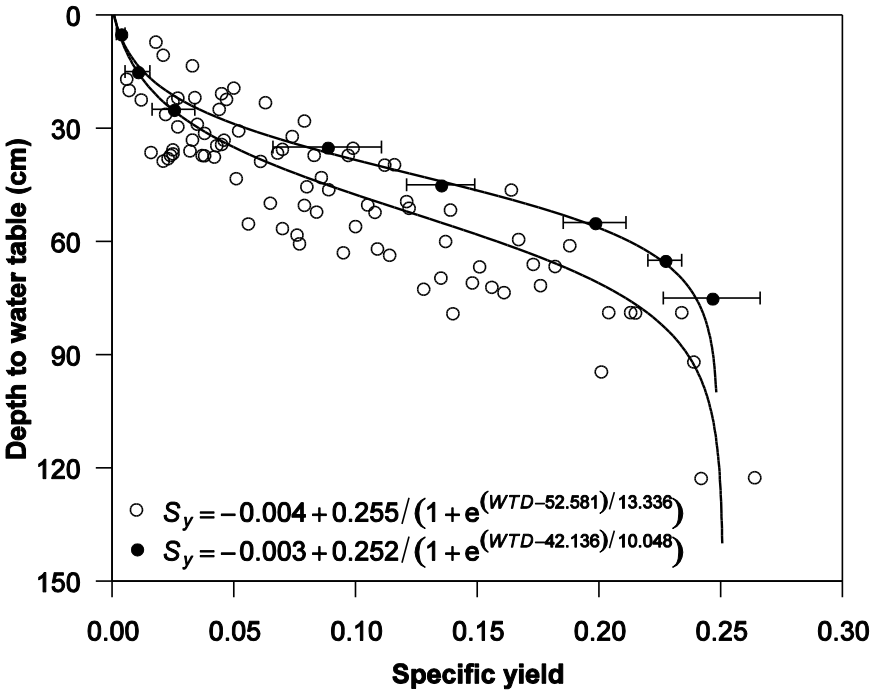

Figure 4.4 Specific yield as a function of depth to water table from drainage experiments (●) and water table response to rainfall (○).The error bars represent one standard deviation from the mean. Well data form all three sites were used to derive specific yield from water table response to rainfall.

The S_y values calculated from the field water table response to rainfall were smaller than those obtained from drainage experiments, especially at the middle range of depths to water table. The difference in S_y obtained under falling and rising water table conditions may be due to hysteresis (entrapped air) in the soil water characteristic and air encapsulation below water table, where there is a difference in the volume of water able to be held at saturation and the volume able to be fully drained (Fayer and Hillel, 1986;

Nachabe, 2002). Encapsulated air is likely to reduce the value of specific yield achieved from a rising water table compared with that determined by drainage from near full saturation situation in the laboratory. Similar discrepancies in S_y under wetting and drying conditions have been found by others (Said et al., 2005; Shah and Ross, 2009; Logsdon et al., 2010). It can also be partially due to the difference in spatial scales used in the S_y determination (ten-meter vs sub-meter). The rainfall-water table response method is able to provide information about the variation of specific yield with depth, but it is expected to give an overestimate of S_y due to the inclusion of infiltrating rainwater retained by the soil (Logsdon et al. 2010; Carlson Mazur et al. 2013). Logsdon et al. (2010) investigated the effect of soil wetting on S_y estimation in a crop field. They indicated the rainfall-rise method produced much higher S_y values if the amount of vadose zone water was not subtracted from rainfall depth, suggesting caution is required when applying the method when soils are dry prior to a rainfall event. We thus ignored all the rainfall events with long previous dry periods in this study. Only the rainfall events with recent rainfall where soil moisture was likely to be replenished and resulted in water level rises were considered.

Crosbie et al. (2005) tested different methods to estimate S_y and found that the rainfall-water table response provided the most reasonable estimates for recharge, which they attributed to S_y being calculated using the same temporal and spatial scale in which it was applied. Therefore, S_y from the water table response to rainfall was adopted to obtain estimates of recharge, whereas S_y determined by the drainage experiments was used to estimate ET_g since it corresponded to draining conditions.

4.3.3 Groundwater recharge under the three vegetation covers.

The relationship between the rate of water table decline and depth to water table (Figure 4.5) shows that the higher the water table is, the greater the decline rate. On average, the rate of water table decline decreased from ~5 cm d^{-1} to less than 1 cm d^{-1} as the water table elevation decreased from near the ground surface to 1.0 m below the surface. The decline rate incorporated factors affecting water level decreases, e.g., groundwater evapotranspiration, lateral flow in and out. A negative power function was fitted between the bin median of discharge rate and depth to water table. We presume that the water table recession behavior is unique to each site, which largely depends on the rates of discharge from the recharge site to the central swale or the ocean. The grassland site shows a higher rate of water table decline than forested sites.

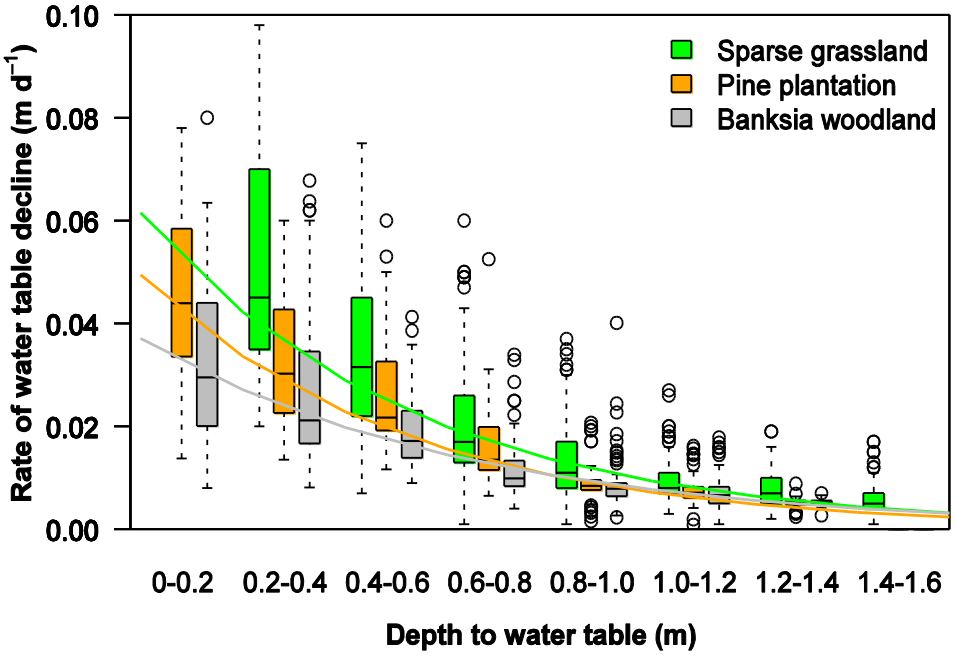

Figure 4.5 Box plots of water table decline rate binned into 0.2 m intervals by depth to water table.

Recharge for each monitoring well was estimated by multiplying the groundwater level rise by the specific yield corresponding to the average level during each rainfall event using the equations in Figure 4.4. There is an obvious seasonal trend in the estimated recharge with the major recharge occurring during the wet summers and autumns (Figure 4.6). Generally, the recharge pattern is similar to that of gross rainfall, with largest amounts of rainfall and recharge in December and January 2012, January and February 2013, during which the heavy rainfall replenished soil moisture and generated groundwater recharge. Although the annual recharge averaged from three vegetation sites amounted to 620 mm (40% of annual average net rainfall), the monthly average recharge distributions showed significant variations. The monthly average recharge estimated for the year 2011–2012 ranged from 11 mm in October 2012 to 208 mm in December 2011, representing 9%–73% of the monthly average net rainfall (Figure 4.6). For the year 2012–2013, the monthly average recharge varied from 8 mm in September 2013 to 221 mm in January 2013 (11%–67% of the monthly average net rainfall).

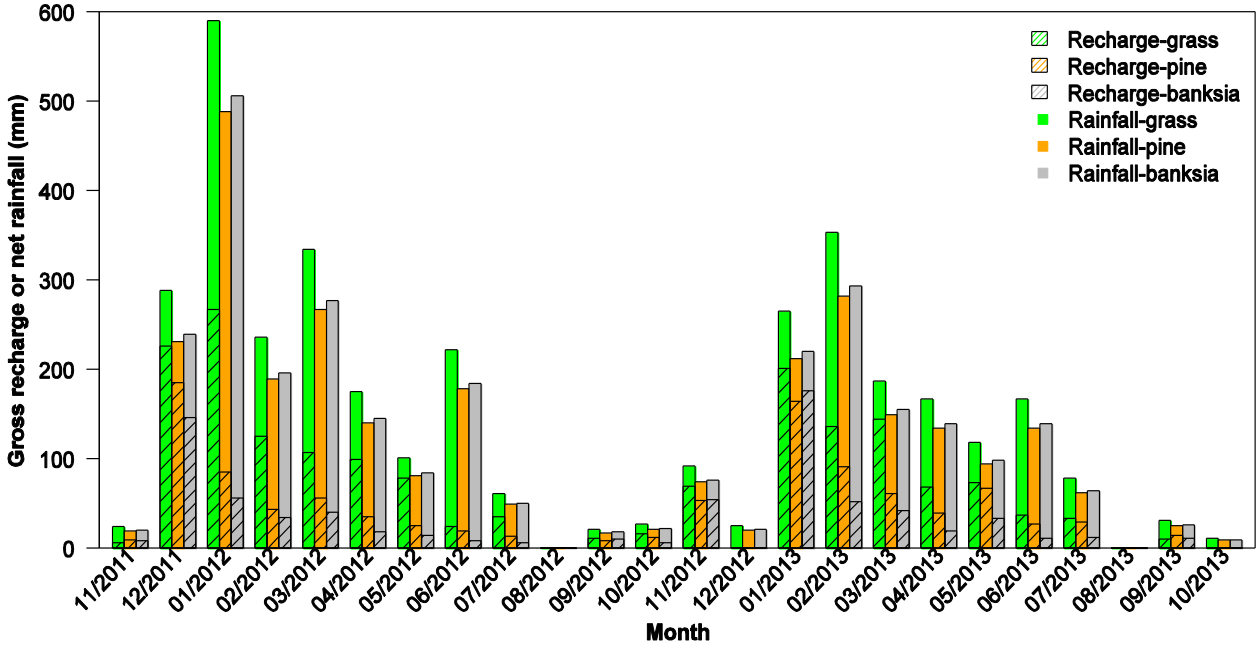

Figure 4.6 Distribution of estimated monthly gross recharge and observed monthly net rainfall at each site over the 2-year period.

The reduction in recharge as a percentage of monthly net rainfall in late summer and autumn is due to the greater influence of the shallow water table, whereas the low percentage of recharge in winter and early spring is mainly ascribed to drier soils with higher moisture holding capacity and smaller rainfall events. There were several rainfall events that did not cause an increase in the water table elevation during the dry season, particularly at the grassland site with its thicker unsaturated zone. During these periods, most infiltrating rainwater was stored in the unsaturated zone and did not apparently recharge the shallow aquifer. Hence, major groundwater recharge primarily occurred in the early summer following the dry season. In this case, the lower water table and drier vadose zone had the largest capacity to accept more recharge after the significant replenishment of soil moisture by the frequent heavy summer storms in our subtropical coastal environment (Figure 4.6).

Temporal recharge patterns for the three field sites are similar due to the similar rainfall patterns between sites; however the magnitude of recharge is different. In the pine plantation, annual recharge amounted to 521 mm (31% of net rainfall) for year 2012 and 589 mm (49% of net rainfall) for year 2013, whereas annual recharge in the banksia woodland was less, with 357 mm (21% of net rainfall) for year 2012 and 449 mm (36% of net rainfall) for year 2013. Much greater annual recharge occurred in the grassland, where total recharge amounted to 1037 mm (49% of net rainfall) and 830 mm (56% of net rainfall)

for years 2012 and 2013, respectively. Lower recharge values in the pine plantation and banksia woodland can be expected since ~20% of gross rainfall was intercepted by forest canopies. This was also due to the generally shallower water table at the forest sites limiting recharge, whereas the grassland had a relatively larger capacity to capture more infiltrating rainfall as groundwater recharge. The forested sites were lower in elevation and had several continuous weeks of near-saturated soil conditions in the wet season, and therefore, recharge was restricted during these periods. The difference in the annual recharge values at each site between the years 2012 and 2013 was attributed to differences in the rainfall in each year.

Overall, these recharge values are higher than results obtained in other studies on Bribie Island. For example, soil water balance modelling by Ishaq (1980) resulted in a recharge value of 13% of rainfall while Isaacs and Walker (1983) calibrated a numerical model for the southern part of the island using a recharge value of approximately 20%. Harbison (1998) estimated recharge values of 15% and 30% based on sodium and chloride mass balance respectively. The Department of Natural Resources reported a recharge value of 22% of total rainfall for the whole island using calibrated models (DNR, 1988). However, much lower recharge estimates have also been reported for the whole island, e.g., 8% by the Department of Natural Resources (DNR, 1996) and 7% by Harbison (1998). Since the estimated recharge values obtained by the water table fluctuation method were event-based gross recharge compared with the steady-state recharge rates estimated by above modelling and chemical methods, higher recharge percentages were expected in this study. Using the WTF method, Crosbie et al. (2005) estimated recharge for 6 field sites in a similar coastal sand-bed aquifer of Newcastle, Australia. The reported recharge percentage values ranged from 58% to 65% of gross rainfall. A deeper average water table (~2 m) than ours was recorded, which probably accepted more infiltrating rainwater and resulted in higher available recharge than that in our shallower water table environment. The water table fluctuation method appeared to produce reasonable recharge values in our study, but the uncertainties in recharge estimates directly resulted from the uncertainty in specific yield under rising water table condition has to be acknowledged. Despite this, the water table fluctuation method was useful to compare the relative influence of various vegetation on groundwater recharge in this environment.

Applying a water balance method, Brauman et al. (2012) found recharge for both cattle pastures and native forests in the highly permeable basalt catchments of tropical leeward Hawaii island were close to 100% of gross rainfall (range = 87%–106 %), where difference

in recharge under different vegetation covers was attributed to the direct fog interception by native forests. They concluded vegetation has small effects on water quantity in areas with highly permeable substrates and intense storms due to fast percolation of water beyond the rooting zone. In our study, the estimated annual recharge was lower (25%–35%) in native and planted forests than that of grassland (50%). In contrast to fewer interception losses in their study as a result of supplement by fog and clouds, ~20% of gross rainfall was intercepted by tree canopies and evaporated back into the atmosphere at our sites, which greatly reduced the potential recharge. The highly permeable sandy aquifer can potentially accept large amount of net rainfall as they suggested, but our shallow water table led to significant rejection of recharge in the wet season. The excess rainwater acted as overland flow to feed the central swale or the wetland through drainage channels along the tracks.

4.3.4 Groundwater discharge via evapotranspiration under the three vegetation covers

Groundwater evapotranspiration was estimated by multiplying the total daily fall of water table by the specific yield corresponding to the daily average level using the equations in Figure 4.4. The White method was not applied during recharge events or when the water table was below the maximum rooting depth. Over the 2-year study period, this method was applied to 82 days in 2012 and 87 days in 2013 for banksia woodland and pine plantation. The results show that the daily ET_g generally decreases from summer to winter (Figure 4.7). The decline in ET_g during the winters reflects the decrease in the transpiration rate as the atmospheric evaporative demand is three times lower than that in the summer. The highest daily ET_g rates were observed in January 2012 and February 2013. The annual cumulative ET_g estimated by the White method amounted to 208 mm in 2012 and 217 mm in 2013 for pine plantation, while the corresponding values for banksia woodland were 111 mm and 131 mm, respectively. The daily ET_g for days in which ET_g was greater than zero over the year 2012 averaged 2.8 mm d^{-1} (range=1.0 to 5.1 mm d^{-1}) in plantation and 1.5 mm d^{-1} (range=0.4 to 4.1 mm d^{-1}) in woodland, while the corresponding values in 2013 were 2.9 mm d^{-1} (range=0.5 to 5.8 mm d^{-1}) and 1.7 mm d^{-1} (range=0.3 to 3.7 mm d^{-1}), respectively. The estimated ET_g for pine plantation was closer to the PET (0.8–6.8 mm d^{-1}) compared to banksia woodland. This was partially caused by the difference in PET between the pine plantation and the banksia wood since the PET was only calculated using parameters from the pine plantation. Although the seasonal patterns of ET_g between banksia and plantation were similar, the estimated ET_g for banksia woodland is

approximately half of the corresponding values for pines. The higher ET_g at the pine plantation is largely explained by much higher tree density. The ET_g for banksia can also be restricted by weaker sensible heat transfer at the canopy surface caused by greater boundary layer resistance from its relatively broad leaves (Oke, 1978) and the higher aerodynamic resistance due to its lower canopy height (Valente et al., 1997).

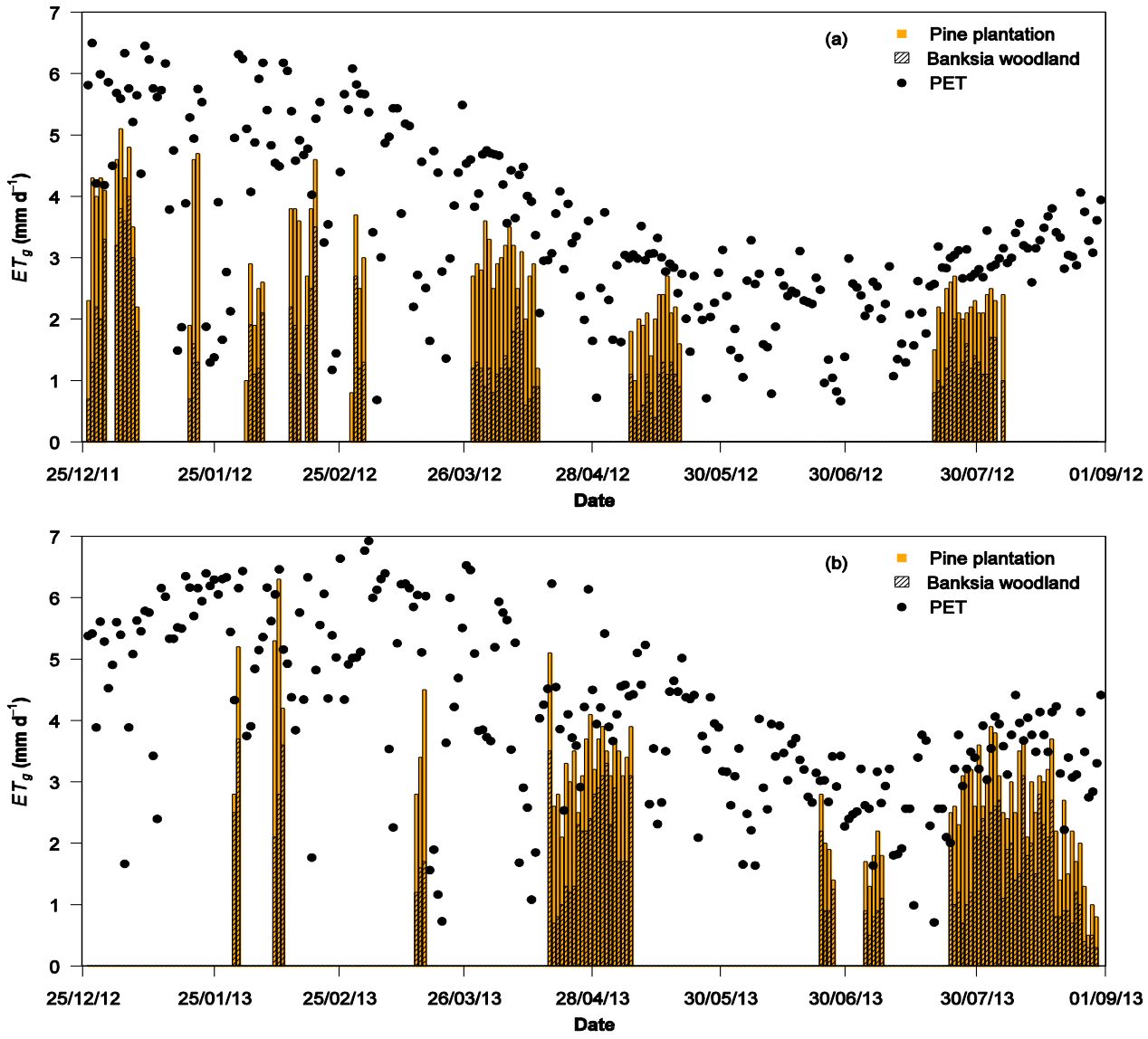

Figure 4.7 Daily potential evapotranspiration (PET) and estimated groundwater evapotranspiration (ET_g) by pine plantation and banksia woodland (a) from 26/12/2011 to 31/08/2012 and (b) 26/12/2012 to 31/08/2013. Due to recharge events or depths to water table larger than maximum root depths, no ET_g was detected between days with ET_g and beyond the above periods over the two years.

Our daily ET_g estimates (0.3–5.8 mm d^{-1}) are generally lower than other ET_g estimates for pines and woodland species using White methods. For example, Vincke and Thiry (2008) found the estimated ET_g for a Scots pine (*Pinus sylvestris* L.) stand growing on a sandy

soil in Belgium ranged from 0.7 to 7.5 mm d^{-1} (PET=1.0–8.5 mm d^{-1}). Gribovszki et al. (2008) obtained ET_g rates of 3.2–10.5 mm d^{-1} (PET=5.0–16.5 mm d^{-1}) for a phreatophyte ecosystem dominated by alder (*Alnus glutinosa* L. Gaertn.) in Hungary. Butler et al. (2007) obtained ET_g rates of 2.9–9.3 mm d^{-1} for a cottonwood forest (*Populus* spp.) with less amounts of mulberry (*Morus* spp.) and willow (*Salix* spp.) in USA. However, our ET_g estimates are comparable with estimated ET_g rates (1.7–6.3 mm d^{-1}) for oak (*Quercus* spp.) and maple (*Acer* spp.) trees by Nachabe et al. (2005) using diurnal fluctuations in the total moisture of sandy soil above a shallow water table (PET=2.0–7.5 mm d^{-1}). In the above studies, the PET was generally higher than our PET estimates of 0.8–6.8 mm d^{-1}, which probably resulted in the higher ET_g estimates accordingly as the ET_g are largely driven by the meteorological variables that control PET such as net radiation, temperature and humidity (Butler et al. 2007; Gribovszki et al. 2008). This difference can also result from differences in depth to water table and forest characteristics. However, the White method seems to be applicable for comparison of ET_g between exotic and native tree species in subtropical coastal environments.

The relationship between ET_g and PET was further analyzed (Figure 4.8), which confirmed that the groundwater discharge via root water uptake by both forests correlates strongly with PET, with higher daily ET_g rates corresponding to higher daily PET. Generally, there is a positive linear correlation between ET_g and PET for both forests, with substantial scatter around the trendline. This scatter is likely the result of changes in other environmental factors such as soil moisture availability, which can impact evapotranspiration and are not included in the PM equation.

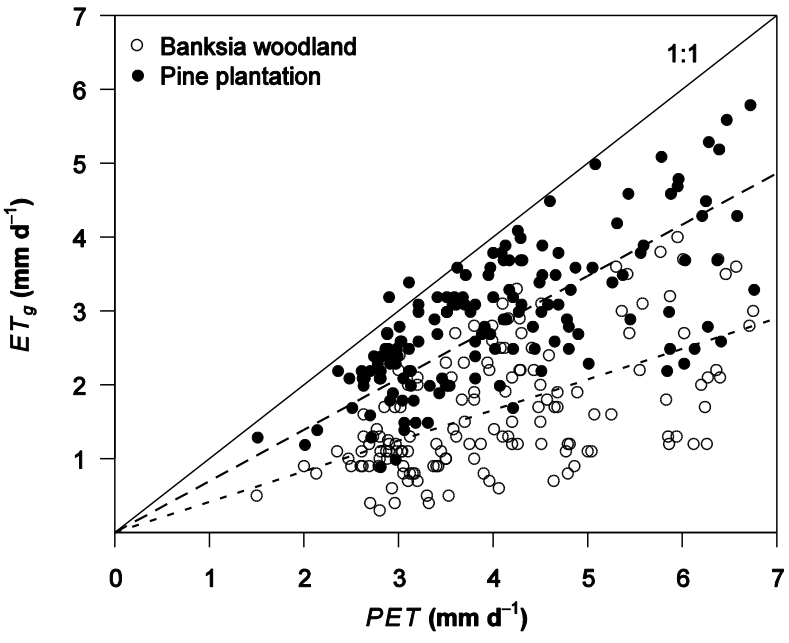

Figure 4.8 Relationship between daily groundwater evapotranspiration (ET_g) and potential evapotranspiration (PET) at the pine plantation and banksia woodland.

Depth to water table is another important factor determining the groundwater contribution to transpiration. The ratio of ET_g to PET can reflect the fraction of ET that is derived from the groundwater. The ET_g/PET ratio increases for depths to water table which range from near-surface to ~30 cm for banksia woodland and to ~45 cm for pine plantation, and then decreases as the water table falls below these thresholds (Figure 4.9). Using numerical simulations, Shah et al. (2007) identified similar thresholds (31–36 cm) for forests with extinction depths of ~2.5 m in sandy soils. Root water uptake by trees was most likely stressed under anaerobiosis conditions when the water table was close to the land surface (Feddes et al., 1978). The roots gradually became active due to increased oxygen in the unsaturated soil as the water table fell towards the threshold depths. The ET_g fraction reached maximum value at threshold depths, when estimated ET_g rates were closer to PET. However, the ET_g fraction started to decrease when water table exceeded the thresholds as a result of a decreasing root density with depth and tended to a value of zero when water table approached maximum rooting depth. Although difference in PET between the pine plantation and the banksia wood was expected, the tendency of ET_g/PET ratio with depth to water table was considered to be similar.

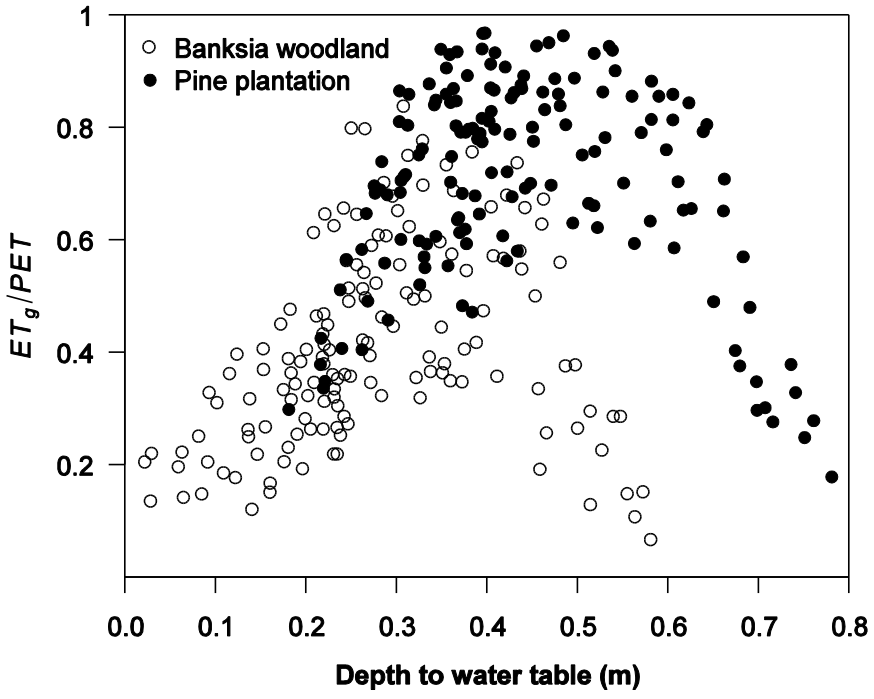

Figure 4.9 Ratio of groundwater evapotranspiration (ET_g) to potential evapotranspiration (PET) as a function of depth to water table at the pine plantation and banksia woodland.

A representative estimation of the net inflow rate throughout the day is required in the White method, because the used assumption of constant inflow rate is questionable in most cases due to changing hydraulic gradients between the recovery source and the monitoring site (Troxell 1936; Loheide and Steven 2008; Fahle and Dietrich 2014). Various modifications have been developed for the original White method to improve ET_g estimates by deriving a time-dependent inflow rate (Gribovszki et al. 2008; Loheide and Steven 2008) or an average rate across the day (Miller et al. 2010). Fahle and Dietrich (2014) evaluated different inflow estimation methods using hourly flow data measured from the lysimeter experiments. Compared to the original White method, better estimates of the inflow rate were obtained when using a two-night average value suggested by Loheide (2005) over longer time spans (6 p.m.–6 a.m.). Thus, the average inflow rate estimated from the two-night values between midnight and 6 a.m. in this work was considered to be representative of the net inflow rate throughout the day of interest.

4.4 Conclusions and implications

In this study, water table measurements in a sandy aquifer under three adjacent vegetation covers were collected over a 2-year period on Bribie Island in subtropical coastal Australia. Water table fluctuations were analyzed to estimate groundwater recharge and discharge through ET_g. The results show substantial seasonal variations in water table depth. The water table at the forested sites displayed a diurnal fluctuation at a depth of up to ~1.0 m, whereas the grassland site exhibited no diurnal fluctuations. For the two years studied, the estimated annual recharge at the sparse grassland site (49–56% of net rainfall) was larger than that at the pine plantation (31–49% of net rainfall), which in turn was larger than that at the banksia woodland (21–36% of net rainfall). The annual cumulative ET_g rates estimated by the White method were higher in the pine plantation than in the banksia woodland, with an average daily ET_g of 2.9 mm d^{-1} in pine plantation and 1.6 mm d^{-1} in banksia woodland for a total of 169 days during hydrological years 2012 and 2013.

The results from this study suggest recharge in the shallow sandy aquifer is dominated by early wet season rainfall but restricted by wet antecedent soil moisture conditions when the water table approaches the soil surface. Groundwater evapotranspiration was largely driven by meteorological variables, but also moderated by depth to water table. Considering the similar net annual recharge (gross rainfall minus ET_g) between the pine plantation and banksia woodland, which is much lower than net annual recharge at the

grassland, the conversions from native vegetation to exotic pine plantations may reduce the local water yields and lower the groundwater level in these areas, especially during the dry seasons and years. Future work will expand upon this study by examining total tree water use to better understand the hydrological effects of vegetation cover changes in shallow sandy aquifer systems.

Chapter 5. Quantifying Spatiotemporal Dynamics of Root-zone Soil Moisture in a Mixed Forest on Subtropical Coastal Sand Dunes Using Surface ERT Combined with Spatial TDR

5.1 Introduction

In sandy coastal environments, forests can significantly affect a catchment's water balance, e.g., through evapotranspiration (*ET*) and patterns of infiltration and groundwater recharge (Bosch and Hewlett, 1982; Zhang et al., 2001; Ford et al., 2011). The latter is mainly a result of rainfall interception by the canopy and soil water extraction by roots. Characterizing the spatiotemporal dynamics of root-zone soil moisture is essential to understand its effect on local hydrology (Vereecken et al., 2008, 2013). A detailed study of spatiotemporal heterogeneity and drivers of root-zone soil moisture dynamics is also necessary for appropriate design and calibration of soil-vegetation-atmosphere models (Western et al., 2003). Nevertheless, quantitatively evaluating spatial and temporal evolutions of subsurface moisture content with high spatial and temporal resolution remains challenging in practice (Jayawickreme et al., 2008).

Time domain reflectometry (TDR) and capacitance probes are commonly used to measure soil moisture in shallow soils (Schwartz et al., 2008; Calamita et al., 2012; Beff et al., 2013). However, these methods only provide information about a relatively small volume of soil (often limited to tens of centimeters around the sensors). Monitoring larger-scale moisture distribution for water balance purpose using a network of such point-scale moisture sensors is expensive and intrusive. Airborne remote sensing methods are useful to detect soil moisture distribution at regional scale, but its investigation depth is restricted to a few centimeters and the spatial resolution is too coarse (Robinson et al., 2012). At intermediate scales (decameter to hectometer), geophysical techniques, such as electromagnetic induction (EMI), ground penetrating radar (GPR) and electrical resistivity tomography (ERT), have proven to be promising alternatives to infer soil moisture down to several meters (e.g., Huisman et al., 2003; Brunet et al., 2010; Robinson et al., 2012; Steelman et al., 2012; Brillante et al., 2014).

Surface ERT is a noninvasive tool to produce two- or three-dimensional (2D or 3D) variations of the subsurface electrical resistivity, which can be related to variations of soil moisture content (Zhou et al., 2001). It has been widely used for hydrological investigations, *e.g.* water infiltration (e.g., Michot et al., 2003; French and Binley, 2004;

Lehmann et al., 2013), potential recharge (Schwartz and Schreiber, 2009) and groundwater fluctuation (Yamakawa et al., 2012). Recently, it has also been deployed to explore vegetation and soil moisture interactions. For example, Jayawickreme et al. (2008, 2010) identified large difference in soil moisture distributions beneath adjacent forest and grassland biomes. Surface ERT has also been used to monitor spatial and temporal water uptake by agricultural crops, e.g., corn (Beff et al., 2013) and sorghum (Srayeddin and Doussan, 2009). However, no studies have used time-lapse surface ERT to directly compare seasonal root-zone soil moisture dynamics under forests in response to rainfall redistribution and root water uptake at the tree scale, especially in subtropical coastal environments.

Linking ERT resistivity data and soil moisture content requires the knowledge of petrophysical relationships. These empirical relationships are mostly determined from laboratory calibrations with field-collected soil samples. Uncertainty is introduced due to the relatively small sample size and the altered conditions in soil structure and pore water salinity during laboratory experiments. Although field-calibrated relationships at the scale of ERT measurements are more reliable, only a few point measurements of moisture content from shallow soil depths are typically applied in relatively large model blocks to correlate electrical resistivity with moisture content. This may not be accurately representative of spatially average soil moisture in the model block. Spatial TDR is a novel method potentially providing the required high spatial resolution soil moisture dynamics. Spatial TDR determines continuous one-dimensional (1D) moisture content profiles along elongated probes, based on the inversion of TDR reflectograms. Scheuermann et al. (2009) tested a spatial TDR system with 3-m-long flexible flat ribbon cables as probes inside a full-scale dike model composed of uniform fine sands. They found the spatial TDR was able to determine moisture distributions with a spatial resolution of about ±3 cm and an average absolute deviation of ±0.02 cm^3 cm^{-3}.

In this paper, we quantified soil moisture dynamics in response to rainfall redistribution and water uptake by roots under three adjacent vegetation covers in a mixed sand dune forest by combining two different geophysical methods (surface ERT and spatial TDR). In subtropical coastal Australia, changes in vegetation cover frequently occur with development and land use change. We would like to establish a methodology which will enable us to better assess and understand the potential hydrological impacts of such changes, particularly those related to sustainable groundwater yields. For our subtropical, sandy environment, the primary objectives are to: (1) evaluate and validate the capability

of spatial TDR and surface ERT to monitor 1D/2D moisture distributions in sandy forest soils; (2) explore and compare seasonal dynamics of subsurface soil moisture under various vegetation types; and (3) investigate how rainfall redistribution by canopy and root water uptake affect the spatial distribution of root-zone moisture content and subsequent deep drainage.

5.2 Materials and methods

5.2.1 Site description

Field observations were carried out in a sand dune area covered by open mixed forests mainly consisting of exotic slash pine (*Pinus elliottii* Engelm), native wallum banksia (banksia *aemula* R.Br.) and understory grass (*Lomandra elongata* Ewart) on North Stradbroke Island (Figure 1.1). A detailed site description is presented in the overview of study sites in Chapter 1. Over the one-year study period (November 2012–October 2013), the total annual rainfall amounted to 2200 mm (Figure 5.1), which was higher than the long-term annual rainfall of 1600 mm (Australian Bureau of Meteorology). The depth to water table varied between 8.42 m and 9.63 m during the study period (Figure 5.1), with largest depth to water table occurring just before the onset of rainy period (end of January), and smallest depth to water table in middle April. The sandy aquifer mainly consists of unconsolidated fine-grained sands based on soil-texture observations in three boreholes collected below the ERT transect after the geophysical surveys (Table 5.1).

Table 5.1 Physical analyses of soil particle size distribution, bulk density (BD), saturated moisture content (θ_s) and saturated hydraulic conductivity (K_s) for soil samples from the field site. Soil properties were determined using intact samples from sand pits in upper 1.5 m of soil but using disturbed samples in lower 2.5 m of soil.

Depth (m)	Particle size distribution (%)			BD (g cm^{-3})	θ_s (cm^3 cm^{-3})	K_s (m d^{-1})
	50-100 µm	100-250 µm	250-500 µm			
0.2	29.0	60.5	10.5	1.42	0.33	2.54
0.5	34.1	57.5	8.4	1.45	0.31	1.68
1.0	17.2	68.4	14.4	1.51	0.29	1.10
1.5	31.6	59.8	8.6	1.52	0.28	1.57
2.0	43.9	44.9	11.2	1.55	0.31	2.06
3.0	18.8	65.3	15.9	1.50	0.28	2.34
4.0	24.7	64.6	10.7	1.56	0.30	1.33

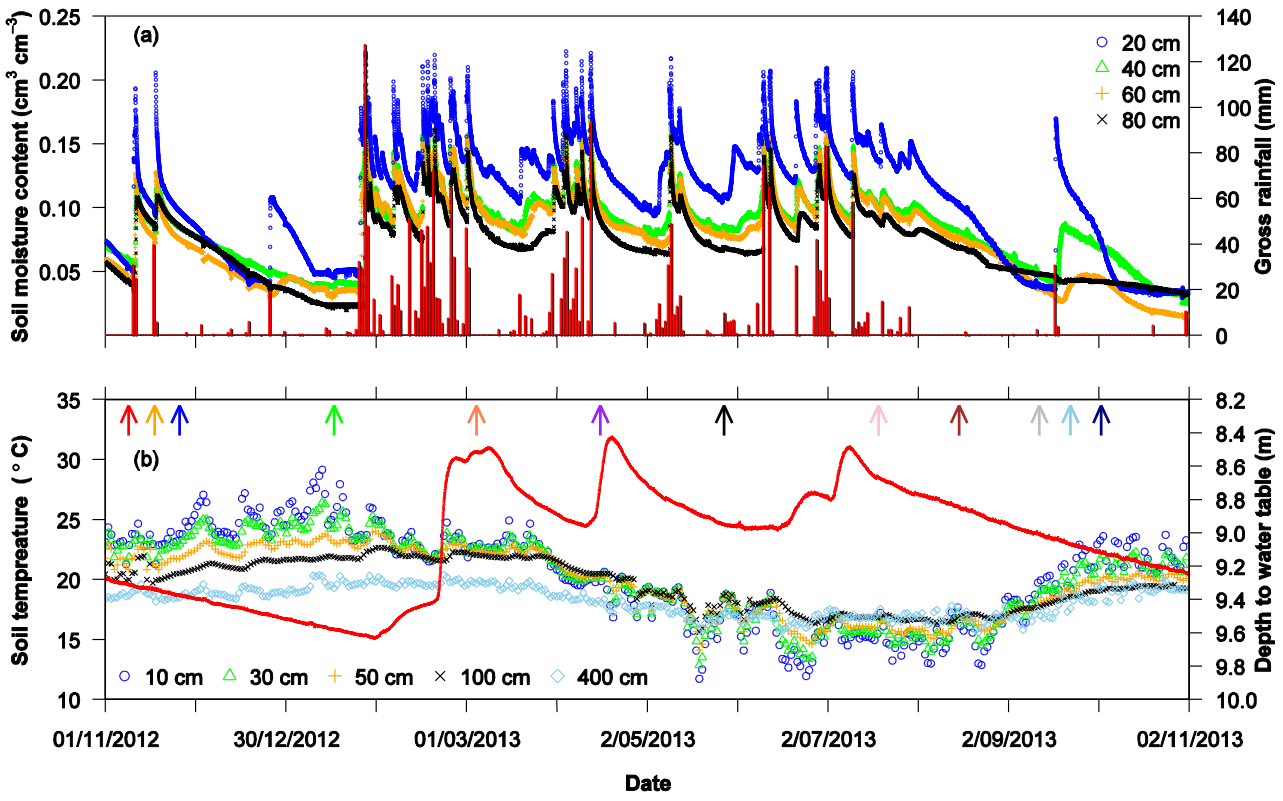

Figure 5.1 (a) Soil moisture content at four depths and daily gross rainfall over the study period; (b) soil temperature at five depths and water table fluctuation. Dates for surface ERT and spatial TDR measurements were indicated by colored arrows.

5.2.2 Surface electrical resistivity tomography

5.2.2.1 Data acquisition

Between November 2012 and October 2013, 18 surface ERT surveys were conducted using a ten-channel SYSCAL Pro Switch resistivity meter (IRIS Instruments, France), of which 12 were presented here showing the seasonal soil moisture cycle (Figure 5.1). During this period, a total of 48 electrodes were permanently installed along a gentle slope (~12 degrees) on the sand dune, regularly spaced at a horizontal interval of 0.5 m. The relative elevation of each electrode point was surveyed using a dumpy level and staff. The ERT transect along the downslope crossed a mixed pine-grass-banksia ecosystem (Figure 5.2). Two-dimensional measurements of apparent soil resistivity were acquired with classic electrode configuration of Dipole-Dipole to take advantage of its highest spatial resolution and better depth coverage (Samouëlian et al., 2005). All ERT surveys were carried out in both normal and reciprocal modes to assess data quality (Koestel et al., 2008). To reduce contact resistance between the electrode and the soil under dry climatic conditions, the soils within a few centimeters around the electrodes were slightly wetted. Each

measurement cycle contained 874 measurement points at 12 data levels with a maximum investigation depth of 4.0 m and took ~40 min to complete.

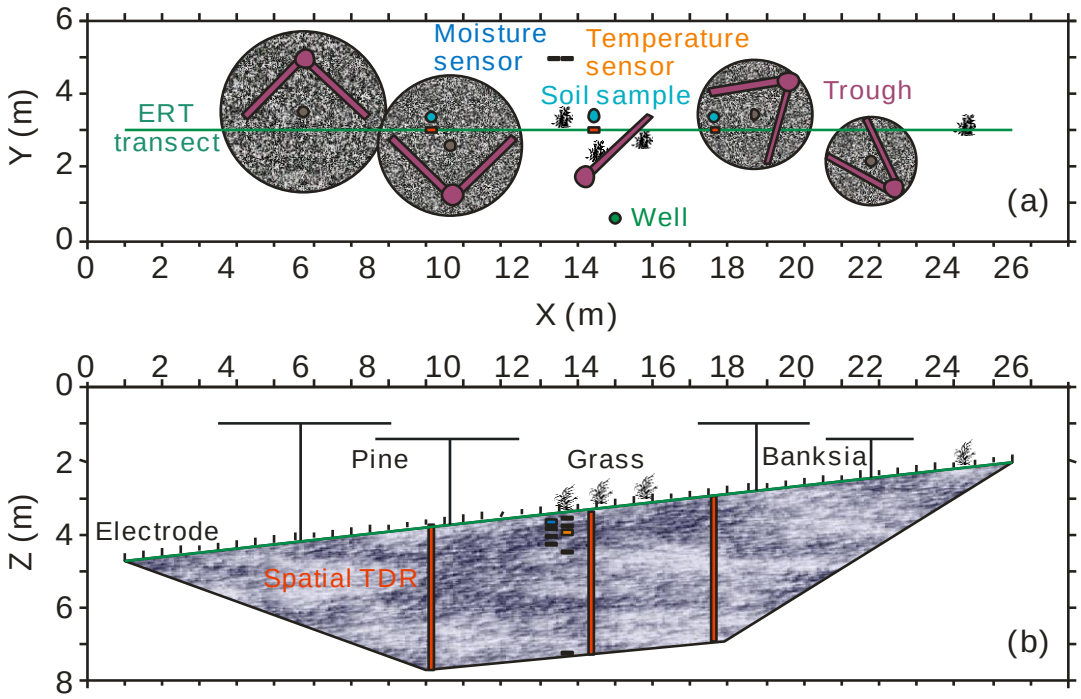

Figure 5.2 Scheme of experimental plot: (a) plan view and (b) elevation view, with positions of three contrasting vegetation types, ERT transect with 48 electrodes, three spatial TDR sensors, nine throughfall troughs, four moisture sensors, five temperature sensors and three soil sampling sites. The stippled circles represent the approximate tree canopy areas. Tree height was not scaled.

5.2.2.2 Data inversion

Prior to data inversion, the apparent resistivity data from the ERT measurements were filtered to remove noisy data. Data points with injected current less than 0.01 A or reciprocal errors larger than 5% were omitted from the inversion processes, which resulted in an elimination of 2% to 6% of measurement points collected from each dataset. To obtain the “true” subsurface resistivity distribution, we inverted the apparent resistivity data using the iterative tomographic inversion scheme of the RES2DINV software (Loke and Barker, 1995). To minimize artefacts produced by numerical inaccuracies from inverting each dataset separately, the time-lapse inversion method was applied which uses a common reference model to jointly invert datasets from different dates (Loke, 2013). We inverted the first dataset collected on 8 November 2012 to produce the starting and reference model for the subsequent time-lapse inversions. Inversions of the datasets typically converged after 3–5 iterations, indicated by a change in root mean square error

(RMSE) between consecutive iterations of less than 5%. Topographic corrections were also taken into account in the inversion processes. We used a finite-difference mesh with a width of half the unit electrode spacing and a height of 25 cm at the surface, increasing by 6% for each deeper layer, which produced a total of 394 model blocks.

5.2.3 Spatial time domain reflectometry

To correlate soil electrical resistivity with moisture content, one-dimensional (1D) soil moisture distribution along flexible flat ribbon cables was monitored. The flat ribbon cables (6-cm-wide and 1-mm-thin) were made of three copper wires covered with polyethylene insulation (Scheuermann et al., 2009). In June 2012, three spatial TDR with 4-m-long flat ribbon cables were vertically installed in the soil along the ERT transect to ensure the comparability of surface ERT and spatial TDR (Figure 5.2). To achieve this, boreholes (D=12.5 cm) were drilled down to a depth of 4.0 m using a hand auger. The flat ribbon cables were manually pushed against on one side of the augered boreholes. The coaxial cable, which was connected with the bottom end of the flat ribbon cable, was placed on the opposite side of the boreholes to avoid disturbance to the sensitive area of flat ribbon cables. To maintain original soil material and similar density for each soil layer, the boreholes were backfilled at 50 cm intervals with retrieved sands from corresponding layers. We started the spatial TDR measurements after a series of heavy rainfall events and a dry period in 2012, allowing the backfilled sands to consolidate naturally.

Spatial TDR measurements were performed from both ends of the flat ribbon cables to improve the spatial resolution. Through a multiplexer (SDMX50 Campbell Scientific), the flat ribbon cables were connected to a TDR device (Campbell Scientific TDR100) with two coaxial cables at ends of the flat ribbon cables. Spatial TDR data were acquired immediately after each ERT survey. The measured TDR signal was subsequently processed into spatial distributions of the permittivity and the volumetric moisture content along the individual cables using the reconstruction algorithm of Schlaeger (2005). Each reconstruction process took about three minutes to complete. Moisture content readings with spatial TDR were calibrated in the laboratory by the field-collected soil samples using Topp's equation (Topp et al., 1980). Detailed information on the principle and inversion algorithm of the spatial TDR was previously presented by Scheuermann et al. (2009).

5.2.4 Petrophysical relationship between soil electrical resistivity and moisture content

Soil electrical resistivity depends on several soil properties, e.g., soil texture, pore water resistivity, moisture content, temperature and sometimes root biomass in vegetated soils (Samouëlian et al., 2005). The similar particle size distributions and bulk densities of the soil samples collected from different depths at three locations in the experimental area indicated that the study area was relatively homogeneous (Table 5.1). Here, we neglected the effect of pore water resistivity on soil resistivity since it was found relatively constant compared to the moisture content variation (Michot et al., 2003; Brunet et al., 2010; Jayawickreme et al., 2010).

Comparisons of electrical resistivity measurements require the expression of the electrical resistivity at a reference temperature, because temperature variations in the soil influence soil electrical resistivity. During experiments, the daily soil temperature varied on the surface from 12 to 29 °C and at 100 cm depth it varied from 16 to 23 °C (Figure 5.2). At 400 cm depth, it remained ~19 °C throughout the year due to the delayed response of deep soil temperature to surface air temperature. Seasonal temperature variations over depth were evident during the ERT surveys, indicating that temperature correction was necessary. We assumed the temperature to be laterally uniform and temperature distribution was linearly interpolated over depth. To account for temperature effects, we corrected resistivity values after ERT data inversions with the equation by Keller and Frischknecht (1966) at a reference temperature of 25 °C:

$$\rho_{ref} = \rho_{soil}\left[1+\alpha\left(T_{soil}-T_{ref}\right)\right] \tag{5.1}$$

where ρ_{ref} (Ω m) is the corrected resistivity at a reference temperature T_{ref} (℃), usually 25℃; ρ_{soil} (Ω m) is the inverted resistivity at soil temperature T_{soil} (℃) and α is the correction factor, equal to 0.025.

The petrophysical relationship linking electrical resistivity to moisture content was then applied to ρ_{ref} at 25 ℃, using the simplified Archie's law (Yamakawa et al., 2012):

$$\rho_{ref} = A\theta^{-n} \tag{5.2}$$

where θ (cm^3 cm^{-3}) is the soil moisture content, A is the empirical coefficient and n is the saturation exponent.

To estimate the fitting parameters, the temperature-corrected resistivities from ERT surveys were plotted against the moisture content values retrieved from spatial TDR

during the first six surveys, while the spatial TDR measurements from the remaining surveys were used to validate the ERT-derived moisture content. For each measurement, soil moisture data along spatial TDR cables were spatially averaged over each corresponding block depth of the inversion model to make the soil moisture and resistivity spatially comparable. Two relationships were developed here to account for the effect of roots on soil resistivity measurements. The soil profile was thus divided into two layers: sand-root layer (0–100 cm) and sand layer (100–400 cm), considering the majority (> 90% of root biomass) of tree roots were found located in the upper 100 cm soil layer.

5.2.5 Additional measurements

The study site was equipped with a weather station located in a nearby clearing, which recorded gross rainfall, air temperature, relative humidity, solar radiation, wind direction and speed. To obtain net rainfall under tree canopies and in between trees, throughfall was collected using 9 U-shaped troughs connected to 5 HOBO RG3 tipping-bucket rain gauges (Onset Computer Corp., Bourne, USA). The troughs were made of split UPVC pipes, 2.5 m long by 0.1 m wide (Figure 5.2). All the tipping-bucket rain gauges were calibrated to 0.2 mm per tip in the lab and recalibrated after deployments in the field (Llorens et al., 1997). Soil temperature was continuously logged with temperature sensors (type 107, Campbell Scientific, USA) at 10, 30, 50, 100 and 400 cm depths. Point-scale soil moisture was also continuously logged with four EC-5 moisture probes (Decagon Devices, Pullman, USA) at 20 cm, 40 cm, 60 cm and 80 cm depths (Figure 5.2).

5.3 Results and discussion

5.3.1 Monitoring 1D soil moisture profile using spatial TDR

Figure 5.3 presents several volumetric moisture content profiles along three spatial TDR cables under three vegetation covers. The continuous vertical distribution and seasonal evolution of soil moisture content were well captured by spatial TDR. The moisture profiles measured using spatial TDR sensors under the pine, grass and banksia showed similar patterns but the magnitude varied as a function of depth and vegetation. Generally, higher moisture content was observed under grasses than pine and banksia trees, particularly in the upper 200 cm of soil.

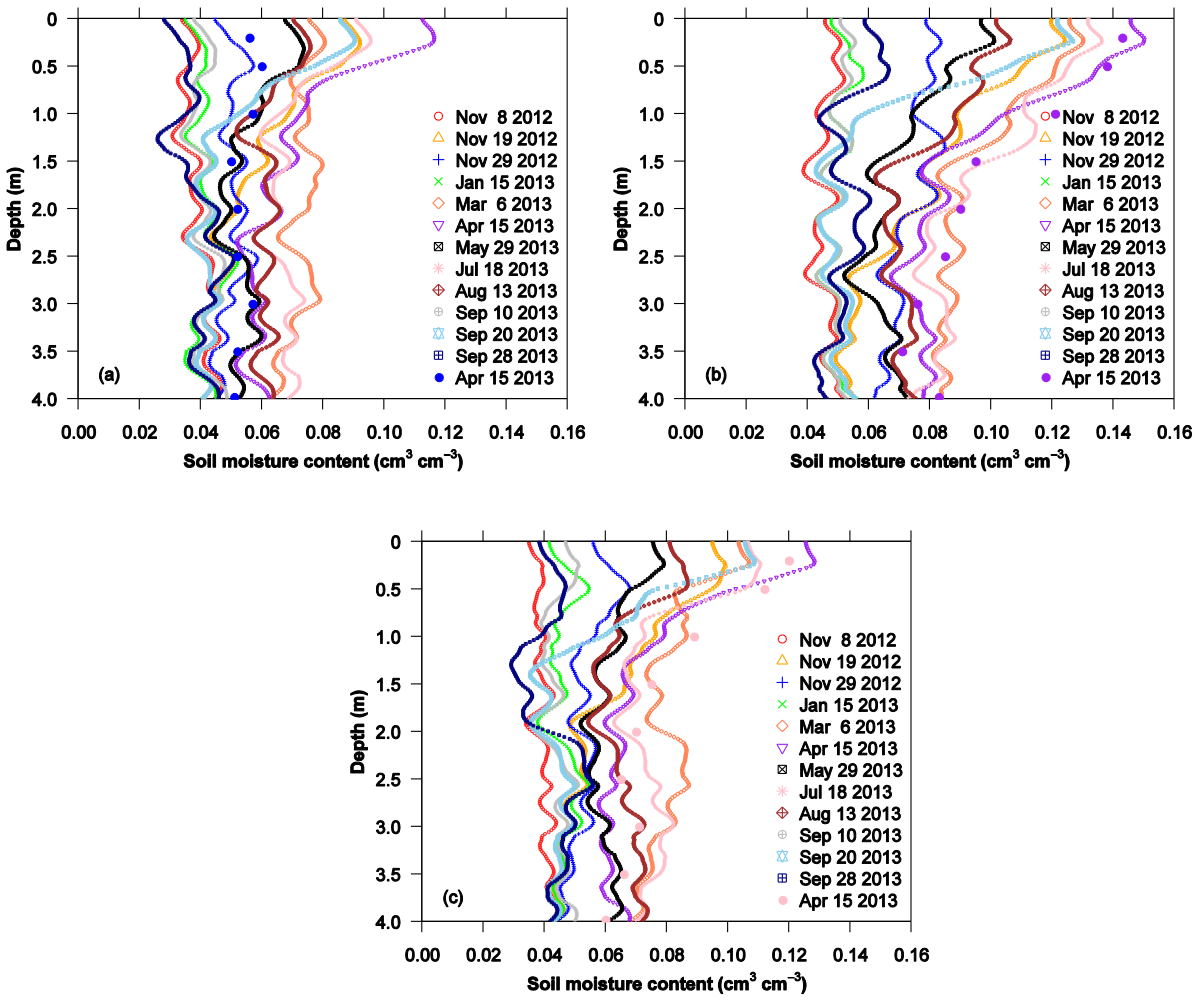

Figure 5.3 One-dimensional soil moisture content profiles along three spatial TDR sensors at different dates under three contrasting vegetation types: (a) pine, (b) grass and (c) banksia. Next to the spatial TDR data, point-scale moisture content values (solid circles) from soil sampling at three different dates are shown.

At the beginning of the spatial TDR measurements (8 November 2012), all three monitored profiles exhibited a similar and relatively low soil moisture (~0.04 cm^3 cm^{-3} averaged over 0–400 cm depth). For all vegetation types, an increase of soil moisture content was observed on 19 November 2012 after three rainfall events, but moisture content tended to decline to initial values following a dry period until 20 February 2013. The rates of increase and decrease in moisture and amplitude varied depending on the vegetation type. During the wet season, soil moisture was significantly replenished, ranging from 0.09 cm^3 cm^{-3} to 0.15 cm^3 cm^{-3} in the upper 100 cm soil and from 0.06 cm^3 cm^{-3} to 0.09 cm^3 cm^{-3} in the lower layer. However, soil moisture was further depleted following the later dry period starting 10 September 2013. Between the first (8 November 2012) and the last (28 September 2013) spatial TDR surveys, soil moisture content in the whole soil profile was close to each other (Figure 5.3).

To evaluate the performance of spatial TDR measurements in the field, we compared continuous moisture content profiles measured by spatial TDR sensors with point-scale volumetric moisture content obtained with soil sampling at different depths (Figure 5.3). Generally, the soil moisture profile was captured by spatial TDR. The maximum absolute deviation was less than 0.02 cm^3 cm^{-3}, which was consistent with the accuracy by Scheuermann et al. (2009). Some difference was expected since the soil sampling sites were 0.3 m from the locations of spatial TDR sensors. The undulations in the measured moisture content profiles are most likely caused by the differences in the density of different backfilled soil layers. No obvious undulations were identified by Scheuermann et al. (2009) in their homogeneously constructed dike model probably because the spatial TDR sensors were installed in uniform sands compared with our less uniform sands in the natural sand dune environment.

Installation of soil moisture sensors in vertical boreholes is likely to change the soil structure and properties, which may produce preferential flow and not be representative of natural soil moisture measurements (Dahan et al., 2007). For unconsolidated fine sands in this study, although slight changes in soil density is expected, it is possible to allow soils being measured in a minimally disturbed condition after soil reorganization naturally. However, a proper installation method is required for other heavy-textured materials to permit soil to be measured with minimum disturbance (Scheuermann et al., 2009). Dahan et al. (2007) developed a technique for the attachment of capacitance probes on flexible sleeves, which was inserted into angled boreholes and filled with liquid resin to press the sensors against the borehole walls. This method could be applicable for installation of our flat ribbon cables in the slanted boreholes.

5.3.2 Mapping spatial variation of soil electrical resistivity using surface ERT

Figure 5.4 presents the spatial variations of the temperature-corrected soil electrical resistivity monitored during various ERT surveys. The data inversion models produced generally lower error statistics (RMSE<2%) during the wet season than those during the dry season (RMSE=2%–4%) most likely due to the better soil conductivity. A spatial heterogeneity of resistivity was observed under the three vegetation covers. Generally, the resistivities taken under pine trees were higher than these under grasses and banksia. These differences were particularly evident during the dry periods.

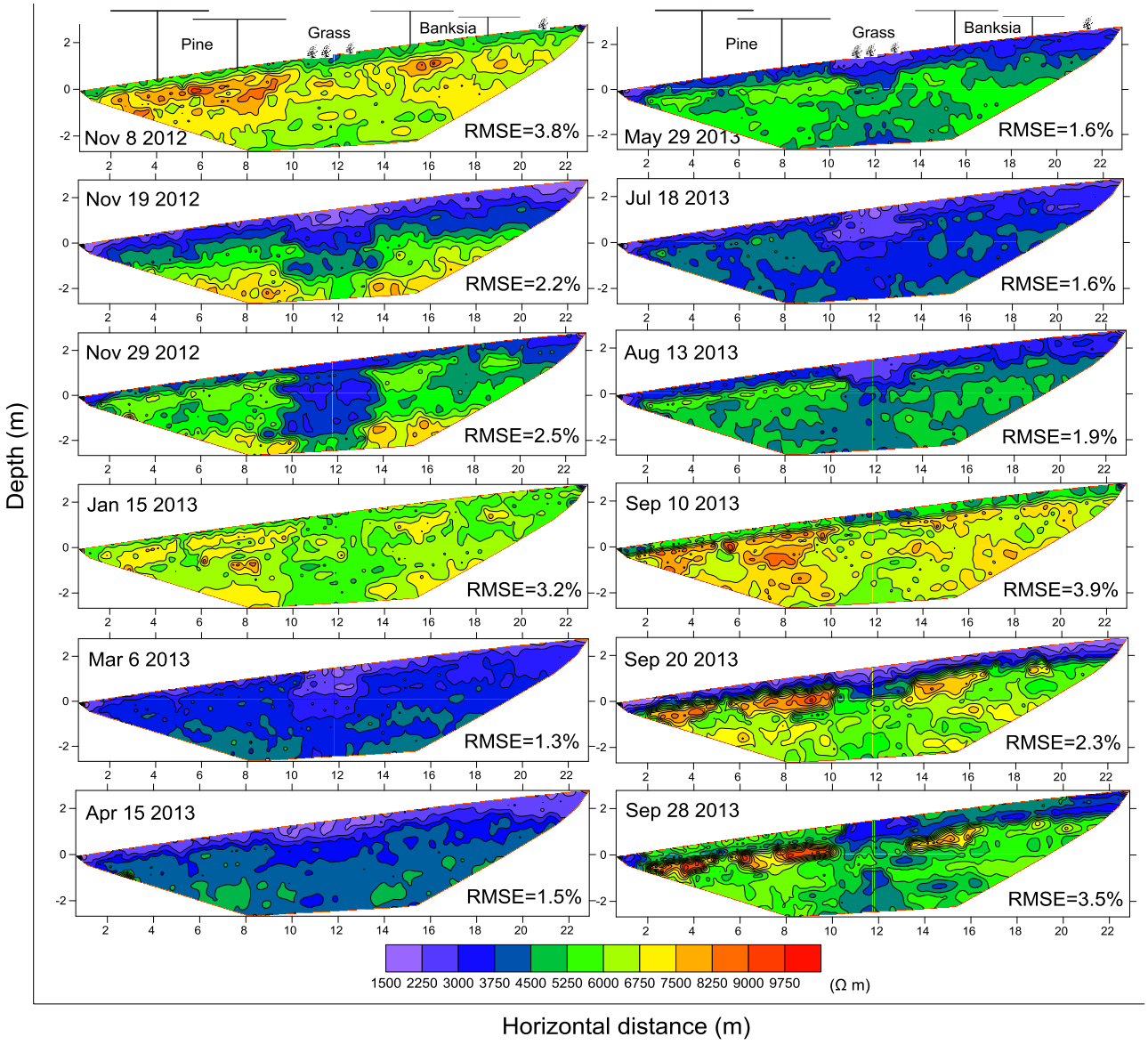

Figure 5.4 Spatial variations of the temperature-corrected soil electrical resistivity monitored during various ERT surveys.

Very high electrical resistivity was observed at the beginning of the ERT surveys, ranging between 5000 Ω m and 9000 Ω m. Specifically, the higher resistivities persisted deeper (~3 m) under the pine trees than the other vegetation types. A similar pattern was observed for banksia but restricted to the top 1.5 m. On 19 November 2012, regions with resistivity < 4000 Ω m were observed in the upper soils and resistivity in other areas of the soil fell inside the range of approximately 4000 to 5000 Ω m. On 29 November 2012, regions with resistivity < 3700 Ω m were observed under the grasses in the middle part of the soil profile. On 15 January, resistivity values in most of the soil profile region were between 5500 Ω m and 6500 Ω m, although patchy anomalies with higher resistivity (> 7500 Ω m) were still observed under the pine tree. During the rainy season, much lower soil electrical resistivity was observed, particularly in the upper 1 m soil layer (< 2500 Ω m),

indicating the effect of rainfall on soil resistivity. Contrarily to the top layer, the electrical resistivity was slightly higher at greater depth (2500–4000 Ω m). On 29 May and 13 August 2013, the resistivity profiles were almost the same with lower resistivity near the surface. On 10 September 2013, similar resistivity distribution was observed as that at the beginning of the measurements. During the last two ERT measurements, relative uniform resistivities (4500–5500 Ω m) were observed within the whole soil profile, except for the lower resistivity near the surface and patches of extreme resistivity zones observed under pine trees.

5.3.3 Conversion of soil electrical resistivity into moisture content

We used the temperature-corrected electrical resistivity data and soil moisture from spatial TDR to establish the site-specific relationships between the two variables for two soil layers (Figure 5.5). For the sand-root layer (layer 1, 0–100 cm) and the sand layer (layer 2, 100–400 cm), we obtained slightly different petrophysical relationships with the parameters of the simplified Archie's model. The optimized parameters were A=218.9, *n*=1.068 for layer 1 and A=172.4, *n*=1.175 for layer 2. The determined parameter *n* was within the low range of typical values (1.0 to 2.7) for unconsolidated sands (Ulrich and Slater, 2004). The fit for Archie's law in the first layer (R^2=0.921, RSME=0.013, *n*=54) is slightly better than the second layer (R^2=0.851, RSME=0.019, *n*=162). These correlations suggest that surface ERT can be used to quantitatively evaluate temporal variations in moisture values using the field-calibrated relationships between soil moisture and resistivity values.

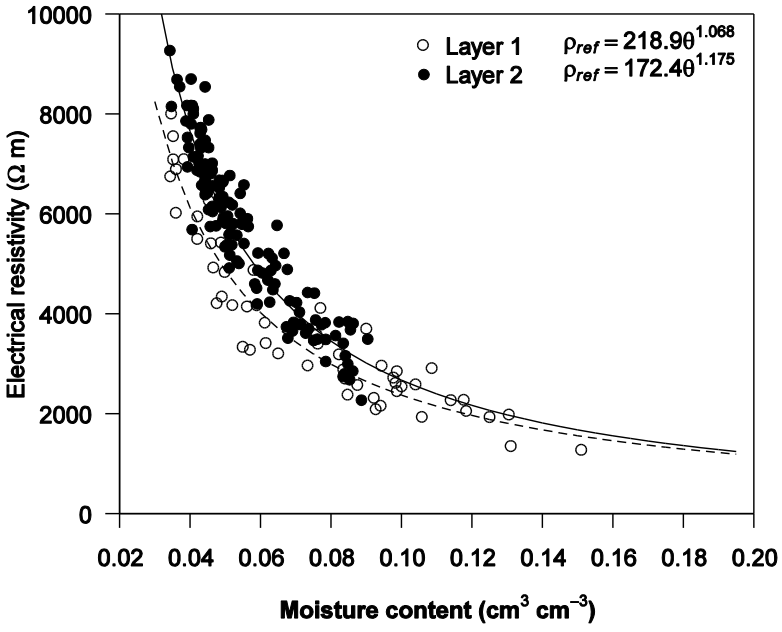

Figure 5.5 Relationship between soil electrical resistivity (ρ_{ref}) and spatially averaged moisture content (θ) obtained from spatial TDR for the sand-root layer (layer 1) and the sand layer (layer 2).

As expected, soil electrical resistivity decreases as moisture content increases. For moisture content < 0.10 cm^3 cm^{-3}, the electrical resistivity rapidly decreases with increasing moisture content. However, at high moisture contents (> 0.15 cm^3 cm^{-3}) only very little change in resistivity is observed when soil content increases or decreases, which indicates accurate estimation of higher moisture content can be difficult using the petrophysical functions. As found by other laboratory and field studies (Fukue et al., 1999; Michot et al., 2003; Samouëlian et al., 2005), the moisture content threshold between low and high electrical resistivity variation was around 0.15–0.20 cm^3 cm^{-3}. However, the natural soil moisture in the sand dunes during ERT surveys generally changes at small and medium moisture contents (0.03–0.15 cm^3 cm^{-3}) compared with saturated moisture content of ~0.30 cm^3 cm^{-3}. Additional moisture measurements at shallow soil depths confirmed moisture content seldom exceeded 0.20 cm^3 cm^{-3} due to low water holding capacity and fast percolation (Figure 5.1).

The first soil layer exhibited larger variations of soil moisture than the second soil layer. The measured resistivity at the same moisture content for the first horizon is smaller than that for the second layer, especially at the high resistivity range, indicating the effect of roots on soil resistivity measurement. This was consistent with the finding by Amato et al. (2008) who found that root biomass exerted more effect at high resistivity, and at lower values the response of resistivity to roots was too weak to be discriminated from the effect of variations of other soil properties. Beff et al. (2013) found no obvious improvement on calibration of petrophysical functions when splitting the data into that with and without the presence of roots. In contrast, Werban et al. (2008) observed two distinct petrophysical relationships in presence or absence of lupine fine roots. Plant roots can potentially affect the soil resistivity measurements due to the high water content and solute concentrations in root xylem (Nadler and Tyree, 2008). However, the major root surface area, especially for large mature tree roots, is considered relatively non-conductive (Furman et al., 2013), and root biomass and volume only account for a small fraction of the root zone area. Thus, we presume that the conductivity of larger roots in our study played a relatively less significant role on soil electrical resistivity compared with the more conductive finer roots of lupine.

5.3.4 Quantifying 2D distribution and seasonal evolution of soil moisture content

Two-dimensional soil moisture distributions over time were determined using the temperature-corrected ERT sections and the petrophysical relationships for the two soil layers. Differences in spatial moisture distribution under various vegetation types and seasonal root-zone moisture content were obvious during the study period (Figure 5.6). The root-zone soil was very dry during the two dry periods (November 2012 to January 2013, August to October 2013) but replenished by rainfall events during the wet season (February to July 2013), with an average wet-season moisture content of ~0.09 cm^3 cm^{-3} in the whole soil profile. Two-dimensional soil moisture distributions showed distinct variations in the moisture content between the three vegetation covers, with relatively lower moisture content under pine trees than those under grasses and banksia.

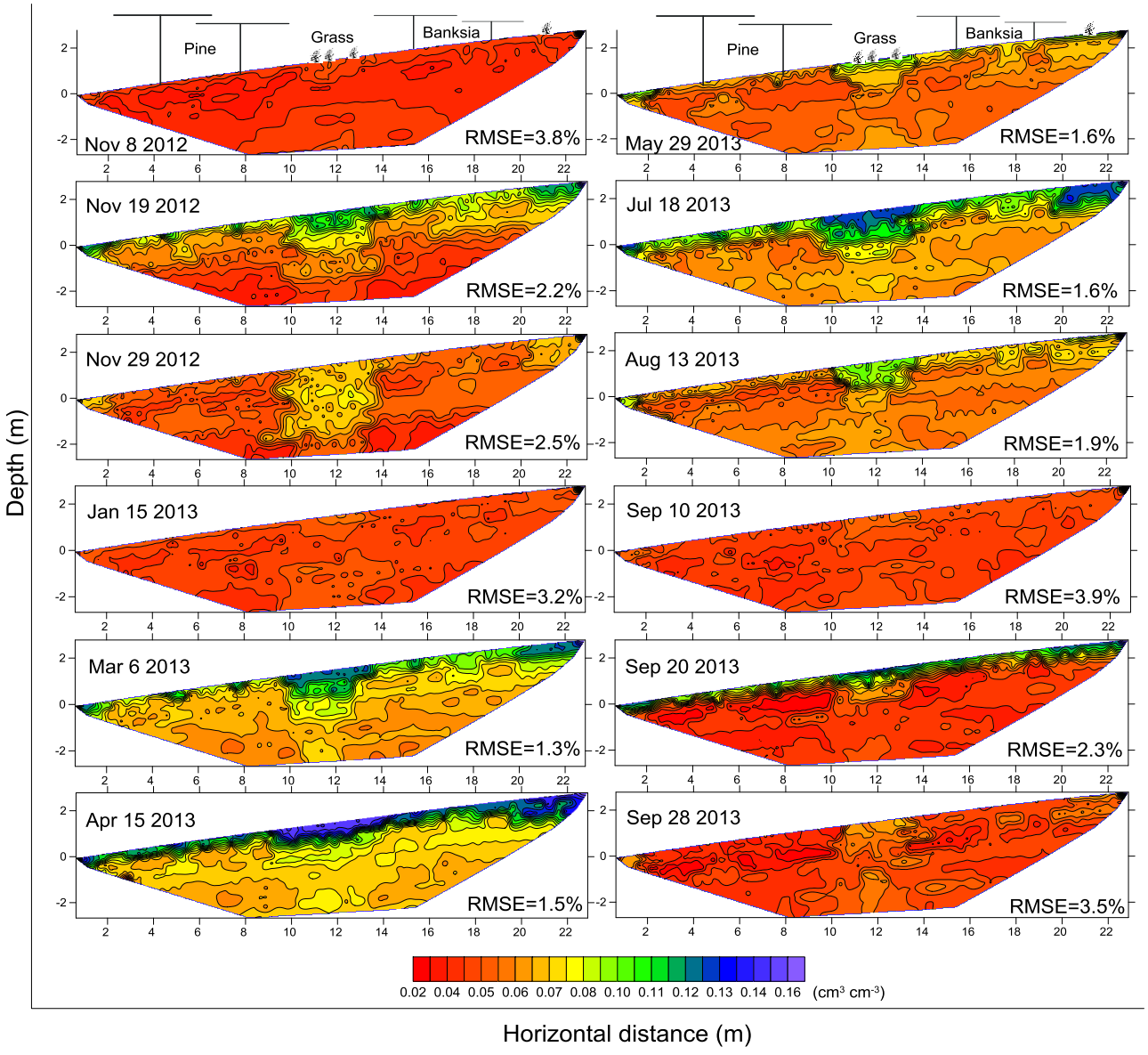

Figure 5.6 Spatial variations of the soil moisture content monitored during various ERT surveys.

At the beginning of the ERT campaign (8 November 2012), following a dry period from August to October in 2012, the estimated moisture content across the site was quite low and relatively uniform, averaged at ~0.04 cm^3 cm^{-3}. After three rainfall events (total rainfall 100 mm), the moisture content was partly replenished, mainly in the upper 1.5 m of soil. The moisture content then gradually declined until the end of this dry period, prior to the beginning of the wet season. A series of high intensity rainfall events over the next month (total rainfall 300 mm) significantly replenished the soil, ranging from 0.08 cm^3 cm^{-3} at a depth of 4.0 m to 0.15 cm^3 cm^{-3} at soil surface. During this period, a large portion of rainfall percolated through the vadose zone, reached the water table and recharged the groundwater (Figure 5.1). The moisture content stayed high over the subsequent four months due to replenishment by periodic rainfall events, with highest moisture content in the middle of April 2013. Two months later, following a further dry period, moisture content significantly decreased, particularly at the top layers (1 m). At the end of the ERT measurements, the moisture content declines towards its initial state, except for the surface moisture which was due to a recent rainfall event. From the above results, soil moisture can be fast replenished after rainfall events and percolate down due to high hydraulic conductivity and low water holding capacity of the sands.

Both spatial TDR and surface ERT enables the measurements of moisture content of sandy forest soils at high spatial and temporal resolutions down to a depth of 4 m, which is the maximum rooting depth for the majority of vegetation types (Canadell et al., 1996). This capability makes it very useful for the detection of root zone processes and predicting the deep drainage in forested ecosystems. With spatial TDR measurements, the dynamics of continuous soil moisture distribution can be successfully monitored with high spatial resolution and accuracy, but the distribution is limited to one dimension. It is therefore advantageous to combine spatial TDR with surface ERT measurements to quantify the spatial distribution of soil moisture at a larger scale (both laterally and in depth) since they can complement each other. Surface ERT would help guide the installation location of point-scale soil moisture sensors (e.g., at canopy and intercanopy areas) to obtain better mean estimation of soil moisture balance in the forested ecosystems.

5.3.5 Effect of rainfall redistribution and root water uptake on soil moisture heterogeneity

To obtain a better understanding of the effects of rainfall redistribution by canopy and water uptake by roots on soil moisture variability and the potential of this monitoring approach, we quantified the differences in 2D soil moisture during two short-term (~10 d)

wetting and drying cycles (Figure 5.7), i.e., W1 (8 to 19 November 2012, rainfall=100 mm), D1 (19 to 29 November 2012), W2 (10 to 20 September 2013, rainfall=30 mm) and D2 (20 to 28 September 2013).

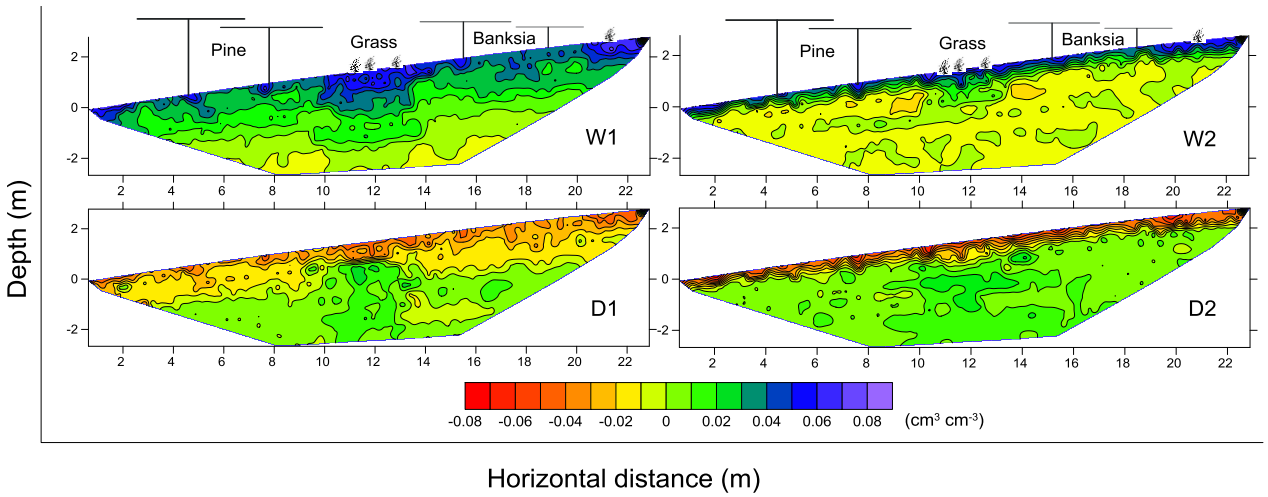

Figure 5.7 Two-dimensional soil moisture evolutions during wetting and drying cycles: W1 (8 to 19 November 2012), D1 (19 to 29 November 2012), W2 (10 to 20 September 2013), and D2 (20 to 28 September 2013). Zero means no changes in the soil moisture content during the comparison period. Values above or below zero indicate an increase or a decrease in soil moisture content during each comparison period, respectively.

After a cumulative rainfall of 100 mm during W1 and 30 mm during W2, an increase of soil moisture in the soil profile was observed with surface ERT for both periods (Figure 5.7). The increase was mainly located under grasses, followed by banksia and pine trees. Specifically, the differences in water storage of the whole soil profile during W1 were 67 mm, 92 mm and 73 mm under pine, grassland and banksia trees, respectively. The corresponding values during W2 were 14 mm, 24 mm and 19 mm, respectively. Considering the evapotranspiration and deep drainage was minimal during these dry periods due to low soil moisture level in the soil profile (~4%), these differences were most likely due to the surface water input. Similar to finding by (Fan et al., 2014), the pine tree intercepted more rainfall (24.3% of gross rainfall) than the banksia tree (18.5% of grass rainfall), while the rainfall interception by the grasses was negligible (1.4% of gross rainfall). The reduced amount of infiltrating rainwater under the trees was thus ascribed to their higher interception losses. However, a locally higher increase in soil moisture was identified around all tree trunks except for one banksia tree, reaching similar levels of moisture content to that under the grasses. This was similar to findings by Michot et al. (2003) who identified preferential infiltration of rainwater under corn plants caused by stemflow. They found the preferential infiltration tended to homogenize the moisture under

the corn row and under the inter-row when a significant rainfall occurred. However, the relatively small portion of stemflow water for our trees and rainfall was insufficient to compensate for the water loss by large tree roots around the tree stem. No localized increase was found around the grasses due to limited stemflow. No increase in soil moisture was identified around the base of one banksia tree likely due to the ERT transect being located 0.8 m from its trunk. The ERT suggests that stemflow is likely to affect a radius of less than 0.5 m from a tree trunk in sandy soils (Cattan et al., 2009; Nikodem et al., 2010).

During the drying periods D1 and D2, ET caused a decrease of moisture content in the soil profile. The differences in water storage throughout the soil profile during D1 were 47 mm, 13 mm and 35 mm under pine, grassland and banksia trees, respectively. The corresponding values during D2 were 10 mm, 5 mm and 13 mm, respectively. Since deep drainage was minimal during these periods due to the small rainfall events and thick vadose zone (4 m), these differences were ascribed to the ET processes. In the upper 1 m soil of the treed area, higher moisture depletion was observed around the tree trunks relative to the intercanopy area. This is similar to Michot et al. (2003) who also observed a higher decrease of moisture content under the corn rows due to root water uptake. However, Srayeddin and Doussan (2009) found the soil moisture decreased mainly under the inter-rows in the upper 1 m of soil, because the moisture content at the surface and under the corn rows was relatively low and moisture depletion occurred in the deeper zones and in the inter-row area. The soil moisture in the lower soil layers below the trees slightly increased (~0.01 cm^3 cm^{-3}), yet values at similar depths below the grassland exhibited a higher increase (~0.03 cm^3 cm^{-3}), indicating most of the infiltrating rainwater below the grassland drained deeper within the profile as a result of lower root water uptake by grasses and higher percolation rates due to higher initial moisture content.

Both spatial rainfall distribution (e.g., throughfall and stemflow) and root water uptake were influencing the patterns of moisture and its variation. Both rainfall interception and root water uptake reduce infiltrating water under trees and reduce potential recharge at our site. Vegetation cover change from native ecosystems (banksia and grasses) to pine plantation in the study area is likely to have reduced soil moisture content and the relatively lower percolation of rainwater through the root zone, would thus reduce the potential recharge in the underlying aquifer. However, a large portion of rainfall still percolated beyond the root zone following heavy summer storms and reached groundwater table due to the high saturated hydraulic conductivity (~180 cm d^{-1}) of our dune sands (Figure 5.1).

5.3.6 Comparison between soil moisture content obtained by surface ERT and spatial TDR

Soil moisture data measured by surface ERT and spatial TDR for the two soil layers during the last six surveys were compared in Figure 5.8. We obtain a reasonably good agreement between ERT-derived and TDR-derived moisture content values (layer 1: RMSE=0.0154 cm^3 cm^{-3}, R^2=0.88, *n*=54; layer 2: RMSE=0.0182 cm^3 cm^{-3}, R^2=0.73, *n*=162). This difference is similar to the error associated with the calibrated petrophysical relationships. The estimate precision quantified by RMSE indicates that the ERT-derived moisture content for the second layer is worse than that for the first layer, with a maximum absolute deviation of 0.03 cm^3 cm^{-3} for the bottom 100 cm soil layer. The larger differences between surface ERT than for spatial TDR measurements at the bottom layer can be largely explained by the decrease in resolution with depth of ERT signal and associated smoothing artifacts from inversion (Marescot et al., 2003). The mean error (ME) values of -0.0075 cm^3 cm^{-3} (layer 1) and 0.0043 cm^3 cm^{-3} (layer 2) indicated that surface ERT generally underestimated moisture content in the upper 100 cm of soil but slightly overestimated moisture content in the deeper layer. Brunet et al. (2010) compared the moisture content obtained from ERT with local measurements made with TDR at ten different times and found absolute deviations up to 0.05 cm^3 cm^{-3}. Michot et al. (2003) reported a RMSE of 0.036 cm^3 cm^{-3} and a ME of 0.0145 cm^3 cm^{-3} for their ERT-based estimates of moisture content. These studies introduced higher errors than what was observed in our study, indicating combining ERT and spatial TDR can improve the accuracy of moisture content estimation.

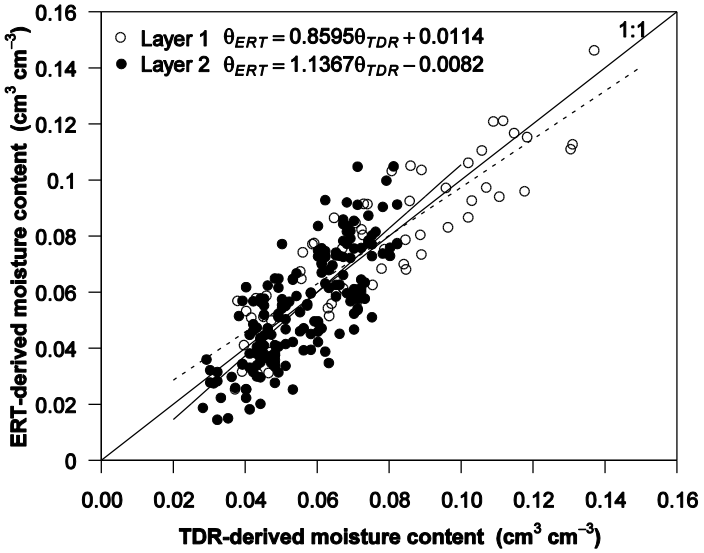

Figure 5.8 Comparison of moisture content derived by surface ERT (θ_{ERT}) and average moisture content measured by spatial TDR (θ_{TDR}) for the sand-root layer (layer 1) and the sand layer (layer 2) during the last six ERT surveys. The dashed and solid lines represent the linear regressions.

5.4 Conclusions

Geophysical instruments are becoming increasingly attractive for high-resolution investigation of subsurface flow processes with minimized disturbance to soils. In this study, we used 2D surface ERT combined with 1D spatial TDR to monitor root-zone moisture dynamics of sandy soils in a subtropical coastal environment. Spatial variation was primarily due to rainfall partitioning by vegetation and root uptake under three vegetation types at the site. The resulting 2D ERT images exhibited clear horizontal and vertical variations of soil electrical resistivity, which were quantitatively related to soil moisture content changes with in-situ calibrated petrophysical relationships using spatial TDR data. Soil moisture evolutions throughout the year were successfully identified by soil electrical resistivity changes. Temperature variations in the soil profile and root effects were both accounted for in the ERT data processing.

Analysis of field resistivity and moisture data between November 2012 and October 2013 confirmed the potential of surface ERT and spatial TDR for use in monitoring spatial and temporal soil moisture dynamics. Relative to traditional point-scale TDR probes, spatial TDR can provide continuous 1D moisture content measurements with high spatial resolution and accuracy (absolute deviation < 0.02 cm^3 cm^{-3}). With a series of continuous soil moisture profiles, percolation of wetting front throughfall the root zone can be well traced at high spatial resolution and the water percolation rates are thus better calculated. In comparison with spatial TDR, surface ERT gives 2D information integrated over a greater volume of soil. In our case, the measurements have reasonable accuracy (RMSE < 0.02 cm^3 cm^{-3}) compared with soil sampling methods. Combination of surface ERT and spatial TDR methods can improve the accuracy of soil moisture monitoring with a better spatial resolution than obtained separately or by point methods.

The rainwater infiltration after canopy redistribution, the drying out of the soil by root water uptake and the surface drainage of the soil moisture were successfully identified by joint use of surface ERT and spatial TDR methods. Soil infiltration and drainage were lowest under the pine trees due to higher rainfall interception and root water uptake. Better positioning of point-scale soil moisture sensors can be guided by surface ERT for soil

moisture balance estimates in heterogeneous forests. The rainfall interception by the canopy played a major role in redistribution of water at the soil surface before it infiltrated. The effect of the root uptake on deep drainage appeared to be limited in sands with high hydraulic conductivity under intensive rainfall in the wet season.

Chapter 6. Modelling Canopy and Root Effects on Soil Moisture and Deep Drainage in a Subtropical Coastal Forest

6.1 Introduction

Accurate representation of spatial and temporal groundwater recharge in groundwater models is necessary for effective water resources management (Assefa and Woodbury, 2013). Traditionally, most regional-scale groundwater models often simplify fundamental recharge processes in the vadose zone (Twarakavi et al., 2008), generally assuming recharge is a simple percentage of rainfall. For example, MODFLOW (Harbaugh et al., 2000), the most commonly used groundwater flow model, was originally designed with independent recharge and evapotranspiration (*ET*) packages (REC-ET packages), which defines a specified downward recharge flux to the groundwater and simulates discharge of water to evaporation and transpiration with a maximum *ET* rate and a *ET* extinction depth. The oversimplified representation of vadose zone flow appears to be arbitrary and subject to very large uncertainty because groundwater and surface water are in continuous dynamic interaction.

To better characterize vadose zone processes, three packages with different level of complexity have been recently developed for MODFLOW to couple groundwater and vadose zone models, i.e., the Variably Saturated Flow (VSF) package (Thoms et al., 2006), the Unsaturated Zone Flow (UZF1) package (Niswonger et al., 2006), and the HYDRUS package (Seo et al., 2007). Among them, the HYDRUS package appears more promising because it incorporates the one-dimensional Richards equation to reasonably represent vadose zone processes in groundwater models with balanced computational efficiency and accuracy. The water transfer within the soil-vegetation-atmosphere system is, however, more complex than is represented in lumped one-dimensional models, with spatial heterogeneity not only in vertical but all directions (Van Dam et al., 1997). As a prerequisite, the uncertainties of modelling water flow with simple one-dimensional vadose zone models compared to two- or three-dimensional models need to be determined in order to confidently model recharge.

Vadose zone soil moisture and water fluxes are influenced by interactions of the meteorological, vegetative and geological conditions. Vegetation acts as the primary link between the atmosphere and subsurface water as its canopy intercepts atmospheric water (primarily rainfall) before it reaches the soil surface, and its roots extract soil water for

transpiration. In forested ecosystems, water fluxes in the subsurface can vary spatially between the canopy and intercanopy zones. On the one hand, infiltrating rainwater is distributed unevenly due to canopy rainfall interception and partitioning into throughfall and stemflow (Raat et al., 2002; Keim et al., 2005; Liang et al., 2007, 2009; Fan et al., 2014). On the other hand, root water uptake is also spatially variable in the subsurface due to highly heterogeneous root distribution of woody species (Clothier and Green, 1994; Green and Clothier, 1999; Vrugt et al., 2001; Deb et al., 2013). These spatial phenomena have important hydro-ecological consequences because they significantly affect the magnitude and distribution of groundwater recharge and solute transport (Tanaka et al., 1996; Guswa and Spence, 2012; Nikodem et al., 2013).

Physically-based soil-vegetation-atmosphere models, e.g., HYDRUS (Radcliffe and Šimuunek, 2010), WAVES (Zhang and Dawes, 1998) and SWAP (Van Dam et al., 1997), are useful tools to improve our understanding of vegetation-related hydrological processes. The HYDRUS 1D and HYDRUS 2D models were used to simulate the soil water regime in a Podzol under a beech canopy, where considerably different infiltration fluxes were found due to stemflow and throughfall (Nikodem et al., 2010). The HYDRUS 3D program was used to simulate spatially distributed drainage fluxes accounting for throughfall and stemflow under banana plants (Sansoulet et al., 2008). Liang et al. (2009) also developed a 3D model and applied it to the simulation of water regime on the hillside, taking into account throughfall and stemflow. Vrugt et al. (2001) compared one-, two-, and three-dimensional root water uptake functions using HYDRUS packages. However, few modelling studies have been performed to quantify the combined effects of rainfall redistribution and non-uniform root systems on the spatial pattern of soil moisture and water percolation.

The general purpose of this work is to investigate spatial subsurface water flow associated with vegetation structure at the tree scale in a coastal sand dune forest of subtropical Australia, by taking into account the non-uniformity of surface rainfall due to canopy redistribution and the spatial position of roots. Specific objectives are: (1) to explore the variability of the rainfall redistribution across a canopy-intercanopy transect and the spatial root distribution at the tree scale; (2) to examine the spatiotemporal dynamics of the soil moisture and deep drainage across a canopy-intercanopy transect using calibrated HYDRUS 2D/3D model; (3) to investigate the effects of different model inputs of rainfall and root distributions on water fluxes estimation; and (4) to investigate how to appropriately represent the two-dimensional variation of vegetation structure in one-

dimensional models to obtain effective equivalent outputs, considering the canopy and intercanopy phenomena.

6.2 Materials and methods

6.2.1 Study area

Field observations were undertaken in a coastal sand dune area covered by open forests mainly consisting of exotic slash pine (*Pinus elliottii* Engelm) on North Stradbroke Island (Figure 1.1). A detailed site description is presented in the overview of study sites in Chapter 1. The extensive unconfined aquifer consists of fine-grained sands based on particle size distribution (Table 6.1).

Table 6.1 Soil physical properties and hydraulic parameters of soil water retention and conductivity functions (Van Genuchten-Mualem model) determined for four soil layers. Values in the parentheses indicate calibrated hydraulic parameters. *BD* is the bulk density of soils; θ_r and θ_s are the residual and saturated water contents; α and n are empirical parameters determining the shape of the hydraulic function; K_s is the saturated hydraulic conductivity and l is the pore-connectivity parameter.

Soil layer (cm)	50-100 µm (%)	100-250 µm (%)	250-500 µm (%)	*BD* (g cm^{-3})	θ_r (cm^3 cm^{-3})	θ_s (cm^3 cm^{-3})	α (cm^{-1})	n	K_s (cm d^{-1})	l
0–25	29.0	60.5	10.5	1.43	0.02	0.33	0.092 (0.127)	2.98 (2.08)	254 (325)	0.5
25–75	34.1	57.5	8.4	1.47	0.03	0.31	0.112 (0.104)	2.13 (2.28)	168 (188)	0.5
75–150	17.2	68.4	14.4	1.52	0.02	0.29	0.154 (0.146)	2.14 (2.37)	145 (219)	0.5
150–400	24.7	64.6	10.7	1.54	0.01	0.30	0.135 (0.095)	3.48 (2.44)	215 (272)	0.5

6.2.2 Data acquisition

6.2.2.1 Throughfall and stemflow measurements

From 1 May 2013 to 31 October 2013, the measurements of throughfall and stemflow were conducted simultaneously. To obtain the spatial distribution of rainfall on the soil surface, eight RG3-M tipping-bucket rain gauges (177 cm^2 orifice, Onset Computer Corp., Bourne, USA) were situated along a canopy-intercanopy transect, at 50, 100, 150, 200, 250, 300, 350 and 400 cm from the tree trunk. The rain gauges were positioned at 0.5 m above the ground to avoid rain splash and prevent damage by animals. The stemflow was measured on one representative pine tree using spiral-type stemflow collars constructed

from wired rubber. The stemflow collar was fixed around the tree trunk and sealed with silicon sealant. The collected stemflow was diverted to a tipping-bucket rain gauge using a rubber hose with 2.5 cm in diameter. All the tipping-bucket rain gauges were calibrated to 0.2 mm per tip in the lab and recalibrated after deployments in the field (Llorens et al., 1997).

6.2.2.2 Fine root sampling and analysis

Considering the vertical and radial variations of the tree root distribution, the two-dimensional depth- and radial-wise distributions of pine roots were measured using a hand auger after the field experiments. The inside diameter of the auger was 12.5 cm and the auger head was 30 cm high. Soil cores were taken in two cardinal directions (east and north) and the average value was used to represent the two-dimensional root distribution. The points of root sampling were located at 10, 25, 50, 75, 100, 150, 200, 300, 400 cm from the tree trunk. Soil cores were taken at 10–50 cm intervals in the vertical direction, and the maximum depth of soil sampling was 300 cm as few roots were found in the deeper soil. The position of each sample was recorded, including the radial distance from the trunk and the depth to the midpoint of each sample. Small and large fine roots (< 2 mm and 2–5 mm in diameter, respectively) were separated from the soils using a 1 mm sieve (Vanninen and Makela, 1999). The roots from each sample were oven-dried and root weight density was determined by dividing the total root weight by the corresponding core volume.

6.2.2.3 Determination of soil physical and hydraulic parameters

Soil samples were taken at different soil depths and horizontal distances from the tree trunk to measure physical and hydraulic properties. Intact soil samples were collected from soil pits down to a depth of 150 cm using sample rings of Ø53 mm×51 mm with closed ring holder (Eijkelkamp-Agrisearch Equipment, Netherlands) at three locations (50, 200 and 350 cm from the trunk) along the canopy-intercanopy transect. For each location, three soil samples were collected at 25 cm depth intervals. The soil samples were wrapped in plastic bags and transported to the laboratory for analysis of soil particle size distribution, bulk density, hydraulic conductivity and water retention curve. For soil profiles between 1.5 m and 4.0 m, disturbed soil samples were obtained using a hand auger and soil hydraulic properties were determined using disturbed soil samples. The saturated hydraulic conductivity was measured with a constant head permeameter (Eijkelkamp-Agrisearch Equipment, Netherlands). Soil bulk density was measured by the standard core method

(De Vos et al., 2005) after determination of soil hydraulic properties. Particle size distribution was obtained from sieve analysis (Gee and Bauder, 1986) to estimate the soil texture and readily available specific yield (Loheide et al., 2005). Soil water retention curve was measured at 6 matric potentials, at 10, 20 and 30 hPa suctions using a sandbox, whereas that for 60, 100 and 500 hPa was measured by a suction plate.

6.2.2.4 Meteorological variables

Meteorological data were observed from an automatic weather station mounted on a 6-meter-high mast in a nearby clearing. Air temperature and relative humidity were measured with an HMP155 sensor (Vaisala, Vantaa, Finland). Wind speed and direction were measured by a wind sentry set (model 03002, RM Young, Michigan, USA). A CNR4 net radiometer (Kipp & Zonen, Delft, The Netherlands) was deployed to measure net radiation. Two HFP01 soil heat flux plates (Hukseflux, Delft, The Netherlands) were buried at 5 cm depth to measure soil heat flux. Meteorological data were automatically sampled at 5-min intervals and recorded at 15-min intervals by a CR1000 datalogger (Campbell Scientific, Logan, USA). During the study period, soil moisture contents were monitored at depths of 20 cm, 40 cm, 60 cm and 80 cm by EC-5 moisture sensors (On-set Computer Corp., Bourne, USA) at the intercanopy area. These soil moisture sensors were calibrated (RSME=0.012 cm^3 cm^{-3}) using soil samples collected from the study site before their deployment in the field.

6.2.3 Model description

The HYDRUS models are finite element programs to simulate one-, two- or three-dimensional water movement and solute transport within the soil profiles (Šimůnek et al., 2008). The model was developed to consider the main processes that affect water fluxes in the vadose zone, such as rainfall, soil evaporation, root water uptake and deep drainage. There have been many successful HYDRUS applications in water flow with root water uptake (e.g., Vrugt et al., 2001; Rees and Ali, 2006; Deb et al., 2013) and water percolation (e.g.; Jiménez-Martínez et al., 2009; Kurtzman and Scanlon, 2011; Turkeltaub et al., 2014).

6.2.3.1 Governing flow equation

We used HYDRUS 1D and HYDRUS 2D/3D programs to numerically solve the one- and two-dimensional solutions of Richards' equation (Richards, 1931), which is widely

accepted to describe underlying physical processes of water movement in variably saturated soils:

$$\frac{\partial\theta(h)}{\partial t} = \nabla\left[K(h)\nabla(h-z)\right] - S(h) \tag{6.1}$$

where $\theta(h)$ is the volumetric water content, h is the soil water pressure head, t is time, z is the vertical coordinate, K is the unsaturated hydraulic conductivity, and $S(h)$ is the sink term, defined as the volume of water removed from a unit volume of soil per unit time due to root water uptake.

The soil hydraulic properties were modelled using the van Genuchten-Mualem (VGM) constitutive relationships (Mualem, 1976; van Genuchten, 1980):

$$\theta(h) = \begin{cases} \theta_r + \dfrac{\theta_s - \theta_r}{\left[1+\left|\alpha h\right|^n\right]^{1-1/n}} & h < 0 \\ \theta_s & h \geq 0 \end{cases} \tag{6.2}$$

$$K(h) = K_s S_e^l \left\{1-\left[1-S_e^{n/(n-1)}\right]^{1-1/n}\right\}^2 \tag{6.3}$$

$$S_e = \frac{\theta(h)-\theta_r}{\theta_s-\theta_r} \tag{6.4}$$

where S_e is the effective saturation, θ_s is the saturated water content, θ_r is the residual water content, K_s is the saturated hydraulic conductivity, α is the air entry parameter, n is the pore size distribution parameter, and l is the pore connectivity parameter, equal to 0.5.

The sink term $S(h)$ was specified in terms of a potential root uptake rate and a water stress factor following Feddes et al. (1978):

$$S(h) = \gamma(h)\beta(x,z)S_t T_p \tag{6.5}$$

where $\gamma(h)$ is the water stress response function ($0<\gamma<1$) that prescribes the reduction in water uptake that occurs due to drought stress, T_p is the potential transportation rate, $\beta(x, z)$ is the normalized water uptake distribution and S_t is the width of the soil surface associated with the transportation process.

For $\gamma(h)$, we adopted the functional form introduced by Feddes et al. (1978):

$$\gamma(h)=\begin{cases}(h-h_4)/(h_3-h_4), & h_4<h\le h_3\\ 1, & h_3<h\le h_2\\ (h-h_1)/(h_2-h_1), & h_2<h\le h_1\\ 0, & h\le h_4 \ or \ h>h_1\end{cases} \quad (6.6)$$

where h_1, h_2, h_3, h_4 are empirical parameters, which are 0, -50 cm, -70 cm, -200 cm, respectively, for this study.

For $\beta(x, z)$, we used a flexible root water uptake model proposed by Vrugt et al. (2001), assuming axial symmetry in root water uptake:

$$\beta(x,z)=\left(1-\frac{x}{x_m}\right)\left(1-\frac{z}{z_m}\right)e^{-\left(\frac{p_x}{x_m}|x^*-x|+\frac{p_z}{z_m}|z^*-z|\right)} \quad (6.7)$$

where x_m , z_m are the maximum rooting lengths in the x, z directions, x, z are distances from the origin of the tree in the x, z directions, p_x, p_z, $x^*$and z^* are empirical parameters. These parameters were calibrated using the "trial and error" method, by manually matching the patterns between observed and modelled root distribution data.

6.2.3.2 Two-dimensional simulation of water flow

Model setup

A two-dimensional radially symmetric transport domain, 400 cm deep and 400 cm long in the radial direction, was used for the numerical simulations (Figure 6.1). This domain covered half of the canopy area (1–250 cm) and half of the intercanopy area (250–400 cm). The transport domain was discretised into finite elements using a grid spacing of 5 cm and stretching factor of 5. To avoid numerical divergence and create small water mass balance errors (< 1%), the mesh was configured to offer mesh refinement of 0.25 cm at the soil surface where the most significant moisture gradients were expected to occur (Downer and Ogden, 2004; Wang et al., 2014). The transport domain was totally discretised into 31144 triangular 2D elements and 15893 nodes. Based on the field observations, the soil profile was divided into four soil layers (Table 6.1). Four observation nodes were specified at depths of 20 cm, 40 cm, 60 cm and 80 cm at a radial distance of 350 cm from the tree trunk to coincide with soil moisture sensor measurements. Besides, we set four observation nodes at depths of 50 cm, 150 cm, 250 cm and 350 cm under the canopy (50 cm from trunk) and another four nodes at same depths in the intercanopy area (350 cm

from trunk), respectively. Mesh lines were specified at the bottom boundary to obtain spatial distribution of deep drainage.

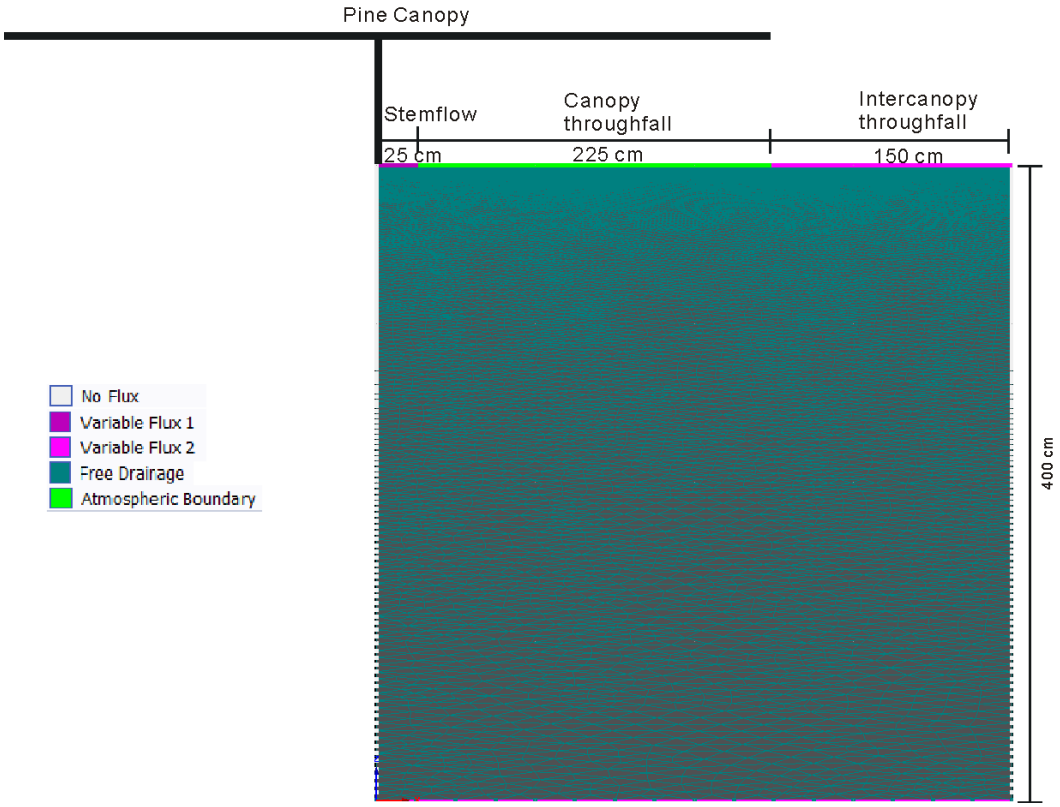

Figure 6.1 Finite element mesh and boundary conditions of the axisymmetric vertical transport domain. The projected canopy area was indicated by the horizontal line. Tree height was not scaled.

Numerical simulations were performed from 1 November 2012 to 31 October 2013. The initial time step was 1 s and the maximum time step was 1 h. The initial conditions employed for the simulations were based on the experimental moisture profile at the start of the period considered. In fact, the profile indicated that the soil was near field capacity at this time following a long dry period. Therefore, initial pressure heads in soil profile were set to field capacity throughout the domain, representing an initial volumetric water content of 0.062, 0.055, 0.049, and 0.057 cm^3 cm^{-3} for different soil layers, respectively.

An atmospheric boundary condition, i.e., the daily potential evaporation (E_p) and transpiration (T_p), and rainfall fluxes, was used as the upper boundary condition. The under-canopy throughfall was used as atmospheric flux boundary condition at the soil surface of the domain and applied at distance from 25 cm to 250 cm from the trunk (Figure 6.1). To simulate different rainfall distribution at the soil surface, stemflow and inter-canopy throughfall were implemented using the time-variable flux boundary conditions as

HYDRUS 2D/3D program allows only one atmospheric boundary condition. These time-variable flux boundary conditions were treated as atmospheric conditions, where water evaporates at E_p as long as the water pressure at the surface remains above a threshold value of -200 cm. The potential stemflow infiltration flux minus potential evaporation was applied around the stem to a radial distance of 25 cm, while the potential daily inter-canopy throughfall infiltration flux minus potential evaporation was used at the remaining top boundary.

Daily potential evapotranspiration (ET_p) was calculated following the Penman-Monteith method using daily weather measurements. The ET_p is partitioned into E_p and T_p according to Beer's equation (Ritchie, 1972):

$$E_p = ET_p e^{-kLAI} \tag{6.8}$$

where k is the radiation extinction coefficient, equal to 0.39, and LAI is the leaf area index. An average of 2.3 m^2 m^{-2} was obtained using a LAI-2000 instrument (LI-COR Bio-sciences, Lincoln, NE). Daily T_p was obtained by subtracting daily E_p from total ET_p.

No flux was allowed through the vertical sides of the transport domain due to symmetry of the half-canopy and half-intercanopy area. A free drainage (unit head gradient) condition was considered at the bottom boundary because the water table at this site was generally located more than 8.5 m below the soil surface and it does not influence the root zone soil water dynamics (Figure 6.2). Figure 6.2 summarizes the applied surface boundary condition, showing daily values of gross rainfall, T_p and E_p.

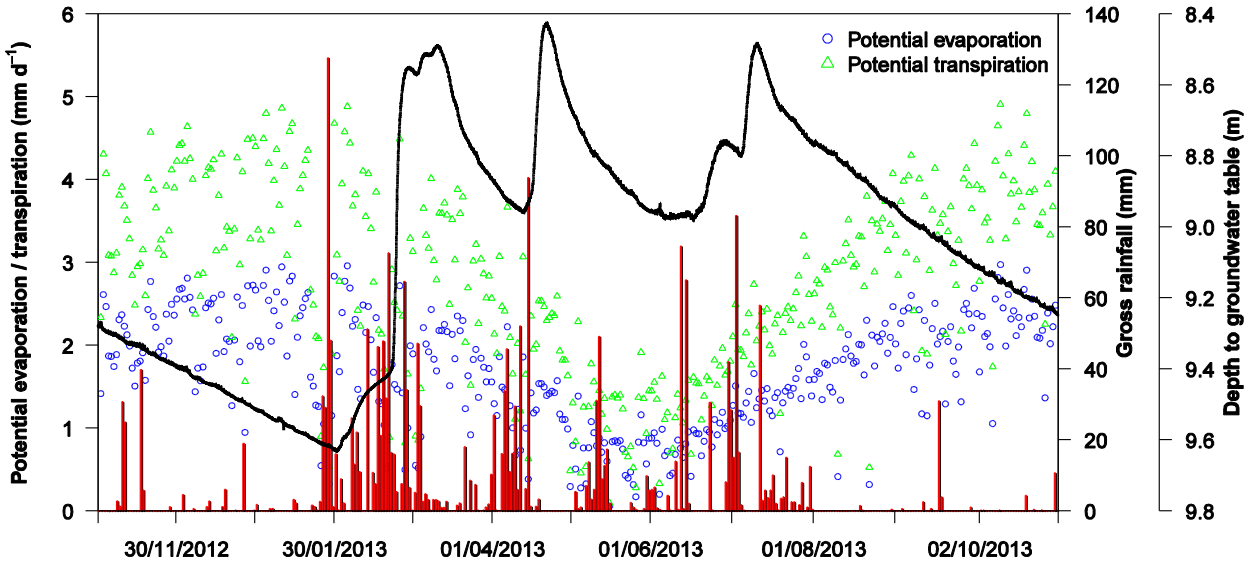

Figure 6.2 Time series of observed daily gross rainfall (red bars), depth to groundwater table (black line), estimated potential evaporation and potential transpiration.

Model calibration and validation

To improve estimates of the soil hydraulic parameters, the HYDRUS 2D/3D calibration was performed for a 182-day period (November 1 2012–April 30 2013) using the Levenberg-Marquardt optimization (Marquardt, 1963) in combination with the HYDRUS 2D/3D model. The model was then validated using the optimized parameters for a 183-day period (May 1 2013–October 31 2013) to evaluate the model performance. Once validated, we also used the validated HYDRUS 2D/3D model to evaluate the spatiotemporal pattern of spatial moisture distribution and deep drainage for the entire year. To avoid unrealistic parameter values during the calibration process, the parameters were confined between a minimum and maximum value. It is generally not recommended to estimate too many parameters simultaneously because of possible correlation among the parameters and resulting uniqueness problems (Hopmans et al., 2002). We estimated the VGM model parameters α, n and Ks simultaneously as they are the most sensitive soil hydraulic parameters (Abbasi et al., 2003; Wang et al., 2014). A total of 12 parameters involved for the layered profiles were thus included in the optimization process. The calibration process was initiated using measured soil hydraulic parameters. Soil water content at measurement soil depths of 20, 40, 60 and 80 cm at the inter-canopy location were used in the objective function during the optimization process. During the HYDRUS 2D/3D calibration and validation, model predictions of water content at depths of 20, 40, 60, and 80 cm were statistically compared to measured values using the root mean square error (RMSE), the mean bias error (ME) (Shen and Louis, 1998), and an index of agreement (d) (Willmott, 1981).

Simulation scenarios

Based on other numerical studies (e.g., Vrugt et al., 2001; Sansoulet et al., 2008; Nikodem et al., 2010, De Silva et al., 2008; Deb et al., 2013), several common used scenarios with different complexity of rainfall and root distributions have been considered to compare water balance components using HYDRUS 2D/3D model (Table 6.2). The baseline scenario represents the most complex field situation, with spatial distribution of stemflow, under-canopy and inter-canopy throughfall at the top boundary and two-dimensional distribution of tree roots based on Vrugt's model. In Scenarios A1, A2 and A3, field-measured spatially variable model inputs of stemflow, under-canopy throughfall and inter-

canopy throughfall was assigned at the top boundary, while a relatively simple one-dimensional root distribution was constructed, with Vrugt's root distribution, linear root distribution (1 at surface and 0 at 3 m) and uniform root distribution models (1 from surface to 3 m), respectively. In Scenarios B1 and B2, two-dimensional root distribution was specified, while variable rainfall without stemflow and weight-averaged rainfall were used on top boundary, respectively. The weight-averaged rainfall was calculated as sums of the stemflow multiplied by the stemflow infiltration area (circle area with diameter of 25 cm) plus canopy throughfall multiplied by the canopy throughfall infiltration area (circle area with diameter of 250 cm minus circle area with diameter of 25 cm) and intercanopy throughfall multiplied by the intercanopy throughfall infiltration area (circle area with diameter of 400 cm minus circle area with diameter of 250 cm), and then all were divided by total infiltration area (circle area with diameter of 400 cm). Under each scenario considered, the spatial moisture distribution is simulated, and the resulting water fluxes within and out from the soil domain through a free drainage boundary is calculated. All the scenarios were conducted with same soil properties and potential *ET* rates. The simulations started from the initial moisture state on November 1 2012, equal to field capacity.

Table 6.2 Scenarios for 1D and 2D simulation experiments with different inputs of surface rainfall and root distribution.

Scenario	Dimension	Surface rainfall	Root distribution
Baseline	2D	Spatially variable	$\beta(x,z)=(1-z/300)(1-x/350)\ e^{-[(1.5/300)\lvert 20-z\rvert+(1.8/350)\lvert 30-x\rvert]}$
A1	2D	Spatially variable	$\beta(z) = (1-z/300)\ e^{-(1.5/300)\lvert 20-z\rvert}$
A2	2D	Spatially variable	$\beta(z)=-z/3+1$
A3	2D	Spatially variable	$\beta(z)=1$
B1	2D	Spatially variable - stemflow	$\beta(x,z)=(1-z/300)(1-x/350)\ e^{-[(1.5/300)\lvert 20-z\rvert+(1.8/350)\lvert 30-x\rvert]}$
B2	2D	Spatially averaged	$\beta(x,z)=(1-z/300)(1-x/350)\ e^{-[(1.5/300)\lvert 20-z\rvert+(1.8/350)\lvert 30-x\rvert]}$
C1	1D	Spatially averaged	$\beta(z) = (1-z/300)\ e^{-(1.5/300)\lvert 20-z\rvert}$
C2	1D	Spatially averaged	$\beta(z)=-z/3+1$
C3	1D	Spatially averaged	$\beta(z)=1$

6.2.3.3 One-dimensional simulation of water flow

We also substituted the two-dimensional soil profile with one-dimensional counterparts to simulate the water flow within the one-dimensional vertical domain using HYDRUS 1D (Šimůnek et al., 2008). The vertical domain was 400 cm deep and discretised into 401 finite elements with node density of 1 at surface and 3 at bottom. The same soil hydraulic parameters for four soil layers and initial conditions were established in the simulations as for the two-dimensional soil profile described above. Boundary conditions were set to allow comparison of the simulation results obtained with both the 1D and 2D models, with atmospheric boundary condition (with a surface layer) and free drainage bottom boundary condition, as with the two-dimensional soil profile. Three simplifying scenarios were developed in one-dimensional simulations to estimate water balance components (Table 6.2). In all Scenarios C1, C2 and C3, weight-averaged rainfall of stemflow, throughfall and gross rainfall was specified at the top boundary, while different kinds of one-dimensional root water uptake model-Vrugt's root distribution over 300 cm depth, linear root distribution (1 at surface and 0 at 3 m) and uniform root distribution (1 from surface to 3 m) were specified, respectively. Under each scenario considered, the spatial moisture distribution is simulated, and the resulting water fluxes within and out from the soil domain through a free drainage boundary is calculated. The water flux through the free drainage represents the potential groundwater recharge in the local aquifer. All the scenarios were conducted with same hydraulic parameters and potential ET rates. The simulations started from the initial moisture state on November 1 2012.

6.3 Results and discussion

6.3.1 Rainfall interception and redistribution

Compared with the long-term mean annual rainfall (1605 mm), the one-year experimental period (November 1 2012–October 31 2013) was characterised by a higher annual rainfall of 2260 mm (Figure 6.2). A significant number of rain events occurred during January and February when temperatures were high. Over the study period of throughfall and stemflow (May 1 2013–October 31 2013), a total gross rainfall of 853 mm was recorded. The throughfall was averaged at 734 mm over the sampled transect area, representing 86.0% of gross rainfall. A total stemflow volume of 452 L was collected, equal to 9 mm rainfall depth over the entire surface area but 2340 mm over the considered stemflow area, which represented 1.0% and 260.0% of gross rainfall, respectively. Interception loss over the study area was estimated by the difference between the measured gross rainfall and net

rainfall (average throughfall plus transect-scale stemflow). The derived interception loss was 110 mm, representing 12.8% of gross rainfall.

The transect-scale stemflow accounted for a small percentage of gross rainfall (1.0%), which was comparable with the other values reported in pine forests, e.g. 1.3% by Llorens et al. (1997), 1.4% by Shachnovich et al. (2008), 0.88% by Shi et al. (2010) and 0.5% by Ghimire et al. (2012). The low stemflow fraction was expected due to the rough bark of pine trees and low stem density in our mixed forests. The observed throughfall was slightly higher than the reported values (80% to 85% of gross rainfall) in other pine forests (Farrington and Bartle, 1991; Shi et al., 2010), whereas the interception loss as calculated in the this study (12.8% of gross rainfall) was lower than those recorded in other pine forests, mainly ranging from 20%–40% (Carlyle-Moses, 2004; Komatsu et al., 2010). The resulting higher throughfall and lower interception was most likely due to the low canopy coverage and leaf area index in the open pine forest.

Figure 6.3 shows the cumulative rainfall as a percentage of gross rainfall measured at different locations along the canopy-intercanopy transect. The distribution of throughfall under canopy and intercanopy was spatially heterogeneous, but the spatial pattern was found to be stable among most rainfall events based on time-stability analysis. Generally, higher throughfall was observed at the intercanopy area, where no leaves and branches existed and the throughfall here was slightly affected by adjacent trees due to rain-shadow effects (Fan et al., 2014). The measured throughfall percentage under canopy ranged between 76% and 82% of gross rainfall, with a mean of 79%. The measured throughfall percentage at the intercanopy site was on average 94% of gross rainfall, ranging from 89% to 96%. The highest throughfall percentage (260% of gross rainfall) next to the tree stem was induced by funnelled stemflow. However, no consistent conclusion has been drawn regarding spatial rainfall distribution under canopy and at intercanopy sites due to tree architecture and climate drivers. Whelan et al. (1998) found less throughfall close to the spruce trunks, whereas Loustau et al. (1992) found the throughfall in between pine trees was the highest for light rainfall but the lowest for heavy rainfall events. Keim et al. (2005) reported higher throughfall close to tree trunks in young coniferous forests, but lower throughfall occurred close to trunks in old stands of conifers.

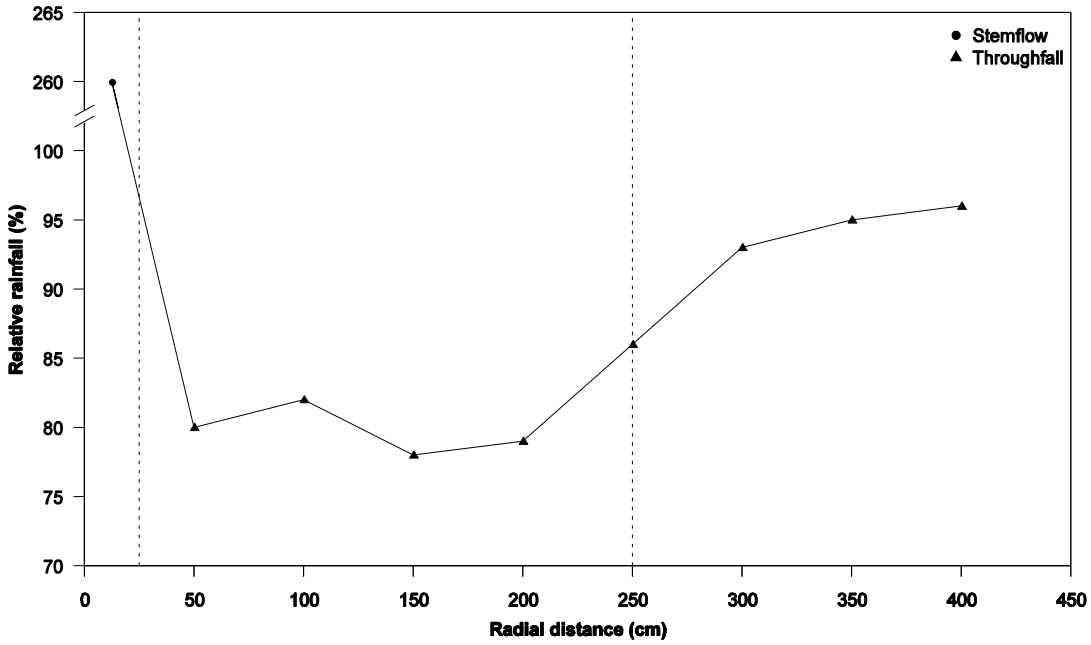

Figure 6.3. Distribution of relative cumulative stemflow and throughfall as a percentage of gross rainfall at different locations along the canopy-intercanopy transect. The two vertical dash lines represent the transition between stemflow, under-canopy and inter-canopy zones, respectively.

6.3.2 Heterogeneous root distribution

Field root sampling revealed a high cumulative root weight density fraction (94% of total root weight density) in the upper 1.0 m (Table 6.3). This is consistent with the finding by Jackson et al. (1996), who found the majority (> 90%) of root biomass were located in the upper 1.0 m soil layer for temperate coniferous forests. Only a small fraction of tree roots was observed beyond the projected canopy area (250–400 cm). However, the field investigation suggests that the root zone developed a maximum root depth of 3.0 m in this study. The maximum root depths of temperate pine species planting on sandy soils are found highly variable (2.0–4.8 m), with a mean maximum depth of 3.2 m±0.8 m (Canadell et al., 1996). The deep rooting systems for pine trees at our sites were associated with their adaptive growths to the low soil holding capacity and deep groundwater table. The dune sands have a low water holding capacity with a total capacity of ~0.05 cm^3 cm^{-3}. This indicates that the soil moisture in shallow vadose zone of sand dunes can be always low and will not be available to vegetation for use. Fast percolation of water through sand under such situation will only increase the deep drainage. Thus, in situation where the dune sand is deep, plant roots have to extend their roots in deep soil to access favourable soil moisture, especially during the dry season with minimal or no rainfall.

Table 6.3 Vertical and radial distribution of fine roots (< 5 mm) for the studied pine tree (mg cm^{-3}).

Soil depth (cm)	Radial distance (cm)									
	10	30	50	70	100	150	200	250	300	350
0-10	1.870	2.142	1.601	1.326	0.954	0.557	0.253	0.177	0.021	0.014
10-30	1.788	3.010	2.008	1.251	0.723	0.245	0.203	0.125	0.008	0.000
30-50	1.496	1.827	1.123	0.753	0.423	0.110	0.070	0.021	0.000	0.005
50-70	0.726	0.865	0.576	0.351	0.212	0.000	0.006	0.000	0.017	0.000
70-100	0.554	0.423	0.000	0.203	0.123	0.052	0.011	0.021	0.000	0.000
100-150	0.253	0.203	0.154	0.186	0.072	0.025	0.000	0.000	0.000	0.000
150-200	0.109	0.000	0.045	0.008	0.003	0.000	0.000	0.000	0.000	0.000
200-250	0.035	0.012	0.000	0.015	0.012	0.040	0.000	0.000	0.000	0.000
250-300	0.014	0.008	0.031	0.000	0.000	0.000	0.000	0.000	0.000	0.000

The two-dimensional distribution of pine roots was simulated with the exponential root distribution model given in Equation 6.7. Based on field investigation, the maximum root lengths in the x, z directions are x_m=350 cm, z_m=300 cm for this study. The maximum root density was located at x*=30 cm, z*=20 cm. The fitted parameter p_x and p_z were 1.8 and 1.5, respectively. Figure 6.4 shows the simulated root distribution using specified root distribution parameters. The comparisons of the measured and simulated distribution show that the section of maximum rooting is similar. There is a slight difference in root distribution at the right bottom corner; however this has little effect for root water uptake because the root fraction at this area is minimal.

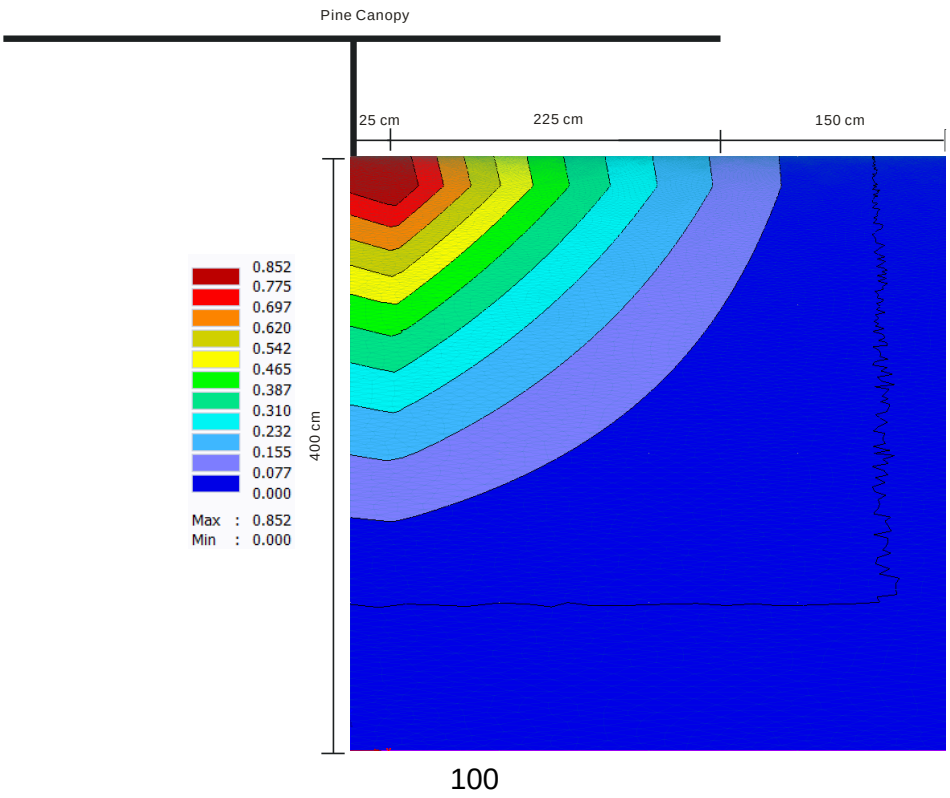

Figure 6.4. Two-dimensional distribution of fine roots as simulated by Vrugt's root distribution model.

6.3.3 Performance of HYDRUS 2D/3D during the calibration and validation processes

We separated the study period into calibration (November 1 2012–April 30 2013) and validation (May 1 2013–October 31 2013) periods to evaluate the performance of the HYDRUS 2D/3D model. The inversely estimated soil hydraulic parameters remained similar to the measured values (Table 6.1). The difference between the measured and calibrated K_S can be explained by considering the anisotropy effect. The constant head permeability test measures only the vertical conductivity and represents local point values, whereas the calibrated parameters represent average effective values over individual soil layer.

Comparisons between simulated and measured water contents at four depths (20, 40, 60 and 80 cm) during the calibration period and during the validation period are shown in Figure 6.5. There was generally a good agreement between simulated and measured water contents for both the calibration and validation periods. Overall model performance was satisfactory as indicated by statistics of mean square error (RMSE), mean bias error (ME) and an index of agreement (*d*). In general, deviations between measured and modelled water contents were small and declined with depth. RMSE varied between 0.016 and 0.018 cm^3 cm^{-3}, ME between 0.005 and 0.010 cm^3 cm^{-3}, and *d* between 0.804 and 0.874 during the calibration period. The validation phases exhibited slightly higher variations than the calibration period, with RMSE varying between 0.013 and 0.027 cm^3 cm^{-3}, ME between 0. 005 and 0.011 cm^3 cm^{-3}, and d between 0.626 and 0.919 for different soil depths.

The HYDRUS 2D/3D predicted both the sharp increase in the water content following rainfall and the gradual decreases during drying periods. However, immediately after a rainfall event, the model predicted slightly lower peak of moisture content at depth of 20 cm but higher peak values at depths of 40, 60, and 80 cm, especially during the validation period (Figure 6.5), which could be explained by the soil water retention behaviour. However, the observed data displayed faster reduction in water content than predicted by the model during the wet season but slower reduction during the dry season. This discrepancy could be attributed to either fast drainage or higher ET rates derived by the pine trees. The ME values (Figure 6.5) indicated that the model generally overpredicted water content at all measurement depths. Small differences between simulated and

measured water content may be partially explained by measurement errors, which are inevitable under field conditions.

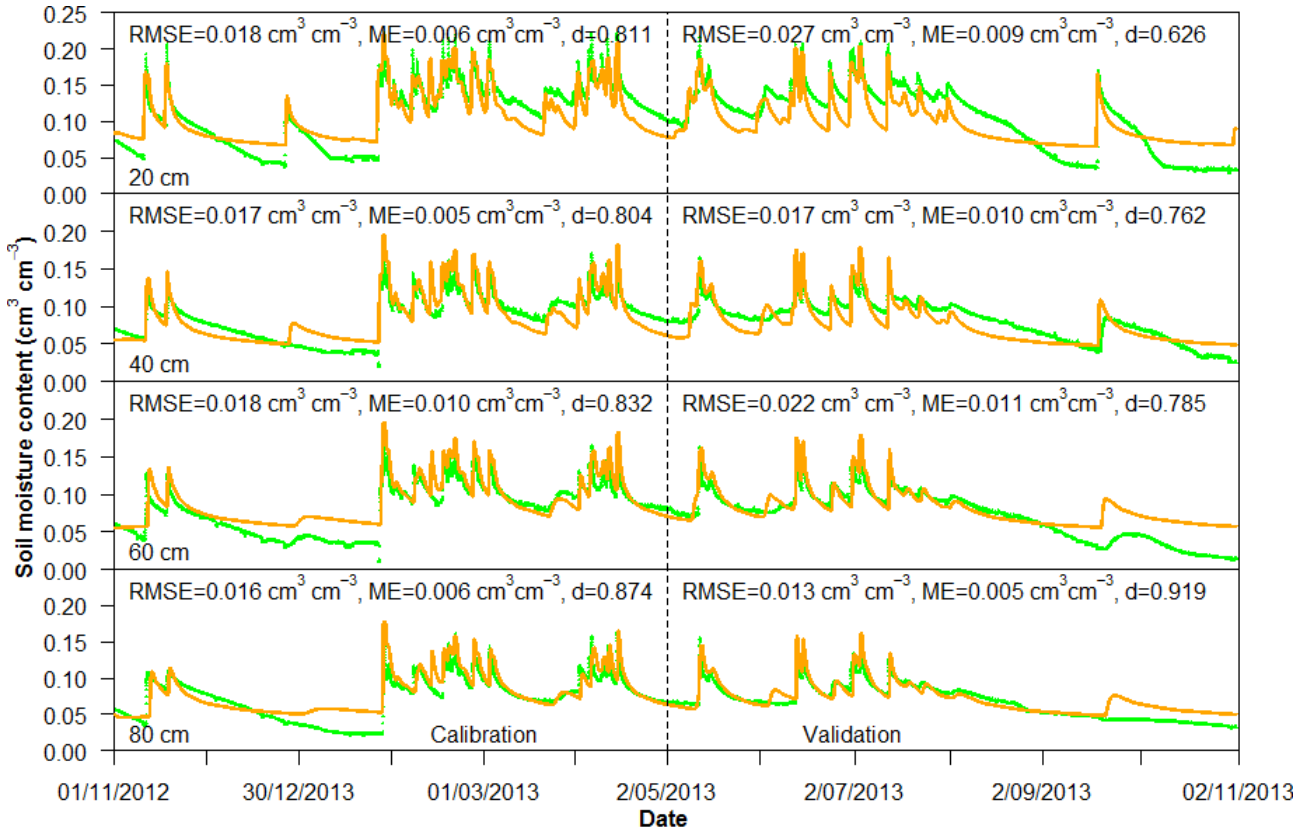

Figure 6.5 Comparision of observed (green) and simulated (orange) soil moisture content at depths of 20, 40, 60, and 80 cm during the calibration and validation processes.

6.3.4 Numerical simulation of two-dimensional water flow

After evaluating the performance of the HYDRUS 2D/3D model, the calibrated model was run over the whole year to evaluate the spatiotemporal pattern of soil moisture and deep drainage at the canopy and intercanopy areas.

6.3.4.1 Spatiotemporal soil moisture distribution

Modelled moisture contents at the under-canopy and inter-canopy sites at four depths (50, 150, 250 and 350 cm) are represented in Figure 6.6. Moisture content recorded under the canopy is, on average, about 0.03 cm^3 cm^{-3} lower than that recorded in the intercanopy area, with maximum difference of 0.11, 0.12, 0.12 and 0.09 cm^3 cm^{-3} for four different depths, respectively. This is mainly ascribed to the lower rainfall infiltration and higher root uptake under the canopy area. Following the rainfall events, the higher soil moisture increase occurred at the soil surface than the deeper soils. Small rainfall events had little influence on the moisture content at deeper depths, explaining why water contents at

deeper depths stayed relatively constant under small rainfall events. Soil moisture closer to the soil surface reacted faster and to a greater extent than those at deeper depth. They were more strongly affected by climatic conditions (rainfall, evaporation and transpiration). Soil moisture contents at deeper depths varied less and were in general lower than at the soil surface. There was a time lag response of soil moisture to rainfall under the canopy than at the intercanopy area largely due to the reduced rainfall input and higher root uptake in this area.

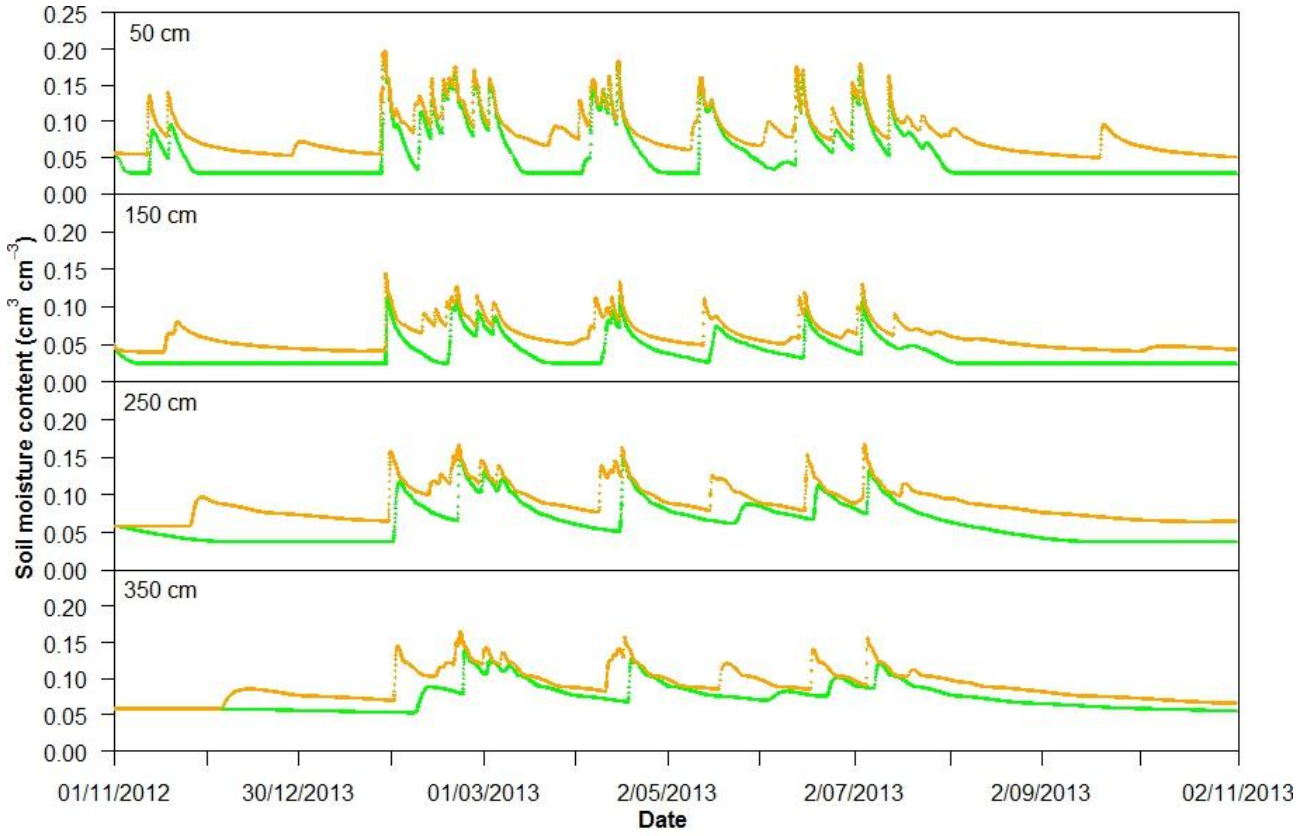

Figure 6.6 Comparision of simulated soil moisture content at depths of 50, 150, 250, and 350 cm under canopy (green) and intercanopy (orange) locations.

In order to explore the effects of rainfall redistribution and root water uptake on spatial soil moisture distribution, we also plotted the two-dimensional maps of simulated moisture across the canopy-intercanopy transect at four simulation days (Figure 6.7). Discontinuity of the simulated soil water contents was caused by the different soil water retention curves for the soil layers. The horizontal variability of infiltration generated by canopy processes leads to variability in soil moisture. From Figure 6.7a (24 January 2013), following a two-month dry period, we can observe the appearance of well-defined soil water content patterns due to the spatially variable root uptake, with smaller moisture contents close to the tree stem. After a cumulative rainfall of 190 mm, an increase of soil moisture in the soil

profile was observed on 27 January 2013 (Figure 6.7b). Higher increase was observed at the intercanopy area compared with the canopy area due to higher rainfall interception under the canopy. However, higher moisture contents comparable to the inter-canopy area were found close the tree stem during the rainfall events. This is due to the preferential infiltration of funnelled stemflow around the stem. These moisture distributions were similar to our field measurement of moisture distribution under similar pine tree and at the inter-canopy area using surface ERT (Fan et al., 2014). Liang et al. (2009) has presented a coupled mechanism termed “double-funneling”, which led to a stemflow-induced preferential infiltration process along root pathways. Apparently, the effects of stemflow serving as highly localized inputs of rainfall on the spatial distributions of soil water in forested ecosystems cannot be ignored. With a further rainfall of 50 mm, the wetting front moved down to deeper soil profiles on 30 January 2013 (Figure 6.7c). Five days later, the infiltrated rainwater redistributed and percolated below the root zone at the inter-canopy area and became deep drainage (Figure 6.7d).

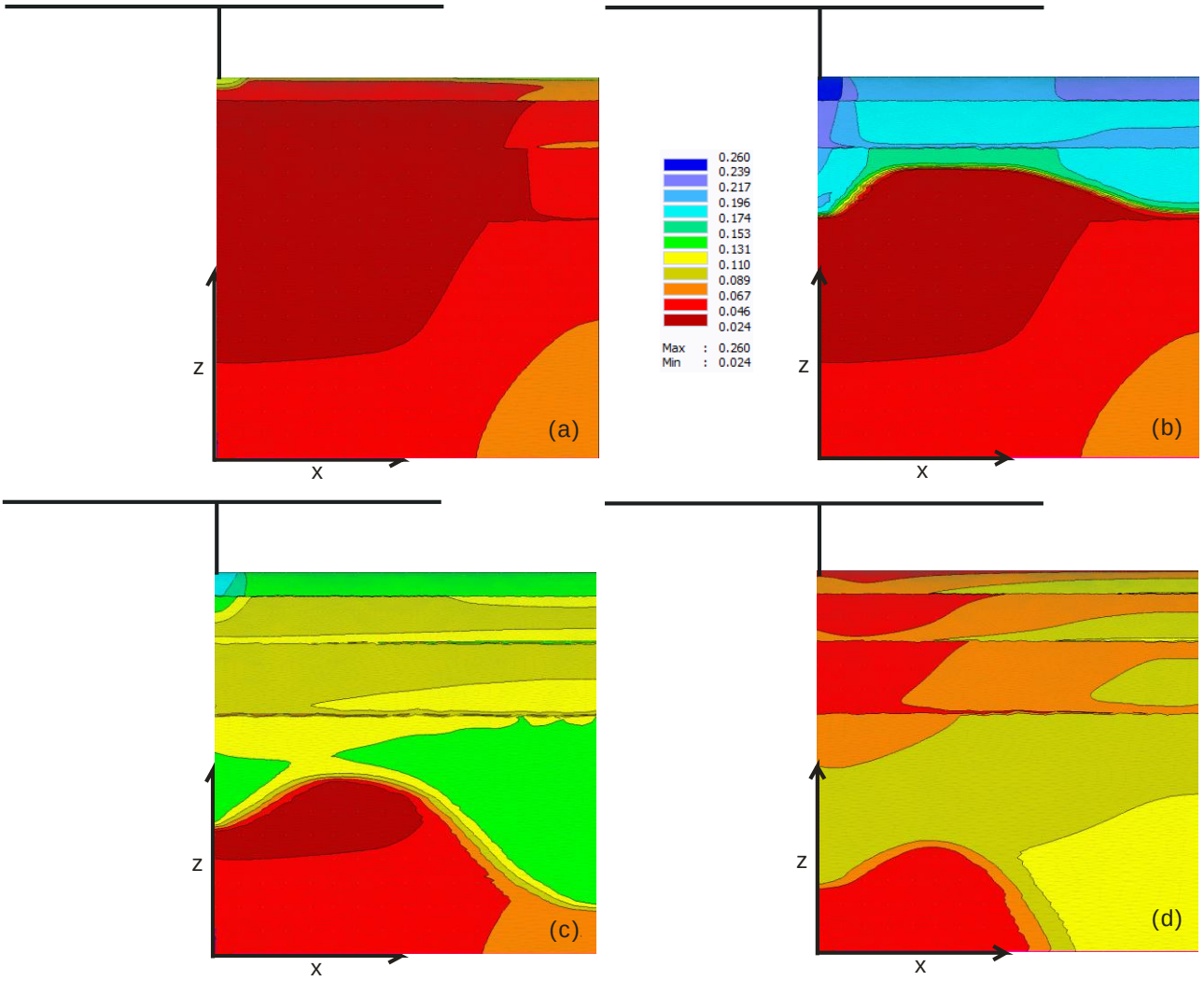

Figure 6.7 Two-dimensional maps of simulated moisture across the canopy-intercanopy transect at four simulation days, i.e. on (a) 24 January, (b) 27 January, (c) 30 January and (d) 4 February 2013.

These results revealed clear variations of moisture content along the transect, so a better observation strategy was needed to obtain the mean soil moisture for the estimation of soil moisture balance when using water balance methods to investigate hydrological processes in forested ecosystems, especially in open forests. To achieve this, we calculated soil water storage for different soil profiles by integrating soil moisture content over the 2D cylindrical radial model domain (Table 6.4). The absolute differences between the soil water storage at each soil profile and average daily soil water storage of the two-dimensional soil profile was also determined. The differences in soil water storage were large and ranged between -6.5 and 97.5 mm. These differences indicated that the sampling of the soil water content at the tree scale is not at all straightforward. The maximum differences were observed close to the middle of the intercanopy area (375 cm from tree trunk).

Table 6.4 Average daily soil water storage of the two-dimensional soil profile (mm) and absolute differences (in parentheses) between the soil water storage at each soil profile and average daily soil water storage of the two-dimensional soil profile (mm).

Date	Soil profile								
	Average	25 cm	75 cm	125 cm	175 cm	225 cm	275 cm	325 cm	375 cm
24 January	186.9	158.8 (-28.2)	155.6 (-31.3)	156.6 (-30.3)	158.4 (-28.5)	170.1 (-16.8)	195.7 (8.8)	240.2 (53.3)	260.1 (73.1)
27 January	361.0	392.5 (31.5)	310.4 (-50.6)	304.2 (-56.8)	307.2 (-53.8)	326.8 (-34.2)	378.9 (17.9)	423.4 (62.5)	444.4 (83.4)
30 January	398.5	383.3 (-15.2)	343.3 (-55.3)	334.0 (-64.5)	344.6 (-54.0)	379.0 (-19.5)	433.2 (34.6)	474.9 (76.4)	496.0 (97.5)
4 February	350.9	295.2 (-55.7)	284.3 (-66.5)	294.4 (-56.4)	322.7 (-28.2)	370.6 (19.7)	405.6 (54.7)	415.6 (64.7)	418.5 (67.7)

Hupet and Vanclooster (2005) observed large differences for the soil water content measured under and in between corn rows and found estimates of mean row scale soil water content by the use of ‘central’ sampling locations in the middle of row led to minimal errors. However, as stated for the estimation of the mean soil water storage in our study, the use of measurements performed at the central location in between trees does not seem very judicious in open forests. Instead, using soil moisture measurements close to the transition zone (250 cm from tree trunk) between under-canopy and inter-canopy areas

provided smallest errors and seems more attractive in most cases. Otherwise, at least two soil moisture profiles (e.g., one under the canopy and one at the intercanopy area) are needed to gain acceptable average soil water balance estimates in open forests.

6.3.4.2 Spatial distribution of deep drainage

Annual deep drainage accumulated to 1350 mm over the one-year study period (Figure 6.8), representing 61% of annual gross rainfall. Based on the water table fluctuation method (Scanlon et al., 2002), gross recharge under the open forest over the year was estimated as 950 mm using a readily specific yield of 0.30 (Loheide et al., 2005), representing 45% of gross rainfall. The difference between modelled deep drainage and measured gross recharge was largely explained by time delay of recharge in the lower aquifer. Deep drainage, commonly considered as potential recharge, is defined as the flux of infiltrated water that moves past the root zone, while recharge is the amount of infiltrated water that actually reaches the aquifer. Deep drainage becomes recharge only when no impeding layers exist that would prevent water from moving down to the aquifer. However, there is often a time lag between deep drainage becoming recharge in situations where land use has changed. This is because it takes some time for the pressure front created by the increase in deep drainage to move downward through the soil to the groundwater, especially for the infiltrating water following the dry period. The modelled high potential recharge percentage is generally comparable with results obtained in other recharge studies in coastal sand aquifers, e.g., 58% to 65% (Crosbie et al., 2005), 54.3% and 53.7% (Chen et al., 2012), ~50% (Petheram et al. 2002; Crosbie et al. 2010), 45%–50% (Green et al., 2007).

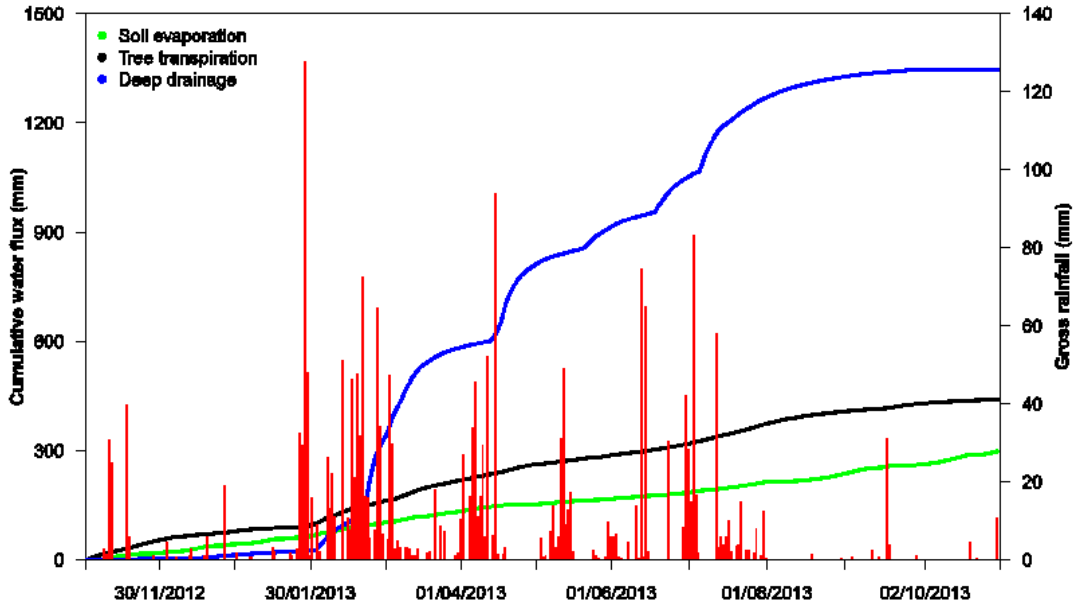

Figure 6.8 Time series of daily gross rainfall (red bars) and cumulative water fluxes (soil evaporation, tree transpiration and deep drainage) simulated over the study period.

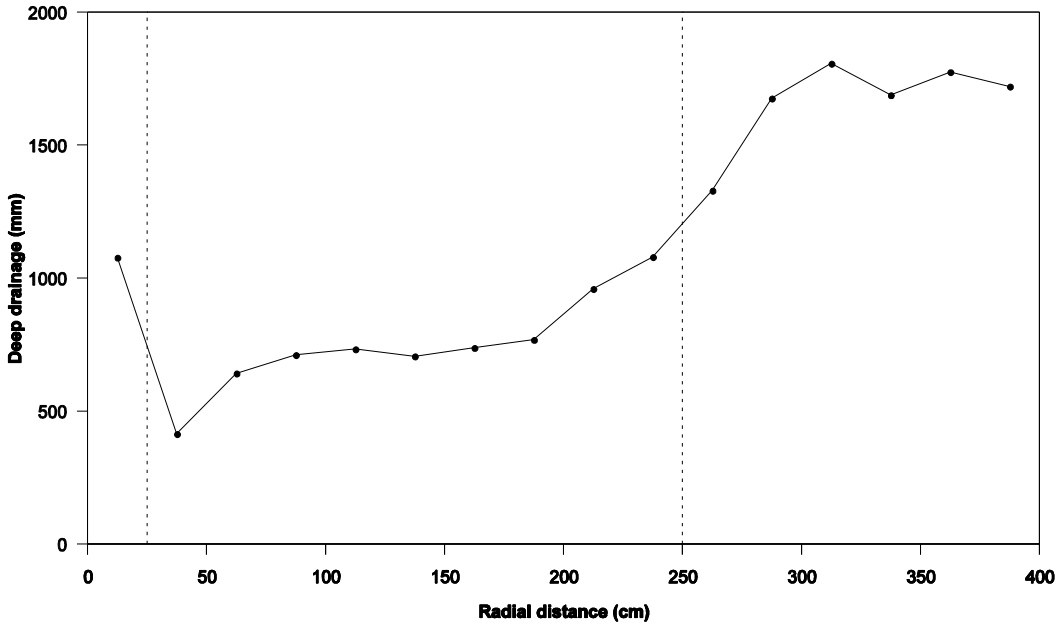

Figure 6.9 Cumulative deep drainage simulated for the study period at different locations under canopy and intercanopy zones. The two vertical dash lines represent the transition between stemflow, under-canopy and inter-canopy zones, respectively.

Canopy and root processes have influenced not only the overall magnitude of potential recharge but also its spatial distribution. At the end of the simulation, cumulative deep drainage over the year was plotted along the canopy-intercanopy transect. Similar to horizontal variability of soil moisture at under-canopy and inter-canopy zones, vegetation also affect the localization of deep drainage. Generally, the model simulations resulted in lower cumulative drainage flux under the canopy than that at the inter-canopy area (Figure 6.9). Deep drainage was spatially variable across the transect, ranging from 413 to 1806 mm with a mean value of 1350 mm and a standard deviation of 476 mm. the relative higher deep drainage close to the stem was due to the preferential infiltration of stemflow. The cumulative deep drainage at the inter-canopy area (250–400 cm) was 103% higher than that under the canopy (0–250 cm). The spatial distribution of drainage was consistent with the fact that water input at the intercanopy is almost 20% higher than that under canopy and the intercanopy area has larger portion of the total surface area of the simulated domain, while both patches share relatively similar soil profiles. The canopy patch is further depleted by root water uptake. Thus, less moisture can percolate below the root zone and becomes potential recharge under the canopy. Similar distribution of deep

drainage has been found by HYDRUS 3D by Vrugt et al. (2001), who found less deep drainage responded to higher root uptake. The variability of drainage justifies the need of two-dimensional rainfall distribution and root uptake models for identifying critical areas, especially when the transport of toxic chemicals beyond the root zone and toward groundwater is of interest at the tree scale (Nikodem et al., 2013).

6.3.5 Comparison of water balance components under different simulation scenarios

Considering various inputs of surface rainfall and root distribution in models, we compared some possible scenarios used in models. To compare the cumulative water fluxes simulated for the 1D and 2D scenarios, the average cumulative fluxes per each boundary unit were calculated, i.e., the simulated cumulative water fluxes were divided by the surface area of the corresponding boundary. The water fluxes at the soil profile top (soil evaporation) and bottom (deep drainage), the root water uptake (tree transpiration) simulated in one- and two-dimensional scenarios are shown in Table 6.5. No runoff was modelled in all scenarios due to the larger soil hydraulic conductivity of the unconsolidated dune sands compared with the rainfall intensities.

Table 6.5 Water balance components in different scenarios and percentage changes (in parentheses) of water balance components in the simulated scenarios relative to the two-dimensional baseline scenario (%).

Water balance component	Scenario									
	Base line	A1	A2	A3	B1	B2	C1	C2	C3	O
Evaporation (mm)	297	308 (3.7)	309 (4.0)	319 (7.4)	322 (8.4)	353 (18.9)	341 (14.8)	327 (10.1)	324 (9.1)	318 (7.1)
Transpiration (mm)	441	592 (34.2)	603 (36.7)	624 (41.5)	446 (1.1)	463 (5.0)	592 (34.2)	603 (36.7)	624 (41.5)	455 (3.2)
Deep drainage (mm)	1347	1217 (-9.7)	1208 (-10.3)	1187 (-11.9)	1317 (-2.2)	1308 (-2.9)	1214 (-9.9)	1207 (-10.4)	1185 (-12.0)	1322 (-1.9)

6.3.5.1 Scenarios A1-A3

The first three scenarios (A1–A3) investigate the effect of representing a one-dimensional root water uptake approach in two-dimensional water flow modelling. Generally, applying simple one-dimensional root distribution models in two-dimensional model with spatial rainfall held at soil surface caused an increase in the values for tree transpiration but decrease in deep drainage and soil evaporation (Table 6.5). Table 6.5 shows the percent of change in the output variables in the simulated scenarios, compared to the baseline scenario. With a Vrugt's root distribution and variable rainfall, deep drainage exhibited the

smallest decrease when compared to the baseline scenario by approximately 9.7%, while in the same scenario tree evaporation increased by 34.2% relative to the baseline scenario. As expected, a uniform root distribution had a much larger effect on tree transpiration than other root models, with an increase of 41.5%. Deep drainage showed the largest percentage decrease (11.9%) when compared to the reference scenario.

6.3.5.2 Scenarios B1 and B2

It is important to note that ignoring stemflow and applying area-weighted rainfall (Scenarios B1) did not result in significant changes in balance components from the reference scenario. For example, deep drainage was underestimated by less than 3% and tree transpiration was within 2% when compared to the reference scenario. Little effects of stemflow were expected over the transect area since it accounted for only a small portion of rainfall (1% of gross rainfall) compared to higher rainfall intensity over the small area around tree stem. Although the preferential infiltration of stemflow does not affect the overall water balance, it can significantly affect the localised water infiltration and nutrition leaching around the tree stem. This can be useful for the growth of vegetation since most root uptake of water and nutrition concurs in this small area. Under Scenario B2, adding area-averaged rainfall and two-dimensional root distribution as model inputs did not impact the water balance components, with a reduction of 2.9% and 5.0% in deep drainage and transpiration, respectively.

6.3.5.3 Scenarios C1–C3

The last three scenarios (C1–C3) reflect the effect of one-dimensional representation of two-dimensional distribution of rainfall and root uptake distribution form canopy and roots. Under all scenarios, the deep drainage was underestimated and tree transpiration and soil evaporation were overestimated. The root water uptake (tree transpiration) depended on root distribution in the root zone (Figures 6.2 and 6.3). Low, moderate, and very high transpiration values were obtained for scenario C1, C2, and C3, respectively. When average rainfall was used coupled with a Vrugt's root distribution, deep drainage was decreased by 9.9%. In the case of average rainfall with the uniform root distribution model, deep drainage was largest underestimated by 12.0%, due to the evapotranspiration increase caused by the growing vegetation. Although water flow in the vadose zone is often simulated in one, two, and three spatial dimensions in most physically-based soil-vegetation-atmosphere models, root water uptake is often considered simply to be a function of the vertical dimension only (Bormann, 2012; Lauenroth and Bradford, 2006;

Sala et al., 1988; Sivandran and Bras, 2012; Teuling et al., 2006). For uniform crops with a spatially uniform water uptake pattern, one-dimensional root distribution functions may be sufficient. However, for large trees in open forests, the process of root water uptake is complex and a two- or three-dimensional representation of roots would be appropriate (Green and Clothier, 1999).

6.3.5.4 Guidance for equivalent one-dimensional model

An understanding of these scenarios could provide a basis to improve the strategies of effectively representing heterogeneous two-dimensional vegetation structure in one-dimensional hydrological models. Results from scenarios A1, A2 and A3 were similar to the water fluxes simulated in scenario C1, C2 and C3 (Table 6.5), which indicates that spatially variable rainfall did not significantly affect the simulated deep drainage. This was further confirmed by comparison between Baseline scenario and Scenario B2, where assuming average rainfall produced similar deep drainage in two-dimensional simulations. This was mainly due to the compensation between less infiltration at the inter-canopy area and higher infiltration under the canopy. The study by Nikodem et al. (2010) also documented that weighted averages of simulated boundary fluxes for two different rainfall intensities (e.g. stemflow and throughfall) might represent approximately average boundary fluxes in the 2D flow system. Whereas water balance simulations are comparable, spatial variability decreased under the uniform rainfall conditions. Under all scenarios, there were reductions in deep drainage. Assuming one-dimensional root distribution will inevitably cause an underestimation of deep drainage due to assumed root distribution at the intercanopy area. To achieve the gains of the baseline scenario in the one-dimensional HYDRUS model, a shallower root distribution thus has to be represented to compensate the wider lateral root distribution, assuming linear root distribution from 1 at soil surface to a maximum depth of 1.25 m in Scenario O (Table 6.5).

6.3.6 Model limitations

The HYDRUS 2D/3D model took into account soil layers with different hydraulic properties, but the soil is considered horizontally homogeneous-average soil properties. It is however known that the soil hydraulic properties can be spatially variable between under-canopy and inter-canopy patches, also within each patch itself. Plants increase the infiltration capacity of the soil by means of their root systems (Gonzalez-Hidalgo and Bellot, 1997), thus limiting runoff and eventual soil erosion. Madsen et al. (2008) showed large changes in surface hydraulic conductivity along a canopy-edge-intercanopy transect in Utah, where

differences in soil hydrophobicity and biological soil crusts appear to have an important control on infiltration. We have not considered the possible horizontal soil because soil properties at our site were mostly similar between canopy and intercanopy locations in soil morphology and surface soil hydraulic conductivities, based on our field investigations of the unconsolidated sandy soils.

The HYDRUS 2D/3D model considered preferential flow caused by funnel stemflow around the tree trunk but neglected other possible preferential water flow. Yet, under certain conditions they change the hydraulic behaviour of soil drastically. For example, macropore flow under saturated conditions (Beven and Germann, 1982; Hendrickx and Flury, 2001; Jarvis, 2007) was not represented in the model. However, the field moisture data indicated surface soil is hardly saturated due to the high infiltration capacity, thus this effect is considered minimal. The model also did not explore the compensation mechanisms in root water uptake via root compensation (extraction at high rates from wet regions, e.g., Šimůnek and Hopmans, 2009; Vogel et al., 2013) and hydraulic redistribution (transport of water from wet soils to dry via the roots, e.g., Katul and Siqueira, 2010). That is, because of local stress in one part of the root system, plants increase local uptake in distant roots beyond the local demand dictated by root density to maintain the overall potential transpiration demand. However, these processes are difficult to represent in modelling framework of Richard model, especially the hydraulic redistribution effect.

6.4 Summary and conclusions

Vegetation canopy and roots can potentially produce variability in soil moisture and hydrological fluxes, e.g., root water uptake and deep drainage. The study focused on investigating the spatial variability of rainfall at soil surface and root distribution in the soil profile. Based on the in situ data, we conducted a series of numerical simulations using HYDRUS 1D and HYDRUS 2D/3D programs to evaluate the effects of this variability on soil moisture dynamics and the water balance in a sand dune forest. Field investigation illustrated the considerable spatial variability of rainfall and roots along the canopy-intercanopy transect. Calibrated HYDRUS 2D/3D model reproduces reasonably well soil moisture distribution during both calibration and validation processes. Soil moisture and deep drainage was generally higher at the inter-canopy area than under the canopy, which suggests the need for improving sampling strategies (e.g., at least two soil profiles, one under the canopy and the other at the inter-canopy site) to obtain unbiased estimates of water content for better soil moisture balance estimation in open forests. Different scenario

simulations showed that root distribution exerted a greater influence on soil water balance than did rainfall distribution from interception. Model simulations resulted in underestimation of deep drainage by 130 mm to 162 mm (9.7%–12.0% drop compared to baseline scenario) as a consequence of representation of two-dimensional rainfall and root distribution in one-dimensional model. Thus, translating the two-dimensional tree structure (rainfall redistribution and heterogeneous roots) to a one-dimensional case needs to be interpreted with caution. In relation to the effective one-dimensional model, uniformly distributed rainfall with a shallower linear root distribution (1 at surface and 0 at depth of 1.25 m) is proposed to produce equivalent deep drainage in this subtropical coastal sand dune forest.

Chapter 7. Conclusions and Recommendations

Using a combination of field measurements and numerical simulations, this study examined the potential effects of vegetation on soil moisture dynamics and groundwater recharge in a subtropical coastal sand dune area of southeast Queensland, Australia. The effects considered were the partitioning of rainfall into throughfall and stemflow (Chapter 2), rainfall interception losses (Chapter 3), groundwater recharge and discharge by vegetation root water uptake in shallow water table environments (Chapter 4), root-zone soil moisture dynamics and water percolation processes in deeper sand dunes (Chapter 5). The application of a commonly used numerical model (HYDRUS) to represent these effects, especially in the context of groundwater modelling, was explored in Chapter 6.

7.1 Conclusions

The results from Chapter 2 and Chapter 6 indicate that throughfall is significantly different between under-canopy and inter-canopy zones in the two studied pine forests. Higher throughfall was found under the canopy on Bribie Island but at the inter-canopy area on North Stradbroke Island. This difference is mainly caused by the spacing between adjacent trees relative to their heights. These spatial patterns were present for most recorded rainfall events in both forests and their persistence is explained by the prevailing easterly wind direction in this coastal environment. The stemflow differs between individual pine trees, which is ascribed to the difference in tree size (e.g. projected canopy area, stem diameter). As indicated by the HYDRUS 2D/3D modelling in Chapter 6, the spatial variability of throughfall and stemflow can significantly affect the heterogeneity of hydrological processes and possibly the associated biochemical processes of forested ecosystems at the tree scale. However, the scenario analyses indicate that spatial variability of rainfall is not important for the larger-scale groundwater balance in our system.

Chapter 3 shows that the annual interception loss in the banksia woodland was lower than that in the pine plantation at our study plots (with areas in the order of hundreds of square meters), which can be explained by the lower canopy storage capacity and higher aerodynamic resistance of the studied banksia woodland. The optimized RGAM and WiMo models can be useful to provide stand-scale interception loss estimates from subtropical coastal forest stands. The results indicate that the characteristics of our pine plot result in an increase in interception losses compared with the cover of the studied native plot and thus reduce the net rainfall input to these systems. However, the effects of larger-scale

development of commercial pine plantations in these areas on potential recharge may be different due to the difference in tree distribution and canopy characteristics at the different scales.

The results of Chapter 4 show that the annual net recharge (gross recharge minus ET_g) at the studied pine plantation was comparable to that of the banksia woodland but only half of the corresponding value at the grassland. The lower recharge values at forested sites resulted from higher rainfall interception and reduced antecedent storage capacity of the vadose zone due to lower surface elevations. That is, in the wet season as the water table elevation increases, there is more storage capacity in the vadose zone beneath the grassland where the surface topography is elevated relative to the forest sites. The results indicate the replacement of native grassland with pine plantation results in less recharge in these areas, but the comparison between banksia and pine forests is difficult due to the difference in tree density, ages and root distribution of the different forest stands. Despite the uncertainties associated with determination of depth-dependent specific yield, results indicate the water table fluctuation method and the White method can be useful to compare the effects of vegetation change on recharge in these subtropical coastal environments.

In Chapter 5, we demonstrate the capacity of both surface ERT and spatial TDR to spatially monitor root-zone moisture dynamics. Measured soil moisture profiles revealed differences in soil moisture dynamics under the different vegetation covers, with highest infiltration and deep drainage occurring under the open grassland compared with treed cover. As discussed earlier, this is likely due to higher rainfall interception and root water uptake by trees. We concluded that surface ERT combined with spatial TDR can be a useful method for quantifying root-zone soil moisture dynamics and understanding tree-scale hydrological processes in these environments. Better positioning of point-scale soil moisture sensors can be guided by surface ERT for soil moisture balance estimates in forest soils. The surface ERT can also be used to obtain larger-scale mean soil moisture balances in these systems.

Simulation results from Chapter 6 show soil moisture and deep drainage was spatially distributed along the canopy-intercanopy transect. Similar to findings by surface ERT in Chapter 5, higher deep drainage was found at the inter-canopy area compared with the under-canopy area due to the reinforced effects of rainfall interception and root water uptake. Estimates of mean transect-scale soil moisture by the use of sampling locations

close to the transition zone between canopy and intercanopy areas would lead to minimum errors in soil water storage estimates of this open forest. The HYDRUS models indicated deep drainage was underestimated as a consequence of uniform representation of spatially varying root systems in equivalent one- or two-dimensional HYDRUS models. Thus, translating the two-dimensional tree structure to one-dimensional lumped models needs to be interpreted with caution. To obtain equivalent deep drainage in the one-dimensional HYDRUS model, a shallower root distribution has to be represented to compensate for the wider lateral root extension.

Overall, the results of this thesis obtained using a range of techniques, confirm that vegetation not only affects the lumped water budget but also the spatial variability of hydrological processes (e.g., rainfall distribution, transpiration and deep percolation). The rainfall interception by the canopy played a major role in redistribution of water at the soil surface before it infiltrates into the soil. The effect of the root uptake on deep drainage appeared to be limited in sands with high hydraulic conductivity under intensive rainfall in the wet season. Based on our plot-scale results, pine plantation may reduce local groundwater recharge and yields, especially during the dry season. Since the pine plantation intercepts relatively more rainfall and uses more groundwater than the native covers, the tree density has to be considered when developing plantations in order to achieve acceptable water management outcomes. This study also indicates estimates of potential recharge based on rainfall data need to take into account the often limited recharge capacity in the wet season in these shallow water table environments. The modelling results indicate that field measurement or modelling of spatially-averaged rainfall interception loss was satisfactory for net rainfall input to vadose models. However, the 2D/3D root distribution has to be investigated in the field and a 1D equivalent root distribution needs to be determined as proper representation in these models.

7.2 Recommendations for further research

To better understand the hydrological effects of vegetation in these subtropical coastal areas, several recommendations for further research based on the findings of this thesis are proposed as follows:

(1) to measure the total water use by pine and banksia forests using sapflow meters or the eddy covariance technique. This study estimated the groundwater use by trees, but the root water uptake form the vadose zone was not examined. Investigation into both water

uses would help identify the water sources for different vegetation under different atmospheric conditions and obtain the whole water balance in these forest systems.

(2) to examine the vegetation-induced variability of soil physical and hydraulic properties. This study mainly focuses on the effects of vegetation on rainfall redistribution and root water uptake, but the effects of leaf litter and vegetation roots on soil hydraulic properties were not considered. Soil properties can differ between the under-canopy and inter-canopy areas due to water repellency and preferential flow. Investigation of heterogeneous soil properties would help further understand the effects of vegetation on variability of hydrological processes at the plant scale.

(3) to improve the ability of HYDRUS model to represent root compensation mechanisms. In this study we considered the water stress function of root water uptake, but compensation mechanisms in root water uptake via root compensation (extraction at high rates from wet regions) and hydraulic redistribution (transport of water from wet soils to dry via the roots) was neglected. Representation of this effect in models would further help understand the interaction between vegetation and soils.

(4) to investigate the effects of vegetation on chemical transport in these environments. This study explored the effects of vegetation on groundwater quantity, but its effects on groundwater quality were not evaluated. The spatial patterns of rainfall and roots can also affect the magnitude and distribution of solute transport in the vadose zone and finally to the groundwater. Further study on chemical transport in these forest systems would provide more information for local groundwater management.

List of References

Abbasi, F., Simunek, J., Feyen, J., Van Genuchten, M.T., Shouse, P.J., 2003. Simultaneous inverse estimation of soil hydraulic and solute transport parameters from transient field experiments: Homogeneous soil. *Transactions of the ASAE* 46, 1085–1095.

Aboal, J.R., Jiménez, M.S., Morales, D., Hernández, J.M., 1999. Rainfall interception in laurel forest in the Canary Islands. *Agricultural and Forest Meteorology* 97, 73–86.

Allen, R.G., Pereira, L.S., Raes, D., Smith, M., others, 1998. Crop evapotranspiration-Guidelines for computing crop water requirements. *FAO Irrigation and drainage paper 56*. FAO, Rome 300, 6541.

Amato, M., Basso, B., Celano, G., Bitella, G., Morelli, G., Rossi, R., 2008. In situ detection of tree root distribution and biomass by multi-electrode resistivity imaging. *Tree Physiology* 28, 1441–1448.

Asdak, C., Jarvis, P.G., Gardingen, P. V., 1998. Modelling rainfall interception in unlogged and logged forest areas of Central Kalimantan, Indonesia. *Hydrology and Earth System Sciences* 2, 211–220.

Assefa, K.A., Woodbury, A.D., 2013. Transient, spatially varied groundwater recharge modeling. *Water Resources Research* 49, 4593–4606.

Baynes J, Dunn GM. 1997. Estimating foliage surface area index in 8-year-old stands of Pinus elliottii var. elliottii Pinus caribaea var. hondurensis of variable quality. *Canadian Journal of Forest Research* 27: 1367–1375.

Beff, L., Günther, T., Vandoorne, B., Couvreur, V., Javaux, M., 2013. Three-dimensional monitoring of soil water content in a maize field using Electrical Resistivity Tomography. *Hydrology and Earth System Sciences* 17, 595–609.

Benyon, R.G., Theiveyanathan, S., Doody, T.M., 2006. Impacts of tree plantations on groundwater in south-eastern Australia. *Australian Journal of Botany* 54, 181.

Bosch J.M., Hewlett J.D., 1982. A review of catchment experiments to determine the effect of vegetation changes on water yield and evapotranspiration. *Journal of Hydrology* 55, 3–23.

Bouillet JP, Laclau JP, Arnaud M, M'Bou, AT, Saint-André L, Jourdan C. 2002. Changes with age in the spatial distribution of roots of Eucalyptus clone in Congo. *Forest Ecology and Management* 171: 43–57.

Brauman, K.A., Freyberg, D.L., Daily, G.C., 2012. Land cover effects on groundwater recharge in the tropics: ecohydrologic mechanisms. *Ecohydrology* 5, 435–444.

Brillante, L., Bois, B., Mathieu, O., Bichet, V., Michot, D., Lévêque, J., 2014. Monitoring soil volume wetness in heterogeneous soils by electrical resistivity. A field-based pedotransfer function. *Journal of Hydrology* 516, 56–66.

Brunet, P., Clément, R., Bouvier, C., 2010. Monitoring soil water content and deficit using Electrical Resistivity Tomography (ERT) – A case study in the Cevennes area, France. *Journal of Hydrology* 380, 146–153.

Brutsaert W., 1979. Heat and mass transfer to and from surfaces with dense vegetation or similar permeable roughness. *Boundary-Layer Meteorology* 16, 365–388.

Bryant, M.L., Bhat, S., Jacobs, J.M., 2005. Measurements and modeling of throughfall variability for five forest communities in the southeastern US. *Journal of Hydrology* 312, 95–108.

Butler, J.J., Kluitenberg, G.J., Whittemore, D.O., Loheide, S.P., Jin, W., Billinger, M.A., Zhan, X., 2007. A field investigation of phreatophyte-induced fluctuations in the water table. *Water Resources Research* 43, W02404.

Calamita, G., Brocca, L., Perrone, A., Piscitelli, S., Lapenna, V., Melone, F., Moramarco, T., 2012. Electrical resistivity and TDR methods for soil moisture estimation in central Italy test-sites. *Journal of Hydrology* 454, 101–112.

Calder IR, Kidd CHR. 1978. A note on the dynamic calibration of tipping-bucket gauges. *Journal of Hydrology* 39, 383–386.

Canadell, J., Jackson, R.B., Ehleringer, J.B., Mooney, H.A., Sala, O.E., Schulze, E.-D., 1996. Maximum rooting depth of vegetation types at the global scale. *Oecologia* 108, 583–595.

Carlson Mazur, M.L., Wiley, M.J., Wilcox, D.A., 2014. Estimating evapotranspiration and groundwater flow from water-table fluctuations for a general wetland scenario. *Ecohydrology* 7, 378–390.

Carlyle-Moses DE, Laureano JSF, Price A. 2004. Throughfall and throughfall spatial variability in Madrean oak forest communities of northeastern Mexico. *Journal of Hydrology* 297, 124–135.

Carlyle-Moses DE. 2004. Throughfall, stemflow, and canopy interception loss fluxes in a semi-arid Sierra Madre Oriental matorral community. *Journal of Arid Environments* 58, 181–202.

Carlyle-Moses, D.E., Price, A.G., 1999. An evaluation of the Gash interception model in a northern hardwood stand. *Journal of Hydrology* 214, 103–110.

Carlyle-Moses, D.E., Price, A.G., 2007. Modeling canopy interception loss from a Madrean pine-oak stand, northeastern Mexico. *Hydrological Processes* 21, 2572–2580.

Cattan, P., Ruy, S.M., Cabidoche, Y.-M., Findeling, A., Desbois, P., Charlier, J.B., 2009. Effect on runoff of rainfall redistribution by the impluvium-shaped canopy of banana cultivated on an Andosol with a high infiltration rate. *Journal of Hydrology* 368, 251–261.

Cheng, D., Li, Y., Chen, X., Wang, W., Hou, G., Wang, C., 2013. Estimation of groundwater evaportranspiration using diurnal water table fluctuations in the Mu Us Desert, northern China. *Journal of Hydrology* 490, 106–113.

Childs, E.C., 1960. The nonsteady state of the water table in drained land. *Journal of Geophysical Research* 65, 780–782.

Ciach GJ, Krajewski WF. 2006. Analysis and modeling of spatial correlation structure in small-scale rainfall in Central Oklahoma. *Advances in Water Resources* 29, 1450–1463.

Clothier, B.E., Green, S.R., 1994. Rootzone processes and the efficient use of irrigation water. Agricultural Water Management 25, 1–12.

Coenders-Gerrits AMJ, Hopp L, Savenije HHG, Pfister L. 2013. The effect of spatial throughfall patterns on soil moisture patterns at the hillslope scale. *Hydrology and Earth System Sciences* 17, 1749–1763.

Crockford RH, Richardson DP. 2000. Partitioning of rainfall into throughfall, stemflow and interception, effect of forest type, ground cover and climate. *Hydrological Processes* 14, 2903–2920.

Crosbie, R., Jolly, I., Leaney, F., Petheram, C., Wohling, 2010. Review of Australian Groundwater Recharge Studies. Clayton, Australia.

Crosbie, R.S., Binning, P., Kalma, J.D., 2005. A time series approach to inferring groundwater recharge using the water table fluctuation method. *Water Resources Research* 41, W01008.

Cuartas, L.A., Tomasella, J., Nobre, A.D., Hodnett, M.G., Waterloo, Maarten J., Múnera, J.C., 2007. Interception water-partitioning dynamics for a pristine rainforest in Central Amazonia, Marked differences between normal and dry years. *Agricultural and Forest Meteorology* 145, 69–83.

Dahan, O., Shani, Y., Enzel, Y., Yechieli, Y., Yakirevich, A., 2007. Direct measurements of floodwater infiltration into shallow alluvial aquifers. *Journal of Hydrology* 344, 157–170.

De Vos, B., Van Meitvenne, M., Quataert, P., Deckers, J., Muys, B., 2005. Predictive quality of pedotransfer functions for estimating bulk density of forest soils. Soil Science Society of America Journal 69, 500–510.

Deb, S.K., Shukla, M.K., Šimůnek, J., Mexal, J.G., 2013. Evaluation of Spatial and Temporal Root Water Uptake Patterns of a Flood-Irrigated Pecan Tree Using the HYDRUS (2D/3D) Model. Journal of Irrigation and Drainage Engineering 139, 599–611.

Deguchi A, Hattori S, Park HT. 2006. The influence of seasonal changes in canopy structure on interception loss, Application of the revised Gash model. *Journal of Hydrology* 318, 80–102.

Deguchi, A., Hattori, S., Park, H.-T., 2006. The influence of seasonal changes in canopy structure on interception loss, Application of the revised Gash model. *Journal of Hydrology* 318, 80–102.

DNR, 1988. A groundwater flow model for Bribie Island. Deparment of Natural Resources, Brisbane.

DNR, 1996. Bribie Island groundwater investigation. Deparment of Natural Resources, Brisbane.

Downer, C.W., Ogden, F.L., 2004. Appropriate vertical discretization of Richards' equation for two-dimensional watershed-scale modelling. *Hydrological Processes* 18, 1–22.

Duke, H., 1972. Capillary properties of soils--influence upon specific yield. Transactions of the ASAE 15, 688–691.

Dykes, A.P., 1997. Rainfall interception from a lowland tropical rainforest in Brunei. *Journal of Hydrology* 200, 260–279.

Fahle, M., Dietrich, O., 2014. Estimation of evapotranspiration using diurnal groundwater level fluctuations, Comparison of different approaches with groundwater lysimeter data. *Water Resources Research* 50, 273–286.

Fan, J., Guyot, A., Oestergaarda, K., Lockington, D., 2014. Measuring and modeling rainfall interception losses by a native banksia woodland and an exotic pine plantation in subtropical coastal Australia. *Journal of Hydrology* 515, 156–165.

Fan, J., Oestergaard, K.T., Guyot, A., Jensen, D.G., Lockington, D.A., 2014. Spatial variability of throughfall and stemflow in an exotic pine plantation of subtropical coastal Australia. *Hydrological Processes*. DOI, 10.1002/hyp.10193

Farrington, P., Bartle, G.A., 1991. Recharge beneath a Banksia woodland and a Pinus pinaster plantation on coastal deep sands in south Western Australia. *Forest Ecology and Management* 40, 101–118.

Fayer, M.J., Hillel, D., 1986. Air Encapsulation, II. Profile Water Storage and Shallow Water Table Fluctuations1. *Soil Science Society of America Journal* 50, 572.

Feddes, R.A., Kowalik, P.J., Zaradny, H., 1978. Simulation of field water use and crop yield.

Fiener P, Auerswald K. 2009. Spatial variability of rainfall on a sub-kilometre scale. *Earth Surface Processes and Landforms* 34, 848–859.

Ford C.R., Hubbard R.M., Vose J.M., 2011. Quantifying structural and physiological controls on variation in canopy transpiration among planted pine and hardwood species in the southern Appalachians. *Ecohydrology*. 4, 183–195.

Ford ED, Deans JD. 1978. The effects of canopy structure on stemflow, throughfall and interception loss in a young Sitka spruce plantation. *Journal of Applied Ecology* 15, 905–917.

French, H., Binley, A., 2004. Snowmelt infiltration, monitoring temporal and spatial variability using time-lapse electrical resistivity. *Journal of Hydrology* 297, 174–186.

Fukue, M., Minato, T., Horibe, H., Taya, N., 1999. The micro-structures of clay given by resistivity measurements. *Engineering Geology* 54, 43–53.

Furman, A., Arnon-Zur, A., Assouline, S., 2013. Electrical Resistivity Tomography of the Root Zone. *Soil-water-root process: advances in tomography and imaging*.

Gash JHC, Stewart JB. 1977. The evaporation from Thetford Forest during 1975. *Journal of Hydrology* 35, 385–396.

Gash, J. H. C., 1979. An analytical model of rainfall interception by forests. *Quarterly Journal of the Royal Meteorological Society* 105, 43–55.

Gash, J.H.C., Lloyd, C.R., Lachaud, G., 1995. Estimating sparse forest rainfall interception with an analytical model. *Journal of Hydrology* 170, 79–86.

Gash, J.H.C., Morton, A.J., 1978. An application of the Rutter model to the estimation of the interception loss from Thetford Forest. *Journal of Hydrology* 38, 49–58.

Gee, G.W., Bauder, J.W., 1986. Particle-size analysis, part 1. Agronomy Monographs. 9.

Ghimire, C.P., Bruijnzeel, L. Adrian, Lubczynski, M.W., Bonell, Mike, 2012. Rainfall interception by natural and planted forests in the Middle Mountains of Central Nepal. *Journal of Hydrology* 475, 270–280.

Gower ST, Norman JM. 1991. Rapid estimation of leaf area index in conifer and broad-leaf plantations. *Ecology* 72, 1896–1900.

Green, S., Clothier, B., 1999. The root zone dynamics of water uptake by a mature apple tree. *Plant Soil* 206, 61–77.

Gribovszki, Z., Kalicz, P., Szilágyi, J., Kucsara, M., 2008. Riparian zone evapotranspiration estimation from diurnal groundwater level fluctuations. *Journal of Hydrology* 349, 6–17.

Guswa AJ, Spence CM. 2012. Effect of throughfall variability on recharge, application to hemlock and deciduous forests in western Massachusetts. *Ecohydrology* 5, 563–574.

Hanchi A, Rapp M. 1997. Stemflow determination in forest stands. *Forest Ecology and Management* 97, 231–235.

Harbaugh, A.W., Banta, E.R., Hill, M.C., McDonald, M.G., 2000. MODFLOW-2000, the US Geological Survey modular ground-water model, User guide to modularization concepts and the ground-water flow process. US Geological Survey Denver, CO, Reston, VA.

Harbison, J.E., 1998. The occurrence and chemistry of groundwater on Bribie Island, a large barrier island in Moreton Bay, Southeast Queensland. Queensland University of Technology.

Healy, R., Cook, P., 2002. Using groundwater levels to estimate recharge. *Hydrogeology Journal* 10, 91–109.

Heppner, C.S., Nimmo, J.R., 2005. A Computer Program for Predicting Recharge with a Master Recession Curve.

Heppner, C.S., Nimmo, J.R., Folmar, G.J., Gburek, W.J., Risser, D.W., 2007. Multiple-methods investigation of recharge at a humid-region fractured rock site, Pennsylvania, USA. *Hydrogeology Journal* 15, 915–927.

Herwitz SR, Slye RE. 1995. Three-dimensional modeling of canopy tree interception of wind-driven rainfall. *Journal of Hydrology* 168, 205–226.

Herwitz, S.R., 1987. Raindrop impact and water flow on the vegetative surfaces of trees and the effects on stemflow and throughfall generation. *Earth Surface Processes and Landforms* 12, 425–432.

Holwerda F, Scatena FN, Bruijnzeel LA. 2006. Throughfall in a Puerto Rican lower montane rain forest, a comparison of sampling strategies. *Journal of Hydrology* 327, 592–602.

Holwerda, F., Bruijnzeel, L.A., Scatena, F.N., Vugts, H.F., Meesters, A.G.C.A., 2012. Wet canopy evaporation from a Puerto Rican lower montane rain forest, The importance of realistically estimated aerodynamic conductance. *Journal of Hydrology* 414–415, 1–15.

Hopmans, J.W., Nielsen, D.R., Bristow, K.L., 2002. How useful are small-scale soil hydraulic property measurements for large-scale vadose zone modeling? *Geophysical Monograph Series* 129, 247–258.

Hopp L, McDonnell JJ. 2011. Examining the role of throughfall patterns on subsurface stormflow generation. *Journal of Hydrology* 409, 460–471.

Hörmann, G., Branding, A., Clemen, T., Herbst, M., Hinrichs, A., Thamm, F., 1996. Calculation and simulation of wind controlled canopy interception of a beech forest in Northern Germany. *Agricultural and Forest Meteorology* 79, 131–148.

Huber A, Iroumé A. 2001. Variability of annual rainfall partitioning for different sites and forest covers in Chile. *Journal of Hydrology* 248, 78–92.

Huisman, J.A., Hubbard, S.S., Redman, J.D., Annan, A.P., 2003. Measuring soil water content with ground penetrating radar. *Vadose Zone Journal* 2, 476–491.

Hupet, F., Vanclooster, M., 2005. Micro-variability of *Hydrological Processes* at the maize row scale, implications for soil water content measurements and evapotranspiration estimates. *Journal of Hydrology* 303, 247–270.

Isaacs, L.T., Lewis T., Walker, F.D., 1983. Groundwater model for an island aquifer , Bribie Island groundwater study.

Ishaq, S., 1980. Bribie Island water supply - hydrogeological reconnaissance of the southern part of Bribie Island. Geological Survey of Queensland, Brisbane.

Jackson, I.J., 1975. Relationships between rainfall parameters and interception by tropical forest. *Journal of Hydrology* 24, 215–238.

Jackson, J.M., 2007. Hydrogeology and groundwater flow model, central catchment of Bribie Island, Southeast Queensland.

Jackson, R.B., Canadell, J., Ehleringer, J.R., Mooney, H.A., Sala, O.E., Schulze, E.D., 1996. A global analysis of root distributions for terrestrial biomes. *Oecologia* 108, 389–411.

Jayawickreme, D.H., Van Dam, R.L., Hyndman, D.W., 2008. Subsurface imaging of vegetation, climate, and root-zone moisture interactions. *Geophysical Research Letters* 35, L18404.

Jayawickreme, D.H., Van Dam, R.L., Hyndman, D.W., 2010. Hydrological consequences of land-cover change, Quantifying the influence of plants on soil moisture with time-lapse electrical resistivity. *Geophysics* 75, WA43–WA50.

Jiménez-Martínez, J., Skaggs, T.H., van Genuchten, M.T., Candela, L., 2009. A root zone modelling approach to estimating groundwater recharge from irrigated areas. *Journal of Hydrology* 367, 138–149.

Kanowski J, Catterall CP, Wardell-Johnson GW. 2005. Consequences of broadscale timber plantations for biodiversity in cleared rainforest landscapes of tropical and subtropical Australia. *Forest Ecology and Management* 208, 359–372.

Keim RF, Skaugset AE, Weiler M. 2005. Temporal persistence of spatial patterns in throughfall. *Journal of Hydrology* 314, 263–274.

Keim, R.F., Tromp-van Meerveld, H.J., McDonnell, J.J., 2006. A virtual experiment on the effects of evaporation and intensity smoothing by canopy interception on subsurface stormflow generation. *Journal of Hydrology* 327, 352–364.

Keller, G.V., Frischknecht, F.C., 1966. Electrical methods in geophysical prospecting.

Kimmins JP. 1973. Some Statistical Aspects of Sampling Throughfall Precipitation in Nutrient Cycling Studies in British Columbian Coastal Forests. *Ecology* 54, 1008–1019.

Klaassen, W., Bosveld, F., De Water, E., 1998. Water storage and evaporation as constituents of rainfall interception. *Journal of Hydrology* 212-213, 36–50.

Klingaman, N.P., Levia, D.F., Frost, E.E., 2007. A comparison of three canopy interception models for a leafless mixed deciduous forest stand in the eastern United States. *Journal of Hydrometeorology* 8, 825–836.

Koestel, J., Kemna, A., Javaux, M., Binley, A., Vereecken, H., 2008. Quantitative imaging of solute transport in an unsaturated and undisturbed soil monolith with 3-D ERT and TDR. *Water Resources Research* 44, n/a–n/a.

Komatsu H, Onozawa Y, Kume T, Tsuruta K, Kumagai T, Shinohara Y, Otsuki K. 2010. Stand-scale transpiration estimates in a Moso bamboo forest, II. Comparison with coniferous forests. *Forest Ecology and Management* 260, 1295–1302.

Krajewski WF, Ciach GJ, Habib E. 2003. An analysis of small-scale rainfall variability in different climatic regimes. *Hydrological sciences journal* 48, 151–162.

Krämer I, Hölscher D. 2009. Rainfall partitioning along a tree diversity gradient in a deciduous old-growth forest in Central Germany. *Ecohydrology* 2, 102–114.

Kurtzman, D., Scanlon, B.R., 2011. Groundwater Recharge through Vertisols, Irrigated Cropland vs. Natural Land, Israel. *Vadose Zone Journal* 10, 662–674.

Laclau JP, Ranger J, Bouillet JP, De Dieu Nzila J, Deleporte P. 2003. Nutrient cycling in a clonal stand of Eucalyptus and an adjacent savanna ecosystem in Congo, 1. Chemical composition of rainfall, throughfall and stemflow solutions. *Forest Ecology and Management* 176, 105–119.

Le Maitre, D.C., F., S.D., Colvin, C., 1999. A review of information on interactions between vegetation and groundwater. Water South Africa.

Lehmann, P., Gambazzi, F., Suski, B., Baron, L., Askarinejad, A., Springman, S.M., Holliger, K., Or, D., 2013. Evolution of soil wetting patterns preceding a hydrologically induced landslide inferred from electrical resistivity survey and point measurements of volumetric water content and pore water pressure. *Water Resources Research* 49, 7992–8004.

Levia DF, Frost EE. 2003. A review and evaluation of stemflow literature in the hydrologic and biogeochemical cycles of forested and agricultural ecosystems. *Journal of Hydrology* 274, 1–29.

Levia DF, Frost EE. 2006. Variability of throughfall volume and solute inputs in wooded ecosystems. *Progress in Physical Geography* 30, 605–632.

Levia DF, Van Stan JT, Mage SM, Kelley-Hauske PW. 2010. Temporal variability of stemflow volume in a beech-yellow poplar forest in relation to tree species and size. *Journal of Hydrology* 380, 112–120.

Levia DF, Van Stan JT, Siegert CM, Inamdar SP, Mitchell MJ, Magee SM, McHale PJ. 2011. Atmospheric deposition and corresponding variability of stemflow chemistry across temporal scales in a mid-Atlantic broadleaved deciduous forest. *Atmospheric Environment* 45, 3046–3054.

Levia, D.F., Carlyle-Moses, D.E., Tanaka, T. (Eds.), 2011. Forest Hydrology and Biogeochemistry. Springer Netherlands, Dordrecht.

Leyton L, Reynolds ERC, Thompson FB. 1967. Rainfall interception in forests and moorland. in Int. Symp. Forest Hydrology, Pergamon Press, Oxford, 163–178.

Li, Q., Cheng, J., Li, T., Liu, F.J., 2007. Ecological function of artificial conifers timber forests in water conservation. *Jilin Forestry Science and Technology* 36, 14–17.

Liang WL, Kosugi K, Mizuyama T. 2007. Heterogeneous soil water dynamics around a tree growing on a steep hillslope. *Vadose Zone Journal* 6, 879–889.

Liang WL, Kosugi K, Mizuyama T. 2009. A three-dimensional model of the effect of stemflow on soil water dynamics around a tree on a hillslope. *Journal of Hydrology* 366, 62–75.

Limousin, J.M., Rambal, S., Ourcival, J.M., Joffre, R., 2008. Modelling rainfall interception in a mediterranean Quercus ilex ecosystem, Lesson from a throughfall exclusion experiment. *Journal of Hydrology* 357, 57–66.

Llorens P, Domingo F. 2007. Rainfall partitioning by vegetation under Mediterranean conditions. A review of studies in Europe. *Journal of Hydrology* 335, 37–54.

Llorens P, Poch R, Latron J, Gallart F. 1997. Rainfall interception by a Pinus sylvestris forest patch overgrown in a Mediterranean mountainous abandoned area I. Monitoring design and results down to the event scale. *Journal of Hydrology* 199, 331–345.

Llorens, P, Gallart, F, 2000. A simplified method for forest water storage capacity measurement. *Journal of Hydrology* 240, 131–144.

Llorens, P., 1997. Rainfall interception by a Pinus sylvestris forest patch overgrown in a Mediterranean mountainous abandoned area II. Assessment of the applicability of Gash's analytical model. *Journal of Hydrology* 199, 346–359.

Llorens, P., Poch, R., Latron, J., Gallart, F., 1997. Rainfall interception by a Pinus sylvestris forest patch overgrown in a Mediterranean mountainous abandoned area I. Monitoring design and results down to the event scale. *Journal of Hydrology* 199, 331–345.

Lloyd C, Marques ADO. 1988. Spatial variability of throughfall and stemflow measurements in Amazonian rainforest. *Agricultural and Forest Meteorology* 42, 63–73.

Loescher HW, Powers JS, Oberbauer SF. 2002. Spatial variation of throughfall volume in an old-growth tropical wet forest, Costa Rica. *Journal of Tropical Ecology* 18, 397–407.

Logsdon, S.D., Schilling, K.E., Hernandez-Ramirez, G., Prueger, J.H., Hatfield, J.L., Sauer, T.J., 2010. Field estimation of specific yield in a central Iowa crop field. *Hydrological Processes* 24, 1369–1377.

Loheide II, S.P., 2008. A method for estimating subdaily evapotranspiration of shallow groundwater using diurnal water table fluctuations. *Ecohydrology* 1, 59–66.

Loheide II, S.P., Butler, J.J., Gorelick, S.M., 2005. Estimation of groundwater consumption by phreatophytes using diurnal water table fluctuations, A saturated-unsaturated flow assessment. *Water Resources Research* 41, W07030.

Loke, M.H., 2013. Rapid 2-D Resistivity & IP inversion using the least-squares method. Man. Res2dinv, version 3, 71.

Loke, M.H., Barker, R.D., 1995. Least-squares deconvolution of apparent resistivity pseudosections. *Geophysics* 60, 1682–1690.

Loustau, D., Berbigier, P., Granier, A., 1992. Interception loss, throughfall and stemflow in a maritime pine stand. II. An application of Gash's analytical model of interception. *Journal of Hydrology* 138, 469–485.

Mair A, Fares A. 2010. Throughfall characteristics in three non-native Hawaiian forest stands. *Agricultural and Forest Meteorology* 150, 1453–1466.

Mao, D., Cherkauer, K.A., 2009. Impacts of land-use change on hydrologic responses in the Great Lakes region. *Journal of Hydrology* 374, 71–82.

Marescot, L., Loke, M.H., Chapellier, D., Delaloye, R., Lambiel, C., Reynard, E., 2003. Assessing reliability of 2D resistivity imaging in mountain permafrost studies using the depth of investigation index method. *Near Surface Geophysics* 1, 57–67.

Marquardt, D.W., 1963. An algorithm for least-squares estimation of nonlinear parameters. *Journal of the Society for Industrial and Applied Mathematics* 11, 431–441.

McClain ME, Boyer EW, Dent CL, Gergel SE, Grimm NB, Groffman PM, Hart SC, Harvey JW, Johnston CA, Mayorga E, McDowell WH, Pinay G. 2003. Biogeochemical hot spots and hot moments at the interface of terrestrial and aquatic ecosystems. *Ecosystems* 6, 301–312.

McConkey B, Nicholaichuk W, Cutforth H. 1990. Small area variability of warm-season precipitation in a semiarid climate. *Agricultural and Forest Meteorology* 49, 225–242.

Meng, G.T., Lang, N.J., Fang, X.J., Li, G.X., Yuan, C.M., Wen, S.L., 2001. Hydrological properties and water balance of Pinus armandii plantation in central Dian Plateau, Yunnan province. *Forest Research* 14, 7–14.

Michot, D., Benderitter, Y., Dorigny, A., Nicoullaud, B., King, D., Tabbagh, A., 2003. Spatial and temporal monitoring of soil water content with an irrigated corn crop cover using surface electrical resistivity tomography. *Water Resources Research* 39.

Molen, M.K. van der, Dolman, A.J., Waterloo, M.J., Bruijnzeel, L.A., 2006. Climate is affected more by maritime than by continental land use change, a multiple-scale analysis. *Global and Planetary Change* 54, 128–149.

Molina AJ, Del Campo AD. 2012. The effects of experimental thinning on throughfall and stemflow, A contribution towards hydrology-oriented silviculture in Aleppo pine plantations. *Forest Ecology and Management* 269, 206–213.

Monteith, J.L., 1965. Evaporation and environment. *Symposia of the Society for Experimental Biology* 19, 205–34.

Moss, P.T., Tibby, J., Petherick, L., McGowan, H., Barr, C., 2013. Late Quaternary vegetation history of North Stradbroke Island, Queensland, eastern Australia. *Quaternary Science Reviews* 74, 257–272.

Mould, D.J., Frahm, E., Salzmann, T., Miegel, K., Acreman, M.C., 2010. Evaluating the use of diurnal groundwater fluctuations for estimating evapotranspiration in wetland environments, case studies in southeast England and northeast Germany. *Ecohydrology* 3, 294–305.

Mualem, Y., 1976. A new model for predicting the hydraulic conductivity of unsaturated porous media. *Water Resources Research* 12, 513–522.

Mululo Sato A, de Souza Avelar A, Coelho Netto AL. 2011. Spatial variability and temporal stability of throughfall in a eucalyptus plantation in the hilly lowlands of southeastern Brazil. *Hydrological Processes* 25, 1910–1923.

Murakami S. 2006. A proposal for a new forest canopy interception mechanism, Splash droplet evaporation. *Journal of Hydrology* 319, 72–82.

Muzylo, A., Llorens, P., Valente, F., Keizer, J.J., Domingo, F., Gash, J.H.C., 2009. A review of rainfall interception modelling. *Journal of Hydrology* 370, 191–206.

Nachabe, M., Shah, N., Ross, M., Vomacka, J., 2005. Evapotranspiration of two vegetation covers in a shallow water table environment. *Soil Science Society of America Journal* 69, 492–499.

Nachabe, M.H., 2002. Analytical expressions for transient specific yield and shallow water table drainage. *Water Resources Research* 38, 11-1–11-7.

Nadler, A., Tyree, M.T., 2008. Substituting stem's water content by electrical conductivity for monitoring water status changes. *Soil Science Society of America Journal* 72, 1006–1013.

Nash J.E., Sutcliffe J.V., 1970. River flow forecasting through conceptual models part I—A discussion of principles. *Journal of Hydrology* 10, 282–290.

Neuman, S.P., 1987. On Methods of Determining Specific Yield. *Ground Water* 25, 679–684.

Nikodem, A., Kodešová, R., Drábek, O., Bubeníčková, L., Boruuvka, L., Pavluu, L., Tejnecky, V., 2010. A numerical study of the impact of precipitation redistribution in a beech forest canopy on water and aluminum transport in a Podzol. *Vadose Zone Journal* 9, 238–251.

Niswonger, R.G., Prudic, D.E., Regan, R.S., 2006. Documentation of the Unsaturated-Zone Flow (UZF1) Package for modeling unsaturated flow between the land surface and the water table with MODFLOW-2005. US Department of the Interior, US Geological Survey.

Nosetto, M.D., Jobbágy, E.G., Brizuela, A.B., Jackson, R.B., 2012. The hydrologic consequences of land cover change in central Argentina. *Agriculture, Ecosystems & Environment* 154, 2–11.

O'Grady AP, Worledge D, Battaglia M. 2005. Temporal and spatial changes in fine root distributions in a young Eucalyptus globulus stand in southern Tasmania. *Forest Ecology and Management* 214, 373–383.

Oke T.R., 1992. Boundary layer climates (Vol. 5). Psychology Press.

Oke, T.R., 1978. Boundary layer climates.

Pinto, C.A., Nadezhdina, N., David, J.S., Kurz-Besson, C., Caldeira, M.C., Henriques, M.O., Monteiro, F.G., Pereira, J.S., David, T.S., 2013. Transpiration in Quercus suber trees under shallow water table conditions, the role of soil and groundwater. *Hydrological Processes*. DOI, 10.1002/hyp.10097

Price, A.G, Carlyle-Moses, D.E, 2003. Measurement and modelling of growing-season canopy water fluxes in a mature mixed deciduous forest stand, southern Ontario, Canada. *Agricultural and Forest Meteorology* 119, 69–85.

Raat, K.J., Draaijers, G.P.J., Schaap, M.G., Tietema, A., Verstraten, J.M., 2002. Spatial variability of throughfall water and chemistry and forest floor water content in a Douglas fir forest stand. *Hydrology and Earth System Sciences* 6, 363–374.

Radcliffe, D.E., Šimůnek, J., 2010. Soil physics with HYDRUS, modeling and applications. CRC press Boca Raton, FL.

Richards, L.A., 1931. Capillary conduction of liquids through porous mediums. *Physics* (College. Park. Md). 1, 318.

Ritchie, J.T., 1972. Model for predicting evaporation from a row crop with incomplete cover. *Water Resources Research* 8, 1204–1213.

Ritter A, Regalado CM. 2012. Roving revisited, towards an optimum throughfall sampling design. *Hydrological Processes* 319, 72–82.

Robinson, D.A., Abdu, H., Lebron, I., Jones, S.B., 2012. Imaging of hill-slope soil moisture wetting patterns in a semi-arid oak savanna catchment using time-lapse electromagnetic induction. *Journal of Hydrology* 416, 39–49.

Roth, B.E., Slatton, K.C., Cohen, M.J., 2007. On the potential for high-resolution lidar to improve rainfall interception estimates in forest ecosystems. *Frontiers in Ecology and the Environment* 5, 421–428.

Rutter A.J., Morton A.J., Robins P.C.,1975. A predictive model of rainfall interception in forests. II. Generalization of the model and comparison with observations in some coniferous and hardwood stands. *Journal of Applied Ecology* 12, 367–380.

Samouëlian, A., Cousin, I., Tabbagh, A., Bruand, A., Richard, G., 2005. Electrical resistivity survey in soil science, a review. *Soil Tillage Research* 83, 173–193.

Sansoulet, J., Cabidoche, Y.-M., Cattan, P., Ruy, S., Šimůnek, J., 2008. Spatially Distributed Water Fluxes in an Andisol under Banana Plants, Experiments and Three-Dimensional Modeling. *Vadose Zone Journal* 7, 819.

Scanlon, B., Healy, R., Cook, P., 2002. Choosing appropriate techniques for quantifying groundwater recharge. *Hydrogeology Journal* 10, 18–39.

Scanlon, B.R., Christman, M., Reedy, R.C., Porro, I., Simunek, J., Flerchinger, G.N., 2002. Intercode comparisons for simulating water balance of surficial sediments in semiarid regions. *Water Resources Research* 38, 59–1–59–16.

Scanlon, B.R., Jolly, I., Sophocleous, M., Zhang, L., 2007. Global impacts of conversions from natural to agricultural ecosystems on water resources, Quantity versus quality. *Water Resources Research* 43, W03437.

Scanlon, B.R., Reedy, R.C., Stonestrom, D.A., Prudic, D.E., Dennehy, K.F., 2005. Impact of land use and land cover change on groundwater recharge and quality in the southwestern US. *Global Change Biology* 11, 1577–1593.

Scheuermann, A., Huebner, C., Schlaeger, S., Wagner, N., Becker, R., Bieberstein, A., 2009. Spatial time domain reflectometry and its application for the measurement of water content distributions along flat ribbon cables in a full-scale levee model. *Water Resources Research* 45.

Schilling, K.E., 2007. Water table fluctuations under three riparian land covers, Iowa (USA). *Hydrological Processes* 21, 2415–2424.

Schlaeger, S., 2005. A fast TDR-inversion technique for the reconstruction of spatial soil moisture content. *Hydrology and Earth System Sciences* Discuss. Discuss. 2, 971–1009.

Schwartz, B.F., Schreiber, M.E., 2009. Quantifying potential recharge in mantled sinkholes using ERT. *Ground Water* 47, 370–81.

Schwartz, B.F., Schreiber, M.E., Yan, T., 2008. Quantifying field-scale soil moisture using electrical resistivity imaging. *Journal of Hydrology* 362, 234–246.

Seo, H.S., Šimuunek, J., Poeter, E.P., 2007. Documentation of the HYDRUS package for MODFLOW-2000, the US Geological Survey modular ground-water model. International Ground Water Modeling Center.

Shachnovich Y, Berliner PR, Bar P. 2008. Rainfall interception and spatial distribution of throughfall in a pine forest planted in an arid zone. *Journal of Hydrology* 28, 123–133.

Shah, N., Ross, M., 2009. Variability in Specific Yield under Shallow Water Table Conditions. *Journal of Hydrologic Engineering* 14, 1290–1298.

Shen, W., Louis, T.A., 1998. Triple-goal estimates in two-stage hierarchical models. *Journal of the Royal Statistical Society, Series B (Statistical Methodology)* 60, 455–471.

Shi Z, Wang Y, Xu L, Xiong W, Yu P, Gao J, Zhang L. 2010. Fraction of incident rainfall within the canopy of a pure stand of Pinus armandii with revised Gash model in the Liupan Mountains of China. *Journal of Hydrology* 385, 44–50.

Shinohara Y, Onozawa Y, Chiwa M, Kume T, Komatsu H, Otsuki K. 2010. Spatial variations in throughfall in a Moso bamboo forest, sampling design for the estimates of stand-scale throughfall. *Hydrological Processes* 24, 253–259.

Silva IC, Rodríguez HG. 2010. Interception loss, throughfall and stemflow chemistry in pine and oak forests in northeastern Mexico. *Tree Physiology* 21, 1009–1013..

Šimůnek, J., van Genuchten, M.T., Šejna, M., 2008. Development and Applications of the HYDRUS and STANMOD Software Packages and Related Codes. *Vadose Zone Journal* 7, 587.

Singh, R.P., 1987. Rainfall Interception by Pinus wallichiana Plantation in Temperate Region of Himachal Pradesh, India. *Indian Forest* 113, 559–566.

Sophocleous, M., 1985. The Role of Specific Yield in Ground-Water Recharge Estimations, A Numerical Study. *Ground Water* 23, 52–58.

Šraj M, Brilly M, Mikoš M. 2008. Rainfall interception by two deciduous Mediterranean forests of contrasting stature in Slovenia. *Agricultural and Forest Meteorology* 148, 121–134.

Srayeddin, I., Doussan, C., 2009. Estimation of the spatial variability of root water uptake of maize and sorghum at the field scale by electrical resistivity tomography. *Plant Soil* 319, 185–207.

Steelman, C.M., Endres, A.L., Jones, J.P., 2012. High-resolution ground-penetrating radar monitoring of soil moisture dynamics, Field results, interpretation, and comparison with unsaturated flow model. *Water Resources Research* 48, W09538.

Swank W.T., Douglass J.E., 1974. Streamflow greatly reduced by converting deciduous hardwood stands to pine. *Nature* 185, 857–859.

Syed KH, Goodrich DC, Myers DE, Sorooshian S. 2003. Spatial characteristics of thunderstorm rainfall fields and their relation to runoff. *Journal of Hydrology* 271, 1–21.

Taniguchi M, Tsujimura M, Tanaka T. 1996. Significance of stemflow in groundwater recharge. 1, Evaluation of the stemflow contribution to recharge using a mass balance approach. *Hydrological Processes* 10, 71–80.

Taniguchi, M., Tsujimura, M., Tanaka, T., 1996. Significance of stemflow in groundwater recharge. 1, Evaluation of the stemflow contribution to recharge using a mass balance approach. *Hydrological Processes* 10, 71–80.

Thoms, R.B., Johnson, R.L., Healy, R.W., 2006. User's Guide to the Variably Saturated Flow (VSF) Process for MODFLOW. US Department of the Interior, US Geological Survey.

Toba T, Ohta T. 2005. An observational study of the factors that influence interception loss in boreal and temperate forests. *Journal of Hydrology* 313, 208–220.

Topp, G.C., Davis, J.L., Annan, A.P., 1980. Electromagnetic determination of soil water content, Measurements in coaxial transmission lines. *Water Resources Research* 16, 574–582.

Twarakavi, N.K.C., Šimuunek, J., Seo, S., 2008. Evaluating interactions between groundwater and vadose zone using the HYDRUS-based flow package for MODFLOW. *Vadose Zone Journal* 7, 757–768.

Ulrich, C., Slater, L., 2004. Induced polarization measurements on unsaturated, unconsolidated sands. *Geophysics* 69, 762–771.

Valente F, David JS, Gash JHC. 1997. Modelling interception loss for two sparse eucalypt and pine forests in central Portugal using reformulated Rutter and Gash analytical models. *Journal of Hydrology* 190, 141–162.

Valente, F., David, J.S., Gash, J.H.C., 1997. Modelling interception loss for two sparse eucalypt and pine forests in central Portugal using reformulated Rutter and Gash analytical models. *Journal of Hydrology* 190, 141–162.

Valente, F., David, J.S., Gash, J.H.C., 1997. Modelling interception loss for two sparse eucalypt and pine forests in central Portugal using reformulated Rutter and Gash analytical models. *Journal of Hydrology* 190, 141–162.

Van Dam, J.C., Huygen, J., Wesseling, J.G., Feddes, R.A., Kabat, P., Van Walsum, P.E. V, Groenendijk, P., Van Diepen, C.A., 1997. Theory of SWAP version 2.0.

Van Dijk, A.I.J.M., Bruijnzeel, L.A., 2001. Modelling rainfall interception by vegetation of variable density using an adapted analytical model. Part 2. Model validation for a tropical upland mixed cropping system. *Journal of Hydrology* 247, 239–262.

Van Genuchten, M.T., 1980. A Closed-form Equation for Predicting the Hydraulic Conductivity of Unsaturated Soils1. *Soil Science Society of America Journal* 44, 892.

Van Stan JT, Siegert CM, Levia DF, Scheick CE. 2011. Effects of wind-driven rainfall on stemflow generation between codominant tree species with differing crown characteristics. *Agricultural and Forest Meteorology* 151, 1277–1286.

Vanninen, P., Makela, A., 1999. Fine root biomass of Scots pine stands differing in age and soil fertility in southern Finland. *Tree Physiology* 19, 823–830.

Venegas, J.G., Harris, R.S., Simon, B.A., 1998. A comprehensive equation for the pulmonary pressure-volume curve. Journal of Applied Physiology 84, 389–95.

Vereecken, H., Huisman, J.A., Bogena, H., Vanderborght, J., Vrugt, J.A., Hopmans, J.W., 2008. On the value of soil moisture measurements in vadose zone hydrology: A review. *Water Resources Research* 44.

Vereecken, H., Huisman, J.A., Pachepsky, Y., Montzka, C., van der Kruk, J., Bogena, H., Weihermüller, L., Herbst, M., Martinez, G., Vanderborght, J., 2013. On the spatio-temporal dynamics of soil moisture at the field scale. *Journal of Hydrology* 516, 76–96.

Verseghy, D.L., McFarlane, N.A., Lazare, M., 1993. Class-A Canadian land surface scheme for GCMS, II. Vegetation model and coupled runs. *International Journal of Climatology* 13, 347–370.

Villarini G, Mandapaka PV, Krajewski WF, Moore RJ. 2008. Rainfall and sampling uncertainties, A rain gauge perspective. *Journal of Geophysical Research-Atmospheres* 113(D11).

Vincke, C., Thiry, Y., 2008. Water table is a relevant source for water uptake by a Scots pine (Pinus sylvestris L.) stand, Evidences from continuous evapotranspiration and water table monitoring. *Agricultural and Forest Meteorology* 148, 1419–1432.

Vrugt, J.A., van Wijk, M.T., Hopmans, J.W., Šimunek, J., 2001. One-, two-, and three-dimensional root water uptake functions for transient modeling. *Water Resources Research* 37, 2457–2470.

Wallace, J., McJannet, D., 2006. On interception modelling of a lowland coastal rainforest in northern Queensland, Australia. *Journal of Hydrology* 329, 477–488.

Wallace, J., McJannet, D., 2008. Modelling interception in coastal and montane rainforests in northern Queensland, Australia. *Journal of Hydrology* 348, 480–495.

Wang, J., Huang, G., Zhan, H., Mohanty, B.P., Zheng, J., Huang, Q., Xu, X., 2014. Evaluation of soil water dynamics and crop yield under furrow irrigation with a two-dimensional flow and crop growth coupled model. *Agricultural Water Management* 141, 10–22.

Werban, U., Attia al Hagrey, S., Rabbel, W., 2008. Monitoring of root-zone water content in the laboratory by 2D geoelectrical tomography. *Journal of Plant Nutrition and Soil Science* 171, 927–935.

Western, A.W., Grayson, R.B., Blöschl, G., Wilson, D.J., 2003. Spatial variability of soil moisture and its implications for scaling. *Scaling Methods in Soil Physics* 119–142.

Whelan M, Sanger L, Baker M, Anderson J. 1998. Spatial patterns of throughfall and mineral ion deposition in a lowland Norway spruce (Picea abies) plantation at the plot scale. *Atmospheric Environment* 32, 3493–3501.

Whelan, M.J., Anderson, J.M., 1996. Modelling spatial patterns of throughfall and interception loss in a Norway spruce (Picea abies) plantation at the plot scale. *Journal of Hydrology* 186, 335–354.

White, W., 1932. A method of estimating ground-water supplies based on discharge by plants and evaporation from soil, Results of investigations in Escalante Valley, Utah. U.S. Geological Survey Water Supply.

Willmott, C.J., 1981. On the validation of models. *Physical Geography* 2, 184–194.

Wullaert H, Pohlert T, Boy J, Valarezo C, Wilcke W. 2009. Spatial throughfall heterogeneity in a montane rain forest in Ecuador, extent, temporal stability and drivers. *Journal of Hydrology* 377, 71–79.

Yamakawa, Y., Kosugi, K., Katsura, S., Masaoka, N., Mizuyama, T., 2012. Spatial and temporal monitoring of water content in weathered granitic bedrock using electrical resistivity imaging. *Vadose Zone Journal* 11.

Yin, L., Zhou, Y., Ge, S., Wen, D., Zhang, E., Dong, J., 2013. Comparison and modification of methods for estimating evapotranspiration using diurnal groundwater level fluctuations in arid and semiarid regions. *Journal of Hydrology* 496, 9–16.

Zhan W, Zhang Z, Wu J, Xiao J. 2007. Spatial variability of throughfall in a Chinese pine (Pinus tabulaeformis) plantation in northern China. *Frontiers of Forestry in China* 2, 169–173.

Zhang, L., Dawes, W., 1998. An integrated energy and water balance model. CSIRO Land and Water Technical Report.

Zhang, L., Dawes, W.R., Walker, G.R., 2001. Response of mean annual evapotranspiration to vegetation changes at catchment scale. *Water Resources Research* 37, 701–708.

Zhou, Q.Y., Shimada, J., Sato, A., 2001. Three-dimensional spatial and temporal monitoring of soil water content using electrical resistivity tomography. *Water Resources Research* 37, 273–285.

Zhu, J., Young, M., Healey, J., Jasoni, R., Osterberg, J., 2011. Interference of river level changes on riparian zone evapotranspiration estimates from diurnal groundwater level fluctuations. *Journal of Hydrology* 403, 381–389.

Ziegler A, Giambelluca T, Nullet M, Sutherland R, Tantasarin C, Vogler J, Negishi J. 2009. Throughfall in an evergreen-dominated forest stand in northern Thailand, Comparison of mobile and stationary methods. *Agricultural and Forest Meteorology* 149, 373–384.

Zimmermann A, Wilcke W, Elsenbeer H. 2007. Spatial and temporal patterns of throughfall quantity and quality in a tropical montane forest in Ecuador. *Journal of Hydrology* 343, 80–96.